21:00:19 OCA PAD AMENDMENT - PROJECT HEADER INFORMATION 11/17/91

Active

Project #: G-41-613 Cost share #: G-41-316 Rev #: 3
Center # : 10/24-6-R6915-0A0 Center shr #: 10/22-1-F6915-0A0 OCA file #:
Work type : RES
Contract#: AFOSR-90-0158 Mod #: AMENDMENT B Document : GRANT
Prime #: Contract entity: GTRC

Subprojects ? : N CFDA: 12.800
Main project #: PE #:

Project unit: PHYSICS Unit code: 02.010.152
Project director(s):
FOX R F PHYSICS (404)894-5260

Sponsor/division names: AIR FORCE / BOLLING AFB, DC
Sponsor/division codes: 104 / 001

Award period: 900301 to 920930 (performance) 921130 (reports)

Sponsor amount	New this change	Total to date
Contract value	58,659.00	164,395.00
Funded	58,659.00	164,395.00
Cost sharing amount		42,482.00

Does subcontracting plan apply ?: N

Title: ON THE THEORY OF TURBULENT DYNAMICS

PROJECT ADMINISTRATION DATA

OCA contact: Mildred S. Heyser 894-4820

Sponsor technical contact

ARJE NACHMAN
(202)767-4958

AFORSR/NM
BUILDING 410
BOLLING AFB, D.C. 20332-6448

Sponsor issuing office

MARILYN JAMES
(202)767-4958

AFOSR/PKZ
BUILDING 410
BOLLING AFB, D.C. 20332-6448

Security class (U,C,S,TS) : U ONR resident rep. is ACO (Y/N): N
Defense priority rating : supplemental sheet
Equipment title vests with: Sponsor X GIT
GIT RETAINS TITLE IF EQUIP COST < $5000
Administrative comments -
AMENDMENT B ADDS $58,659-EXERCISES THE SECOND ADDITIONAL PERIOD OF RESEARCH CONTINUING THROUGH 9/30/92.

2-1
SR852

GEORGIA INSTITUTE OF TECHNOLOGY
OFFICE OF CONTRACT ADMINISTRATION

NOTICE OF PROJECT CLOSEOUT

Closeout Notice Date 02/03/93

Project No. G-41-613 Center No. 10/24-6-R6915-0A0

Project Director FOX R F School/Lab PHYSICS

Sponsor AIR FORCE/BOLLING AFB, DC

Contract/Grant No. AFOSR-90-0158 Contract Entity GTRC

Prime Contract No.

Title ON THE THEORY OF TURBULENT DYNAMICS

Effective Completion Date 920930 (Performance) 921130 (Reports)

Closeout Actions Required:	Y/N	Date Submitted
Final Invoice or Copy of Final Invoice	Y	930128
Final Report of Inventions and/or Subcontracts	Y	
Government Property Inventory & Related Certificate	Y	
Classified Material Certificate	N	
Release and Assignment	N	
Other	N	

Comments EFFECTIVE DATE 3-1-90. CONTRACT VALUE $164,395.

Subproject Under Main Project No.

Continues Project No.

Distribution Required:

Project Director	Y
Administrative Network Representative	Y
GTRI Accounting/Grants and Contracts	Y
Procurement/Supply Services	Y
Research Property Managment	Y
Research Security Services	N
Reports Coordinator (OCA)	Y
GTRC	Y
Project File	Y
Other HARRY VANN-FMD	Y
FRED CAIN-OOD	Y

NOTE: Final Patent Questionnaire sent to PDPI.

Annual Technical Report for Grant: AFOSR-90-0158, "On the Theory of Turbulent Dynamics", for the time period 900301 to 900930, Ronald F. Fox, P.I., (Georgia Tech Project # G-41-613).

This research program is based on the idea of amplification of intrinsic (i.e. thermal or molecular) fluctuations by chaotic dynamics. Just prior to the initiation of this grant in March, 1990, several papers were written on this subject (there is no citation to this grant on these papers because of the timing): Phys. Rev. Letts. **64**, 249 (1990), Phys. Rev. **A41**, 2952, 2969 (1990), and Phys. Rev. **A42**, 1946 (1990). These papers provide some of the foundational ideas for this program (reprints are attached). Two more papers have also been written, each of which does carry a citation to this grant. The first of these papers: " On the growth of molecular fluctuations for nonstationary systems" has been held up by unusually long refereeing delays. The second paper: "Amplification of intrinsic fluctuations by chaotic dynamics in physical systems" was only recently submitted. This last paper contains a newly discovered technique for the treatment of large scale fluctuations and numerical examples of the amplification effect (preprint attached). It also contains a suggestion about how to see this effect experimentally. Meanwhile, a collaborative effort with my experimental colleague R. Roy has lead to the observation of this effect in a chaotic multi-mode Nd-YAG laser system, and we are going to write a paper about this soon.

Additional research activity directly related to turbulence in fluids has commenced with the AFOSR support of my student, Tim Elston. He is studying the numerical simulation of hydrodynamic flows which may be chaotic. We will ultimately do this with and without the incorporation of intrinsic fluctuations. The numerical techniques, which are quite delicate, are based in large part on the recent work of Brocket et al., "The dynamics of freely decaying two-dimensional turbulence.", J. Fluid Mech. **194**, 333 (1988), of Kida et al. "A route to chaos and turbulence.", Physica **D37**, 116 (1989), and of Canuto, Spectral Methods in Fluid Dynamics, (Springer-Verlag, New York, 1988). To overcome the stiffness of the Navier-Stokes equations (rendered as driven nonlinear coupled ODE's (truncated to a finite set) for the vorticity in our studies), we find that the "second order (stabilized) leapfrog Crank-Nicolson scheme" is effective and apparently state of the art. To this method one can add the fluctuations in accord with the new technique elucidated in the pending paper "Amplification of intrinsic..." referred to in paragraph

1, above. This work is being pursued with computational facilities here at Tech and on the Cray at the Naval Research Laboratory Central Computing Facility. The Cray time was requested to support the research funded by this grant and $5000 of time has been provided. Mr. Elston has successfully run trial programs on the Cray and we are now poised for our research objectives.

As was pointed out in the original proposal for this grant, one approach to this problem is to obtain a master equation underlying the hydrodynamic equations. An extremely interesting development in this direction has come to our attention recently through the paper of G. Eyink: "Dissipation and large thermodynamic fluctuations" (to appear in J. Stat. Phys.). This paper is directly concerned with hydrodynamics and fluctuations in nonequilibrium states and it addresses the issue of master equations. The work of Kawasaki and of Spohn is especially relevant and we are exploring the real possibility that a valid master equation can be exposed by their methods.

Effect of Molecular Fluctuations on the Description of Chaos by Macrovariable Equations

Ronald F. Fox
School of Physics, Georgia Institute of Technology, Atlanta, Georgia 30332

Joel E. Keizer
Institute for Theoretical Dynamics and Department of Chemistry, University of California, Davis, California, 95616

(Received 7 July 1989; revised manuscript received 13 November 1989)

Intrinsic molecular fluctuations are associated with macrovariables whose time evolution is described by macrovariable equations. When the macrovariable equations describe chaotic trajectories, the covariance matrix for the molecular fluctuations diverges rapidly. This implies that the macrovariable equations are not stable and cannot be justified from an underlying molecular description.

PACS numbers: 05.45.+b, 05.40.+j, 05.70.Ln

There is a long tradition behind the description of macroscopic dissipative processes by phenomenological equations, e.g., hydrodynamics, electrical circuits, and mass-action chemical reactions. It is now widely appreciated[1-9] that a complete macroscopic description of these processes must include the deterministic macrovariables as well as their molecular fluctuations, both of which reflect underlying microscopic dynamics.[1,2,8,9] Indeed, these fluctuations provide the basis for our understanding of light scattering,[10,11] electrical noise, and other noise measurements for macroscopic systems.[12]

By considering the thermodynamic limit of Hamiltonian, kinetic theory,[13] and master equation theories,[14-22] numerous investigators have concluded that fluctuations in macroscopic variables—such as the mass, momentum, and internal energy densities used in hydrodynamics—satisfy Langevin-type equations obtained by linearization around the usual phenomenological macrovariable equations. While these equations successfully describe a variety of physical and chemical phenomena for both stationary and nonstationary states,[8,12] recent numerical work suggests that this approach breaks down on chaotic attractors.[23] Here we investigate this phenomenon further by applying hydrodynamic fluctuation theory to the Lorenz model. We show by numerical calculations that the trace norm of the covariance matrix diverges exponentially at twice the rate of the largest Lyapunov exponent. This is a general property of linearized Langevin theories on chaotic attractors, a result that is discussed here but whose proof is reserved for elsewhere.[24]

We focus on the Lorenz model[25] because it has its origins in the hydrodynamic equations (using constitutive relations and thermodynamic identities the internal energy density is replaced by the temperature density,[7,26] for which there is a generally agreed upon hydrodynamic fluctuation theory).[7,9-11] The Lorenz model exhibits chaos in an appropriate parameter range and can be interpreted as a macroscopic, three-mode representation of the Rayleigh-Bénard problem. The well-known, approximate, Galerkin truncation[25] leads to the following coupled equations for the lowest-order amplitudes (macrovariables) of the temperature deviation (Y and Z) and vorticity (X):

$$\frac{d}{dt}X=-\sigma(X-Y)\,,\quad \frac{d}{dt}Y=-XZ+rX-Y\,,\qquad \frac{d}{dt}Z=XY-bZ\,. \tag{1}$$

According to fluctuating hydrodynamics,[7,8,12,26] Eq. (1) represents the conditionally averaged behavior of the amplitudes. Molecular fluctuations in the amplitudes can be obtained in a similar fashion by analyzing fluctuations in the mass, momentum, and temperature densities for the Rayleigh-Bénard problem. Since the fluctuations satisfy linearized equations obtained from the hydrodynamic equations,[7,26] a Galerkin truncation paralleling that used to obtain the Lorenz equations also yields the associated fluctuation equations. Denoting the fluc-

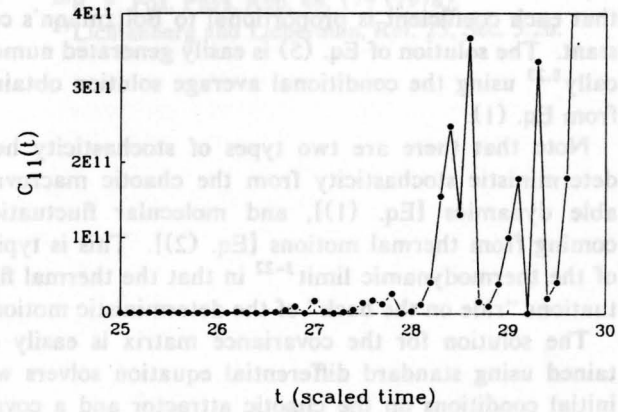

FIG. 1. The variance for δX, C_{11}, grows large and varies wildly.

tuations in X, Y, and Z by δX, δY, and δZ, we obtain[24]

$$\frac{d}{dt}\delta X = -\sigma(\delta X - \delta Y) + f_X ,$$
$$\frac{d}{dt}\delta Y = -X\delta Z - Z\delta X + r\delta X - \delta Y + f_Y , \quad (2)$$
$$\frac{d}{dt}\delta Z = X\delta Y + Y\delta X - b\delta Z + f_Z ,$$

in which f_X, f_Y, and f_Z are the derived Gaussian fluctuating forces.[7,26]

Equation (2) is coupled to Eq. (1) via the Jacobian matrix of coefficients, **J**, which depends explicitly on the time-dependent solution to Eq. (1):

$$\mathbf{J} = \begin{bmatrix} \frac{\partial dX/dt}{\partial X} & \frac{\partial dX/dt}{\partial Y} & \frac{\partial dX/dt}{\partial Z} \\ \frac{\partial dY/dt}{\partial X} & \frac{\partial dY/dt}{\partial Y} & \frac{\partial dY/dt}{\partial Z} \\ \frac{\partial dZ/dt}{\partial X} & \frac{\partial dZ/dt}{\partial Y} & \frac{\partial dZ/dt}{\partial Z} \end{bmatrix} = \begin{bmatrix} -\sigma & \sigma & 0 \\ r-Z & -1 & -X \\ Y & X & -b \end{bmatrix} . \quad (3)$$

It is well known[8,12] that the stochastic differential equations, Eq. (2), produce a nonstationary, Gaussian conditional probability distribution with vanishing mean and covariance matrix, **C**, defined by

$$\mathbf{C} = \begin{bmatrix} \langle\delta X\delta X\rangle & \langle\delta X\delta Y\rangle & \langle\delta X\delta Z\rangle \\ \langle\delta Y\delta X\rangle & \langle\delta Y\delta Y\rangle & \langle\delta Y\delta Z\rangle \\ \langle\delta Z\delta X\rangle & \langle\delta Z\delta Y\rangle & \langle\delta Z\delta Z\rangle \end{bmatrix} , \quad (4)$$

which solves the equation

$$\frac{d\mathbf{C}}{dt} = \mathbf{J}\mathbf{C} + \mathbf{C}\mathbf{J}^{\dagger} + \mathbf{\Gamma} \quad (5)$$

and in which $\mathbf{\Gamma}$ is the matrix of correlation coefficients for the fluctuating forces in Eq. (2). This matrix is completely determined by the fluctuation-dissipation relation for hydrodynamics and involves no free parameters.[26] Its explicit form will be given elsewhere,[24] but we note here that each coefficient is proportional to Boltzmann's constant. The solution of Eq. (5) is easily generated numerically[8,23] using the conditional average solution obtained from Eq. (1).

Note that there are two types of stochasticity here: deterministic stochasticity from the chaotic macrovariable dynamics [Eq. (1)], and molecular fluctuations coming from thermal motions [Eq. (2)]. This is typical of the thermodynamic limit[3-22] in that the thermal fluctuations "ride on the back" of the deterministic motion.

The solution for the covariance matrix is easily obtained using standard differential equation solvers with initial conditions on the chaotic attractor and a covariance matrix that initially vanishes. Figure 1 shows the results for the parameter values $\sigma = 10$, $b = \frac{8}{3}$, and $r = 28$, for which the Lorenz model is chaotic. The one-one element of the covariance matrix (δX-mode variance) is seen both to grow and to fluctuate wildly as it rides along the attractor. Comparable results are found for other matrix elements. Keizer and Tilden[23] previously conjectured that the covariance matrix grows exponentially on a chaotic attractor at twice the rate of the largest positive Lyapunov exponent. In fact, we have found a way to make this conjecture precise[24] using the trace norm, as illustrated by the plot in Fig. 2 of the logarithm of the square root of the trace of the covariance matrix squared. This smooths out the plot enormously, which after a few time units essentially increases linearly with the time. The slope of this linear plot is 1.84, which is precisely twice the largest positive Lyapunov exponent for the attractor as determined by standard methods.[27]

The exponential growth of fluctuations on the chaotic attractor has striking consequences. First, when the square root of a covariance becomes comparable to the size of the macroscopic variables, the deterministic equations lose their meaning. According to Fig. 2, this becomes the case at a scaled time of approximately 20. Using values of the density, viscosity, and aspect ratio typical for water and the Rayleigh-Bénard system, we estimate the actual time required for this to occur in the Lozenz model is about 40 min. This suggests that in hydrodynamic experiments on chaotic systems, the effect of fluctuations may be amplified to macroscopic size on an experimentally accessible time scale. Second, this result suggests that on this time scale the macroscopic, deterministic description for the hydrodynamic variables may break down. A detailed analytic account of this breakdown will appear elsewhere.[24]

The exponential divergence of the covariance matrix for dissipative macrovariable fluctuations on a chaotic attractor is a general property of the usual fluctuation theories in the thermodynamic limit.[8,12,24] In this limit, the macrovariables satisfy the usual kinetic equations [cf. Eq. (1)], and the covariance matrix for the fluctuations solves an equation with exactly the same form as

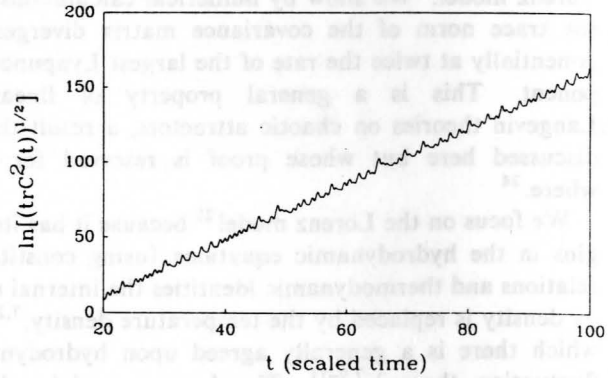

FIG. 2. The Lyapunov exponent is one-half of the slope, i.e., 0.92.

Eq. (5) where **J** is the Jacobian matrix for the macrovariable motion and Γ is the strength of the correlation coefficients for the Gaussian forces. For the coupled system of macrovariables and covariance matrix, it is not difficult to show, either numerically or analytically, that asymptotically in time, on a chaotic attractor, the covariance matrix grows at twice the rate of the largest Lyapunov exponent.[23,24] Specifically, we find that it is possible to define a Lyapunov exponent for the covariance matrix equation [Eq. (5)], denoted by λ_C, and we have proved the identity

$$\lambda_C = 2\lambda , \tag{6}$$

where λ is the Lyapunov exponent for the deterministic macrovariable equation. The proof of this identity follows from the fact that the Jacobi matrix not only determines the time evolution of the covariance matrix [Eq. (5)], but is also responsible for determining the Lyapunov exponent λ for the macrovariable equations.[27] Thus the observed behavior of the fluctuating Lorenz model in the thermodynamic limit is generic.

As a consequence, we expect that, (1) on the time scale of the inverse of the largest (positive) Lyapunov exponent, the average behavior will not be correctly given by the deterministic equations, and (2) on this time scale, molecular fluctuations are sufficiently amplified that a molecular-level description must be used instead of a purely macrovariable description.

It should be emphasized that these results refer only to macroscopic systems for which the dynamical processes are dissipative. For example, they do not apply to conservative Hamiltonian systems in which chaos is also well established. However, they seem relevant for chaotic dynamics in chemistry, as well as in various kinds of hydrodynamic systems. Finally, numerical calculations suggesting that turbulence involves a chaotic attractor make us suspect that a complete description of experimental turbulence will require more than just the Navier-Stokes equations; a more molecular-level description will be necessary.

This work was supported by National Science Foundation Grants No. PHY86-03729, No. 89-02549 (R.F.F.) and No. CHE86-18647 (J.E.K.) and the Institute of Theoretical Dynamics at the University of California, Davis.

[1]G. E. Uhlenbeck and G. W. Ford, *Lectures in Statistical Mechanics* (American Mathematical Society, Providence, RI, 1963).

[2]H. Mori, Prog. Theor. Phys. **33**, 423 (1965).

[3]P. Langevin, C. R. Acad. Sci. Paris **146**, 530 (1908).

[4]G. E. Uhlenbeck and L. S. Ornstein, Phys. Rev. **36**, 823 (1930).

[5]M. C. Wang and G. E. Uhlenbeck, Rev. Mod. Phys. **17**, 323 (1945).

[6]L. Onsager and S. Machlup, Phys. Rev. **91**, 1512 (1953).

[7]R. F. Fox and G. E. Uhlenbeck, Phys. Fluids **13**, 1893 (1970); **13**, 2881 (1970).

[8]J. E. Keizer, *Statistical Thermodynamics of Nonequilibrium Processes* (Springer-Verlag, New York, 1987).

[9]L. D. Landau and E. M. Lifshitz, *Fluid Mechanics* (Pergamon, London, 1959), Chap. XVII.

[10]B. J. Berne and R. Pecora, *Dynamic Light Scattering* (Wiley, New York, 1976).

[11]A. M. S. Tremblay, E. Siggia, and M. Arai, Phys. Rev. A **23**, 1451 (1981).

[12]N. C. van Kampen, *Stochastic Processes in Physics and Chemistry* (North-Holland, Amsterdam, 1981).

[13]T. R. Kirkpatrick, E. G. D. Cohen, and J. R. Dorfman, Phys. Rev. A **26**, 972 (1982); T. R. Kirkpatrick, Doctoral dissertation, Rockefeller University, 1981 (unpublished).

[14]A. Nordsieck, W. E. Lamb, and G. E. Uhlenbeck, Physica (Utrecht) **7**, 344 (1940).

[15]A. J. F. Siegert, Phys. Rev. **76**, 1708 (1949).

[16]H. P. McKean, J. Comb. Theory **2**, 358 (1967).

[17]J. Logan and M. Kac, Phys. Rev. A **13**, 458 (1976).

[18]D. A. McQuarrie, J. Appl. Prob. **4**, 413 (1967).

[19]T. G. Kurtz, J. Appl. Prob. **7**, 49 (1970); **8**, 344 (1971).

[20]N. G. van Kampen, Can. J. Phys. **39**, 551 (1961).

[21]R. Kubo, K. Matsuo, and K. Kitahara, J. Stat. Phys. **9**, 51 (1973).

[22]R. F. Fox, J. Chem. Phys. **70**, 4660 (1979).

[23]J. E. Keizer and J. Tilden, J. Chem. Phys. **93**, 2811 (1989).

[24]R. F. Fox, J. E. Keizer, and J. Tilden (to be published).

[25]A. J. Lichtenberg and M. A. Lieberman, *Regular and Stochastic Motion*, Applied Mathematical Sciences Vol. 38 (Springer-Verlag, New York, 1983), Sec. 7.4.

[26]R. F. Fox, Phys. Rep. **48**, 179 (1978).

[27]Lichtenberg and Lieberman, Ref. 25, Sec. 5.2b.

Chaos, molecular fluctuations, and the correspondence limit

Ronald F. Fox
School of Physics, Georgia Institute of Technology, Atlanta, Georgia 30332-0430
(Received 31 October 1989)

Chaos is characterized by sensitive dependence on initial conditions. Trajectories determined by coupled, ordinary differential equations show sensitive dependence when their associated Liapunov exponent is positive. The Liapunov exponent is positive if the Jacobi matrix associated with the coupled differential equations has an eigenvalue with a positive real part, on the average, as the Jacobi matrix evolves along the trajectory. For macrovariable equations, there are also fluctuation equations which follow the macrovariable trajectories. The covariance matrix for these fluctuations evolves according to an equation in which the Jacobi matrix for the deterministic motion plays the dominant role. For a chaotic trajectory, the covariance matrix grows exponentially. This means that for macrovariable equations that imply chaos, the construction of the macrovariable equations out of an underlying master equation is no longer valid. The macrovariable equations cease to be physical, and the physical description must be done entirely at the master equation level of description where the fluctuations, which are very large scale, can be properly treated. In parallel with this analysis, the correspondence limit connecting the time evolution of the Wigner distribution with Liouville's equation breaks down when the classical motion is strongly chaotic. This implies that strongly chaotic classical dynamics must be treated quantum mechanically in order to properly treat the quantum fluctuations which have grown macroscopically large. Experimental confirmation of these ideas is discussed.

I. WHAT IS CHAOS?

Consider a system of coupled, first-order differential equations of the form

$$\frac{d}{dt}x_i(t)=F_i(\mathbf{x}(t)) , \tag{1}$$

where $i=1,2,\ldots,N$ and $\mathbf{x}(t)$ denotes the N-dimensional vector with components x_i. The functions F_i are generally nonlinear. Because these equations are first order in the time derivative, initial conditions give rise to unique trajectories. Chaos is very sensitive dependence of the trajectory $\mathbf{x}(t)$ on the initial conditions.

This sensitive dependence can be made quantitative by introducing the concept of a Liapunov exponent.[1] First, consider the instantaneous, local linearization around the trajectory $\mathbf{x}(t)$. Let $\Delta\mathbf{x}$ denote a small deviation from $\mathbf{x}(t)$ at time t. For a short time, $\Delta\mathbf{x}$ evolves according to

$$\frac{d}{dt}\Delta x_i=J_{ik}\Delta x_k , \tag{2}$$

in which summation over k is implicit and J_{ik} is the Jacobi matrix defined by

$$J_{ik}=\frac{\partial F_i}{\partial x_k} . \tag{3}$$

The nonlinearity of the F_i's implies that J_{ik} is an explicit function of $\mathbf{x}(t)$. As the trajectory evolves in time, the matrix elements J_{ik} also evolve. At each instant of time, one may compute the eigenvalues of J_{ik}. If at least one eigenvalue has a positive real part, there is an instantaneous, local tendency for the magnitude of $\Delta\mathbf{x}$ to grow, along a direction corresponding to the associated eigenvector. As the trajectory evolves, and J_{ik} also evolves, such a tendency is averaged over the course of the trajectory and this leads to the definition of the Liapunov exponent.

Let

$$d(\mathbf{x}_0,t)=\|\Delta\mathbf{x}(\mathbf{x}_0,t)\| \tag{4}$$

be the length of the deviation vector at time t that started at $t=0$ from $\mathbf{x}=\mathbf{x}_0$. We have used the notation $\|\ \|$ for the Euclidean metric in an N-dimensional space. The Liapunov exponent λ is defined by[1]

$$\lambda=\lim_{\substack{t\to\infty \\ d(\mathbf{x}_0,0)\to 0}}\frac{1}{t}\ln\left[\frac{d(\mathbf{x}_0,t)}{d(\mathbf{x}_0,0)}\right] . \tag{5}$$

If $\lambda>0$, then initially close trajectories exponentiate apart with an initial rate λ. This is what is meant by sensitive dependence on initial conditions. If (1) describes a dissipative dynamics and parameters are chosen so that trajectories approach a globally stable attracting fixed point, then $\lambda<0$. If a limit cycle is the attractor, then $\lambda=0$. But if the attractor is that for a chaotic trajectory (dissipative or Hamiltonian dynamics), then $\lambda>0$.

There is another representation of the dynamics in (1) which will prove useful below. We may describe the dynamics in (1) by a conserved probability flow for the probability distribution $P(\mathbf{x},t)$:

$$\frac{\partial}{\partial t}P(\mathbf{x},t)=-\frac{\partial}{\partial x_j}[F_j(\mathbf{x})P(\mathbf{x},t)] , \tag{6}$$

with the initial condition $P(\mathbf{x},0)=\delta(\mathbf{x}-\mathbf{x}_0)$. Equation (6)

is simply the continuity equation for a conserved probability flow with probability flux $\mathbf{F}P$. Since it is first order on both the left- and right-hand sides, it is straightforward to prove that it has the solution

$$P(\mathbf{x},t)=\delta(\mathbf{x}-\mathbf{x}(t)) , \tag{7}$$

where $\mathbf{x}(t)$ is the solution to Eq. (1). Clearly, if we multiply (6) by x_i and integrate over $d^N x$ we get

$$\frac{d}{dt}\langle x_i\rangle=\langle F_i(\mathbf{x})\rangle , \tag{8}$$

where $\langle\ \rangle$ denotes averaging with respect to $P(\mathbf{x},t)$. Since (7) holds, Eqs. (1) and (8) are identical. Because this probability distribution remains a Dirac δ function for all times, it describes a deterministic motion with no fluctuation whatsoever around the deterministic trajectories implied by (1).

We remark in passing that, although (6) is a linear equation in P, it nevertheless describes chaos. Whenever the $\mathbf{x}(t)$ trajectory is chaotic, the P distribution simply follows the $\mathbf{x}(t)$ trajectory, and also exhibits chaos. One may think of (6) as an example of Liouville's equation, the name we use for it below.

The key points developed here are that the magnitude of the Liapunov exponent is determined by the time-evolving Jacobi matrix, and that Liouville's equation provides a description of the dynamics equivalent to (1) when its solution is the Dirac δ function solution that follows the trajectory. In the following sections of this paper, we will return to these key points for the discussions of both molecular fluctuations and the correspondence limit.

II. MOLECULAR FLUCTUATIONS

Macrovariable equations are phenomenological descriptions of physical or chemical phenomena at the macroscopic level rather than many-particle descriptions at the fundamental microscopic level. We briefly discuss two examples below: hydrodynamics and chemical reactions.

The hydrodynamic equations are[2]

$$\frac{\partial}{\partial t}\rho=-\nabla\cdot(\rho\mathbf{u}) , \tag{9}$$

$$\rho\left[\frac{\partial}{\partial t}u_\alpha+\mathbf{u}\cdot\nabla u_\alpha\right]=-\frac{\partial}{\partial x_\beta}P_{\alpha\beta} , \tag{10}$$

$$\rho\left[\frac{\partial}{\partial t}\varepsilon+\mathbf{u}\cdot\nabla\varepsilon\right]=-\nabla\cdot\mathbf{q}-P_{\alpha\beta}D_{\alpha\beta} , \tag{11}$$

in which ρ is the mass density, $\mathbf{u}$ is the velocity field, ε is the energy field per unit mass, $P_{\alpha\beta}$ is the stress tensor, $\mathbf{q}$ is the heat flux, and $D_{\alpha\beta}$ is the strain tensor. In this form, these equations represent conservation of mass, momentum, and energy, respectively. They do not constitute a closed description,[3] however, because the quantities on the right-hand side, such as $P_{\alpha\beta}$ and $\mathbf{q}$, are not expressed solely in terms of the quantities of the left-hand side. This can be remedied by introducing the constitutive relations and equations of state which then produce a well-posed mathematical description. Usually, one ends up with a closed description in the quantities ρ, $\mathbf{u}$, and T where T is the temperature field. Because these quantities represent macroscopic amounts of matter, they have associated with them molecular fluctuations.[4,5] For example, in the description of the hydrodynamics of water, ρ, $\mathbf{u}$, and T may refer to the quantities found for a cubic micrometer of water (this is a "macroscopic" amount) which contains $\sim 10^{11}$ water molecules. From the macroscopic viewpoint, the cubic micrometer is thought of as a point, but there will be molecular fluctuations associated with ρ, $\mathbf{u}$, and T. The theory for these fluctuations is well worked out and is used to compute light scattering profiles that have been repeatedly confirmed with measurements.[6]

A bimolecular reaction

$$A+B\underset{k_b}{\overset{k_f}{\rightleftarrows}}C+D \tag{12}$$

is described by the mass action equation[7]

$$\frac{d}{dt}\xi=k_f C_A C_B-k_b C_C C_D , \tag{13}$$

in which C_A, etc. are the concentrations of the various chemical species and ξ is the reaction progress variable. C_A is the concentration of species A in the total volume of the reaction and no spatial variations are contemplated. This situation is realized from a macroscopic viewpoint in a "continuously stirred tank reactor." Nevertheless, chemicals are molecules and each concentration has associated with it a molecular fluctuation. Once again, the theory for such fluctuations is well established.[7–9]

A rather general theoretical approach has been developed to deepen our understanding of how fundamental microscopic dynamics gives rise to macroscopic, deterministic equations and their associated molecular fluctuation equations. This is the master equation approach.[8,10] In essence, it is a mesoscopic description of dynamics, intermediate between the truly microscopic, many-particle dynamics and the macroscopic phenomenology. For mass action chemical reactions, the McQuarrie master equation[8] is very well established.[9] For dilute gas hydrodynamics, Boltzmann's equation serves the role of the master equation,[3,5] and for moderately dense gases the Boltzmann-Enskog equation does likewise.[11,12] For liquids, however, no master equation or equivalent is widely accepted, so that one of the upshots of the proposals to be enunciated below will be establishing such a master equation construct for hydrodynamics in order to use it to test other of our proposals. Modern kinetic theory may have already taken us a long way towards this particular goal.

All master equations may be put into the form[10]

$$\frac{\partial}{\partial t}P(\mathbf{c},t)=\int d^N c'[W(\mathbf{c},\mathbf{c}')P(\mathbf{c}',t) -W(\mathbf{c}',\mathbf{c})P(\mathbf{c},t)] , \tag{14}$$

in which $\mathbf{c}$ and $\mathbf{c}'$ denote the macrovariables, $P(\mathbf{c},t)$ is the probability distribution for the macrovariables at time t, and $W(\mathbf{c},\mathbf{c}')$ is the transition distribution for changes in

the macrovariables. $W(\mathbf{c},\mathbf{c}')$ determines how much $\mathbf{c}'$ changes in an infinitesimal time interval, Δt. Normally, this change is by a molecular amount, but at a macroscopic rate. This means the following. Let Ω characterize the macroscopic size of the system (e.g., Ω could be the total volume). Normally, W causes a change in $\mathbf{c}'$ components of size $1/\Omega$ at a rate $\sim\Omega$. We may make this quantitative by looking at the moments of W:

$$K_i^{(1)}(\mathbf{c})=\int d^N c'(c_i'-c_i)W(\mathbf{c}',\mathbf{c}) , \tag{15}$$

$$K_{ij}^{(2)}(\mathbf{c})=\int d^N c'(c_i'-c_i)(\mathbf{c}_j'-\mathbf{c}_j)W(\mathbf{c}'\mathbf{c}) , \tag{16}$$

$$\vdots$$

$$K_{i_1 i_2 \cdots i_p}^{(p)}(\mathbf{c})=\int d^N c' \prod_{j=1}^{p}(c_{i_j}'-c_{i_j})W(\mathbf{c}',\mathbf{c}) . \tag{17}$$

The preceding remarks imply that for large Ω, $K^{(p)}\sim\Omega^{-(p-1)}$. In addition, it may be shown that the master equation (14) is equivalent to the Kramers-Moyal[13–15] partial differential equation

$$\frac{\partial}{\partial t}P=-\frac{\partial}{\partial c_i}(K_i^{(1)}P)+\frac{1}{2}\frac{\partial^2}{\partial c_i \partial c_j}(K_{ij}^{(2)}P)+\cdots + \frac{(-1)^p}{p!}\prod_{j=1}^{p}\frac{\partial}{\partial c_{i_j}}(K_{i_1 i_2 \cdots i_p}^{(p)}P)+\cdots . \tag{18}$$

We are now in a position to take the "macroscopic limit," i.e., $\Omega\to\infty$. The result is the first-order Liouville equation:[15–17]

$$\frac{\partial}{\partial t}P_\infty=-\frac{\partial}{\partial c_i}(K_i^{(1)\infty}P_\infty) . \tag{19}$$

This equation has the Dirac δ solution

$$P_\infty(\mathbf{c},t)=\delta(\mathbf{c}-\mathbf{c}(t)) , \tag{20}$$

where $\mathbf{c}(t)$ solves the equation

$$\frac{d}{dt}c_i(t)=K_i^{(1)\infty}(\mathbf{c}(t)) . \tag{21}$$

Clearly, if we multiply (19) by c_j and integrate over $d^N c$, we get

$$\frac{d}{dt}\langle c_i\rangle=\langle K_i^{(1)\infty}(\mathbf{c})\rangle , \tag{22}$$

where $\langle\ \rangle$ denotes averaging with respect to P_∞. Since (20) holds, Eqs. (21) and (22) are identical. Thus the macroscopic limit yields a deterministic, macrovariable equation. In constructing the master equation for a particular macrovariable dynamics, the goal is to have (21) be identical with the original macrovariable dynamics. Mathematically, there are many W's which can do this, and which one is correct must be decided by the mesoscopic physics underlying the macrovariable equation.

We can also obtain the fluctuations around the deterministic dynamics in (21) by further analysis of the Kramers-Moyal equation (18).[10,15,17] We introduce the scaled deviations $\boldsymbol{\mu}$ (fluctuations) from the deterministic motion $\mathbf{c}(t)$ defined by

$$c_i=c_i(t)+\Omega^{-1/2}\mu_i . \tag{23}$$

Using (21) and replacing $\mathbf{c}$ in (18) by (23) and then Taylor-expanding all functions with respect to $\boldsymbol{\mu}$, yields and equation for the distribution of the fluctuations, $\phi(\boldsymbol{\mu},t)$:

$$\frac{\partial}{\partial t}\phi(\boldsymbol{\mu},t)=-\frac{\partial}{\partial\mu_i}\left[\frac{\partial}{\partial c_j}K_i^{(1)\infty}(\mathbf{c}(t))\mu_j\phi(\boldsymbol{\mu},t)\right] +\frac{1}{2}\frac{\partial^2}{\partial\mu_i\partial\mu_j}R_{ij}^{(2)}(\mathbf{c}(t))\phi(\boldsymbol{\mu},t) , \tag{24}$$

in which $R^{(2)}$ is defined by

$$R_{ij}^{(2)}=\lim_{\Omega\to\infty}\Omega K_{ij}^{(2)}(\mathbf{c}(t)) . \tag{25}$$

Both $K^{(1)\infty}$ and $R^{(2)}$ depend on the determination trajectory, $\mathbf{c}(t)$, determined by (21). In fact, the coefficients of the μ terms in the first part of the right-hand side of (24) (the "streaming term") are precisely the Jacobi matrix for (21):

$$J_{ij}=\frac{\partial K_i^{(1)\infty}}{\partial c_j} . \tag{26}$$

Introduce the covariance matrix C_{ij} defined by

$$C_{ij}=\langle\mu_i\mu_j\rangle , \tag{27}$$

in which $\langle\ \rangle$ now denotes averaging with respect to $\phi(\boldsymbol{\mu},t)$. Equation (24) may be used to prove that C_{ij} satisfies the equation[7]

$$\frac{d}{dt}C_{ij}=J_{ik}C_{kj}+C_{ik}J_{jk}+R_{ij}^{(2)} . \tag{28}$$

Thus, not only does J_{ij} govern the determination of the Liapunov exponent for the deterministic macrovariable equation (21), but it also governs the evolution of the fluctuation covariance matrix through Eq. (28). J_{ij} inherits time dependence from (21) through its explicit dependence on $\mathbf{c}(t)$.

Normally, the dynamics begins with some precise initial state, $\mathbf{c}(0)$ and no initial covariances, $C_{ij}(0)=0$. The $R_{ij}^{(2)}$ term in (28) drives the growth of a nonzero C_{ij}.

Keizer and Tilden[18] studied the growth of C_{ij} for simple limit cycles and for chaotic trajectories generated by the Rossler model.[19] Their numerical studies showed that for a chaotic trajectory, C_{ij} grew exponentially at a rate that appeared to be twice the Liapunov exponent for that trajectory. We have recently proved that this observation is not an accident.[20]

Equation (28) may be considered to be an equation for the evolution of the "vector" C_{ij}. Consider the metric for this space defined by

$$\|C\|=(\mathrm{tr}C^2)^{1/2} . \tag{29}$$

The corresponding Liapunov exponent λ_C is defined by

$$\lambda_C=\lim_{\substack{t\to\infty \\ \mathrm{tr}C^2(0)\to 0}}\frac{1}{t}\ln\left[\frac{[\mathrm{tr}C^2(t)]^{1/2}}{[\mathrm{tr}C^2(0)]^{1/2}}\right] . \tag{30}$$

On account of the common role of J_{ij} for both λ and λ_C, we were able to prove[20]

$$\lambda_C = 2\lambda \ , \tag{31}$$

in which λ is the Liapunov exponent for the dynamics given in (21), and for which λ is defined as in (5).

Before proceeding to the radical consequences of the exponential growth of the covariance matrix for a chaotic macrovariable trajectory, it is important to emphasize the two distinct ways in which we use Eq. (28). For nonchaotic trajectories, that approach stable steady states, the covariance matrix elments remain very small [of order unity for the scaling in (23), which means that the unscaled covariance matrix elements are of order $1/\Omega$], and represent the physically real fluctuations "carried on the back" of the deterministic motion.[7] However, for the chaotic trajectories, for which the covariance matrix elements diverge exponentially, we no longer view them as physically correct since they ultimately grow much too large, and because their origin is in Eq. (24), which followed from (18), provided they are *not* too large. Nevertheless, we have found that Eq. (28) may be used as a purely mathematical device for computing the Liapunov exponent. Thus we have used it to compute Liapunov exponents for the Rossler and Lorenz models[21] and have obtained three-decimal-place agreement with standard methods.[1] Moreover, when (28) implies that the covariance matrix elements diverge for a chaotic trajectory, the real physical fluctuations do indeed grow very large. While (28) is not an accurate way to handle large physical fluctuations, the underlying master equation (14) still is. Therefore we use (28) to compute λ, but we revert to (14) to do the physical treatment of the dynamics.

The radical consequence of chaos for the macrovariable dynamics is that the justification for the macrovariable equation (21) from the underlying master equation (14) breaks down. The reason for this breakdown is that the Dirac δ function solution to (19) given in (20) is not a stable solution to (19). The slightest bit of width added to the Dirac δ distribution leads to exponentially growing covariance matrix elements. Thus any initial distribution other than $P_\infty(\mathbf{c},0)=\delta(\mathbf{c}-\mathbf{c}(0))$ will not evolve like the expression in (20). Consequently, (22) will not reduce to (21) since the average of nonlinear terms such as $\langle K_i^{(1)\infty}(\mathbf{c})\rangle$ does not reduce to the nonlinear functions of the averages $K_i^{(1)\infty}(\langle \mathbf{c} \rangle)$. Simply put, the contraction of the master equation into a deterministic macrovariable equation does not occur. A proper description of the dynamics and its associated, large scale fluctuations must be done at the mesoscopic level of the master equation.

There are several picturesque ways of expressing this result for more specific situations. For example, when the Navier-Stokes equations (hydrodynamics) predict chaos (numerically[22] they are certainly able to do so), the Navier-Stokes equations are no longer valid; or, you cannot get a theory of turbulence from Navier-Stokes alone. Similarly, when the mass action chemical reaction equations imply chaos (numerically), these equations are physically invalid.

There is an important provision to this conclusion and each of its particular realizations. The invalidity of the Dirac δ function solution to (19) which is at the core of our results reflects its instability with respect to any sort of initial probability distribution width. Nevertheless, if the initial width is very small and the Liapunov exponent for the chaotic trajectory is also very small, the instability may take a very long time to manifest itself. Thus the Dirac δ function solution may prove to be a very good approximation over a time interval which is longer than the time taken to do the associated experiment. For example, one may say that Navier-Stokes will work well, for a while, in the case of "weak" turbulence. Clearly, for any given situation, one must determine the Liapunov exponent and size of the initial width in the distribution [this is determined by $R^{(2)}(0)$], in order to decide whether or not to discard the macrovariable equations in favor of the master equation.

Detailed accounts of these phenomena for the Rossler model, the Lorenz model,[23] and the periodically driven Brussellator[24] (a particular chemical reaction with a cubic nonlinearity) may be found in a forthcoming paper coauthored with Keizer, Tilden, and Fox.[20]

III. THE CORRESPONDENCE LIMIT

In Sec. I we showed that there are two equivalent ways to describe the time evolution of an N variable dynamical system. Either N coupled first order, ordinary differential equations are used to determine the unique N variable trajectories, or an $N+1$ variable (N x_i's and t) partial differential equation, the Liouville equation for the conserved probability, is used to obtain a Dirac δ function solution that follows precisely the N variable trajectory. In classical mechanics, these two alternatives also exist, although now we have $2N$ coupled, ordinary differential equations for N coordinates and their N conjugate momenta, or a $2N+1$ variable partial differential equation, Liouville's equation. A quite general treatment of the correspondence limit for the relationship between quantum mechanics and classical mechanics can be developed if we focus on the Liouville equation.

In 1932, Wigner published a paper[25] aimed at obtaining quantum corrections to formulas for thermodynamic equilibrium. In doing so, he formulated a quantum-mechanical generalization of Liouville's equation that becomes Liouville's equation in the correspondence limit (i.e., as $\hbar \to 0$). The remarkable feature of this correspondence limit which we will exploit here is that it is formally isomorphic to the connection between the master equation and the macrovariable equations, specifically to the connection between (18) and (19). Moreover, by applying the same procedure[10,15,17] to get from (18) to (24), we can also obtain an equation for the fluctuations associated with the Wigner-Liouville connection. Throughout this presentation the role of Ω^{-1} is played by $\hbar$, and naturally $\Omega \to \infty$ corresponds with $\hbar \to 0$. The consequences of these considerations for the correspondence limit when the classical dynamics is strongly chaotic are radical.

Consider the Hamiltonian

$$H = \sum_{k=1}^{n} \frac{p_k^2}{2m_k} + V(x_1 x_2 \cdots x_n) \ . \tag{32}$$

The Wigner distribution for this n-coordinated system is defined[25] by

$$W(x_1\cdots x_n p_1\cdots p_n)=\left[\frac{1}{\pi\hbar}\right]^n\int\cdots\int dy_1\cdots dy_n\psi^*(x_1+y_1\cdots x_n+y_n)\psi(x_1-y_1\cdots x_n-y_n)$$
$$\times\exp\left[2\frac{i}{\hbar}(p_1y_1+\cdots+p_ny_n)\right], \tag{33}$$

in which the p_i's are ordinary parameters rather than differential operators as in the quantum interpretation of (32). W is not a probability distribution because it is sometimes negative. However, both of its reduced distributions are the correct probability distributions,[25] as is easily proved: $\int\cdots\int dp_1\cdots dp_n W$ is the probability distribution for the x_i's and $\int\cdots\int dx_1\cdots dx_n W$ is the probability distribution for the p_i's. Wigner showed[25] that the time evolution of W is given by

$$\frac{\partial}{\partial t}W=-\frac{p_k}{m_k}\frac{\partial}{\partial x_k}W+\left[\frac{\partial}{\partial x_k}V\right]\frac{\partial}{\partial p_k}W+\sum_{\substack{\lambda_1+\cdots+\lambda_n\\ \text{odd}}}\left[\frac{\partial^{\lambda_1+\cdots+\lambda_n}}{\partial_{x_1}^{\lambda_1}\cdots\partial_{x_n}^{\lambda_n}}V\right]\frac{\left[\frac{\hbar}{2i}\right]^{\lambda_1+\cdots+\lambda_n-1}}{\lambda_1!\cdots\lambda_n!}\frac{\partial^{\lambda_1+\cdots+\lambda_n}}{\partial_{p_1}^{\lambda_1}\cdots\partial_{p_n}^{\lambda_n}}W, \tag{34}$$

in which the second line is a summation over all $\lambda_1+\cdots+\lambda_n$ that are odd. The remarkable features of this equation are that the $\hbar$-independent terms are identical with Liouville's equation for Hamiltonian (32) treated classically, and the remaining terms are at least of order $\hbar^2$ and contain at least the third derivative of the potential, V. This is the equation that parallels the Kramers-Moyal equation (18) with $\hbar$ in the role of Ω^{-1}. Clearly, all that remains, if $\hbar\to 0$, is the classical Liouville equation, that parallels Eq. (19). It has a Dirac δ function solution that follows the solution to Hamilton's equations of motion:

$$\frac{d}{dt}x_i(t)=\frac{p_i(t)}{m_i}, \tag{35}$$

$$\frac{d}{dt}p_i(t)=-\frac{\partial}{\partial x_i}V(x_1(t)\cdots x_n(t)). \tag{36}$$

In parallel with our treatment of macrovariable fluctuations, Eq. (34) may be analyzed[10,15,17] to determine the quantum fluctuations attending the classical motion. We introduce the scaled deviations, μ_i and q_i, (fluctuations) from the classical motion, $x_i(t)$ and $p_i(t)$, defined by

$$x_i=x_i(t)+\hbar^{1/2}\mu_i, \tag{37}$$

$$p_i=p_i(t)+\hbar^{1/2}q_i. \tag{38}$$

Replacing x_i and p_i in (34) by (37) and (38), and Taylor-expanding V with respect to the μ_i's eventually yields an equation for the distribution of the fluctuations, $\phi(\boldsymbol{\mu},\mathbf{q},t)$:

$$\frac{\partial}{\partial t}\phi(\boldsymbol{\mu},\mathbf{q},t)=-\frac{q_k}{m_k}\frac{\partial}{\partial\mu_k}\phi(\boldsymbol{\mu},\mathbf{q},t)+\left[\frac{\partial^2}{\partial x_j\partial x_k}V\right]\mu_j\frac{\partial}{\partial q_k}\phi(\boldsymbol{\mu},\mathbf{q},t)+O(h^{1/2}). \tag{39}$$

In order to satisfy Heisenberg's uncertainty principle, this equation must have the initial distribution (for minimum uncertainty) given by

$$\phi(\boldsymbol{\mu},\mathbf{q},t)=\prod_{j=1}^{n}\frac{1}{4\pi}\exp\left[-\frac{\mu_j^2}{2\sigma^2}-2\sigma^2q_j^2\right] \tag{40}$$

so that

$$[\langle(\Delta\mu_i)^2\rangle]^{1/2}[\langle(\Delta q_i)^2\rangle]^{1/2}=\sigma\frac{1}{2\sigma}=\frac{1}{2}, \tag{41}$$

which is the scaled version [see (37) and (38)] of the Heisenberg uncertainty requirement. Notice that, unlike (24), Eq. (39) contains no second-order derivatives in μ_i's or q_i's, i.e., no terms like the $R^{(2)}$ terms in (24). This fact reflects the intrinsic difference between macrovariable equations described by either (1) or (14) which are *dissipative*, and Hamiltonian equations described by either (34) or (35) and (36) which are *conservative*. The diffusive $R^{(2)}$ term in (24) also shows up in the covariance equation (28). We will now turn to the analog of (28) for the present case.

Let z_i for $i=1,2,\ldots,2n$ be defined by

$$z_1=x_i,\quad i=1,2,\ldots,n \tag{42}$$

and

$$z_i=p_{i-n},\quad i=n+1,n+2,\ldots,2n. \tag{43}$$

Hamilton's equations (35) and (36) may be written in the form

$$\dot{x}_i=\frac{\partial H}{\partial p_i}, \tag{44}$$

$$\dot{p}_i=-\frac{\partial H}{\partial x_i}. \tag{45}$$

Let the $2n\times 2n$ matrix $\underline{I}$ be defined by

$$\underline{I}=\begin{bmatrix}\underline{0} & \underline{E}\\ -\underline{E} & \underline{0}\end{bmatrix}, \tag{46}$$

in which $\underline{0}$ is the $n\times n$ zero matrix and $\underline{E}$ is the $n\times n$ identity matrix. With $\underline{I}$, Eqs. (44) and (45) may be rewritten in the form

$$\dot{z}_i = I_{ij}\frac{\partial H}{\partial z_j} . \tag{47}$$

(I_{ij} reflects the so-called symplectic structure[26] of Hamiltonian dynamics.) The Jacobi matrix J_{ij} for this dynamics is just

$$J_{ij} = I_{ik}\frac{\partial^2 H}{\partial z_j \partial z_k} , \tag{48}$$

a $2n\times 2n$ matrix. Now, let η_i be defined by

$$z_i = z_i(t) + \hbar^{1/2}\eta_i , \tag{49}$$

i.e.,

$$\eta_i = \mu_i, \quad i = 1,2,\ldots,n \tag{50}$$

$$\eta_i = q_{i-n}, \quad i = n+1, n+2, \ldots, 2n . \tag{51}$$

Therefore (39) becomes

$$\frac{\partial}{\partial t}\phi(\eta,t) = -J_{ij}\eta_i\frac{\partial}{\partial \eta_j}\phi(\eta,t) , \tag{52}$$

which has precisely the same form as the streaming term in (24).

Let the covariance matrix C_{ij} be defined by

$$C_{ij} = \langle \eta_i \eta_j \rangle , \tag{53}$$

in which $\langle\ \rangle$ defined averaging with respect to $\phi(\eta,t)$. Equation (52) implies

$$\frac{d}{dt}C_{ij} = J_{ik}C_{kj} + C_{ik}J_{jk} \tag{54}$$

and (40) implies the initial conditions for C_{ij} given by

$$C_{ij} = \sigma^2\delta_{ij}, \quad i,j = 1,2,\ldots,n \tag{55}$$

$$C_{ij} = \frac{1}{4\sigma^2}\delta_{ij}, \quad i,j = n+1, n+2, \ldots, 2n \tag{56}$$

$$C_{ij} = 0 \quad \text{otherwise} . \tag{57}$$

This differs from (28) since there is no $R^{(2)}$ inhomogeneity. However, for (28) the initial condition on the covariance matrix was that it vanished, and $R^{(2)}$ causes it to become nonzero, reflecting the underlying fluctuation-dissipation relation.[5,7,15] In (54), there is no $R^{(2)}$ term because the underlying dynamics is conservative, but Heisenberg's uncertainty principle requires the initial C_{ij} to be nonzero. Nevertheless, just as with (28), this equation has a Liapunov exponent defined by (30) and satisfying identity (31) where this time λ is the largest positive Liapunov exponent implied by the classical dynamics (47) and governed by the Jacobi matrix (48). This, of course, means that if the classical trajectory is chaotic ($\lambda > 0$), then the covariance matrix will diverge, or, in other words, the quantum fluctuations become macroscopically large.

The correspondence limit applies when a classical-mechanical motion is described using the underlying quantum mechanics. The correspondence limit is verified when one shows that the quantum-mechanical treatment yields the classical motion plus ignorable quantum corrections. As we have shown above, a minimum uncertainty distribution can be chosen so that the coordinates have a very small quantum variance, i.e., σ may be taken to be very small. However, this implies that the covariance for the conjugate momenta goes like $1/2\sigma$. If the expectation values for the momenta are "classical," then it is still possible to have the variances $1/2\sigma$ be very small *compared* to the expectations. This is the essence of the classical correspondence limit for the quantum dynamics. (We may also consider the situation in which the roles of coordinates and momenta are reversed.) Using the Wigner distribution, we see that these conditions translate into Liouville's equation, the classical limit of (34), along with an initial distribution which is essentially a Dirac δ function, since its scaled representation is governed by the initial distribution for (39), i.e., (40), which is as narrow as one would like in both the coordinates (σ) and the conjugate momenta ($1/2\sigma$/momenta expectation value). As long as (39), or equivalently (54), implies that the covariances do not grow large, compared to the expectation values, this classical limit, the "correspondence" limit, is maintained. But chaos in the classical notion clearly invalidates this correspondence because the Jacobi matrix for the classical motion governs the growth of quantum fluctuations through Eq. (54) and creates a positive Liapunov exponent for the classical motion as well as for the covariance matrix equation. Thus, when the classical motion is chaotic, Liouville's equation does not have a Dirac δ function solution for all time. Its solution is not equivalent to Hamilton's equations of motion since averaging over its non-Dirac δ function solution will not reproduce Hamilton's equations [cf. (21) and (22)]. One must not attempt to contract the Wigner equation description in such a case. This means one must simply stay with the original Schrödinger equation for the entire description.

Even though the Schrödinger probability distribution can be made initially to be as sharp as one would like around the initial classical variables, strong chaos makes it grow broad rapidly. These remarks are entirely parallel to our earlier remarks regarding the master equation and the macrovariable equations and chaos. This also means there is an identical proviso, i.e., the need to use quantum mechanics for the description of a chaotic classical-mechanical motion depends on the initial size of the quantum fluctuations ($\hbar$ and σ) and on the size of λ. It is sometimes possible that the quantum fluctuations will not become too large to ignore on the time scale of the computation or experiment involved. One will need to ascertain by simulation whether or not chaos forces the abandonment of the classical description. Surely, chaotic classical motion in the Solar System[27] is an example where the quantum fluctuations may safely be ignored even on an "astronomical" time scale. For more down to Earth examples, the possibility of macroscopically large quantum fluctuations in an otherwise classical system is now seen to be a very real possibility. In parallel with our earlier picturesque statements for macrovariable

chaos, one may say that to properly describe classical-mechanical chaos, one must do quantum mechanics.

In a companion paper,[28] a detailed account of how the correspondence principle works for the nonchaotic or very weakly chaotic classical case, and then fails for the strongly chaotic case, is given for the periodically kicked pendulum. We have used extensive numerical computation to study the rapid growth of quantum fluctuations in this example when the classical dynamics is strongly chaotic.

IV. EXPERIMENTAL CONFIRMATION

There are two specific examples that may readily lead to experimental testing which we will now discuss. One is a macrovariable problem: hydrodynamic turbulence; and the other is an essentially quantum-classical correspondence problem: the laser. Our initial remarks apply to both cases.

There does not appear to be any reason to have to invent new kinds of experiments to test the ideas in this paper. Experimenters already use a statistical approach to these types of problems. There are a wide variety of techniques for measuring moments of variables, entire distribution functions, correlation functions and their power spectra, for doing light scattering, etc. With either a hydrodynamics paradigm or a laser paradigm, there is a set of deterministic equations which are used to model the physical system. These equations are usually deemed appropriate on the basis of equilibrium or steady-state measurements and computations. By obtaining parameter settings that make the solutions to the equations chaotic, the experimenter can attempt to arrange his apparatus settings to mimic the mathematical chaos. In reality, there are various sources of noise that make this comparison difficult. However, noise terms may be added to the equations used as a model and the influences of these noise terms can then be deduced by numerical simulation.[29] The basic point is that the predicted statistics for deterministic equations which include various noise terms (additive and/or multiplicative) are different from the predictions based upon an underlying master equation (or the underlying quantum mechanics). For example, if we add Gaussian fluctuations to Eq. (1), a Fokker-Planck equation can be derived in which the streaming term is governed by the F_i's. However, for chaos, if we take the view expressed in this paper, we must instead use the master equation underlying (1), and since (1) is no longer a valid contraction, the F_i's do not appear anywhere in this alternative description. We clearly get two distinct predictions.

Hydrodynamics presents an extra difficulty to which we alluded in Sec. II. There is as yet no accepted underlying master equation. This can probably be attributed to a combination of the intrinsic difficulty in obtaining one and, till now, not having any compelling reason to construct one.[7,30] Nevertheless, the Navier-Stokes equations produce numerical chaos,[22] and to date no one has been able to claim quantitative agreement between numerical work and physical measurements. The situation is very much better for nonchaotic hydrodynamic states created in the Benard system and in the Taylor-Couette system.[31] The agreement between Navier-Stokes and measurements is then excellent.

The laser problem not only involves the quantum-classical correspondence but also has the character of a macrovariable problem. This is a consequence of using a few, highly contracted, variables to treat the laser, rather than the full density matrix.[32] By now, it is very evident that these equations do not adequately model the behavior of real lasers when the lasers are operated under conditions which the laser equations predict lead to strong chaos.[33] Clearly, one should attempt to do a much better mesoscopic, or even full density matrix, modeling job. The quantum fluctuations have become so large that the contraction down to simple semiclassical equations in terms of intensities and molecular state populations is invalid. Nevertheless, the measurements already undertaken are probably adequate to test these ideas; it is the correct mesoscopic description and treatment which is presently lacking.

Another experimental paradigm for the study of large quantum fluctuations may be the Josephson junction. Its behavior can be treated as a periodically modulated damped pendulum.[34] The Wigner-Liouville correspondence analysis of Sec. III is easily applied to this concrete case in the undamped case. The damping may present an unfortunate difficulty, however.

ACKNOWLEDGMENTS

This work was supported by National Science Foundation Grant No. PHY-8902549. Part of this work was done at the Institute for Theoretical Dynamics at the University of California at Davis, in close collaboration with Joel Keizer. The correspondence limit work has been done in part with B. L. Lan, and has benefited from numerous discussions with Joseph Ford.

[1] A. J. Lichtenberg and M. A. Lieberman, *Regular and Stochastic Motion* (Springer-Verlag, New York, 1983), Sec. 5.2b.

[2] L. D. Landau and E. M. Lifshitz, *Fluid Mechanics* (Pergamon, London, 1959).

[3] G. E. Uhlenbeck and G. W. Ford, *Lectures in Statistical Mechanics* (American Mathematical Society, Providence, RI, 1963), Chap. VII.

[4] D. Forster, *Hydrodynamic Fluctuations, Broken Symmetry, and Correlation Functions* (Benjamin/Cummings, Reading, MA, 1975).

[5] R. F. Fox and G. E. Uhlenbeck, Phys. Fluids **13**, 1893 (1970); **13**, 2881 (1970).

[6] B. J. Berne and R. Pecora, *Dynamic Light Scattering* (Wiley, New York, 1976).

[7] J. E. Keizer, *Statistical Thermodynamics of Nonequilibrium Processes* (Springer-Verlag, New York, 1987).

[8] D. A. McQuarrie, J. Appl. Prob. **4**, 413 (1967).

[9] T. G. Kurtz, J. Appl. Prob. **7**, 49 (1970); **8**, 344 (1971).

[10]N. G. van Kampen, *Stochastic Processes in Physics and Chemistry* (North-Holland, Amsterdam, 1981), Chap. V.
[11]R. Balescu, *Equilibrium and Nonequilibrium Statistical Mechanics* (Wiley, New York, 1975), Sec. 20.4.
[12]J. A. McLennon, *Introduction to Nonequilibrium Statistical Mechanics* (Prentice Hall, Englewood Cliffs, NJ, 1989), Chap. 7.
[13]H. A. Kramers, Physica **7**, 284 (1940).
[14]J. E. Moyal, J. R. Stat. Soc. B **11**, 150 (1949).
[15]R. F. Fox, Phys. Rep. **48**, 179 (1978), Sec. I.5.
[16]N. G. van Kampen, Can. J. Phys. **39**, 551 (1961).
[17]R. Kubo, K. Matsuo, and K. Kitahara, J. Stat. Phys. **9**, 51 (1973).
[18]J. E. Keizer and J. Tilden, J. Chem. Phys. **93**, 2811 (1989).
[19]A. J. Lichtenberg and M. A. Lieberman, Ref. 1, Sec. 7.1b.
[20]J. E. Keizer, J. Tilden, and R. F. Fox (unpublished).
[21]A. J. Lichtenberg and M. A. Lieberman, Ref. 1, Sec. 7.4a.
[22]R. G. Deissler, NASA Technical Memorandum No. 101983, 1989 (unpublished).
[23]E. N. Lorenz, J. Atmos. Sci. **20**, 130 (1963).
[24]K. Tomita, Phys. Rep. **86** (1982).
[25]E. Wigner, Phys. Rev. **40**, 749 (1932).
[26]V. I. Arnold, *Mathematical Methods of Classical Mechanics* (Springer-Verlag, New York, 1978), Chap. 8.
[27]J. Wisdom, Proc. R. Soc. London, Ser. A **413**, 109 (1987); Icarus **72**, 241 (1987).
[28]R. F. Fox and B. L. Lan, preceding paper, Phys. Rev. A **41**, 2952 (1990).
[29]S. Zhu, A. W. Yu, and R. Roy, Phys. Rev. A **34**, 4333 (1986).
[30]N. G. van Kampen, Ref. 10, Chap. XII.
[31]H. L. Swinney, Physica **7D**, 3 (1983).
[32]M. Sargent, M. O. Scully, and W. E. Lamb, *Laser Physics* (Addison-Wesley, Reading, MA, 1974).
[33]E. Arimondo (private communication).
[34]P. Bak, T. Bohr, M. H. Jensen, and P. V. Christiansen, Solid State Commun. **51**, 231 (1984).

Chaos and the correspondence limit in the periodically kicked pendulum

Ronald F. Fox and Boon Leong Lan
School of Physics, Georgia Institute of Technology, Atlanta, Georgia 30332-0430
(Received 23 August 1989; revised manuscript received 8 September 1989)

The correspondence limit is illustrated for the periodically kicked pendulum. The classical dynamics of this system can be represented by a discrete map. A corresponding quantum map is derived and then rendered in the Ehrenfest formulation for expectation values. The Ehrenfest representation is studied for a minimum uncertainty Gaussian wave packet. It is shown that as $\hbar$ gets very small, followed by a decrease in the variance of the wave packet, the quantum map shadows the classical map with an error approaching zero for a length of time approaching infinity. The Gaussian form of the wave packet is preserved by the time evolution provided $\omega_0 T \ll 1$. This constraint implies that the classical map is predominantly not chaotic with very small regions of very weak chaos. As $\omega_0 T$ approaches 1, where the classical map becomes strongly chaotic, the propagation in time of the Gaussian wave packet completely breaks down. The possible significance of this breakdown is discussed.

I. INTRODUCTION

Generalizing the ideas associated with chaos in classical dynamical systems to the quantum-mechanical context has proved to be less than straightforward. In the classical-mechanical context chaos is characterized[1] by the existence of a positive Liapunov exponent, that represents quantitatively the extreme sensitivity of phase-space trajectories to initial conditions. It is not immediately obvious how to implement this characterization quantum mechanically where the idea of a precise classical trajectory in a phase space has been replaced by the time evolution of a probability amplitude in a Hilbert space. One approach to "quantum chaos" is to accept this incompatibility at the outset, and to define[2] quantum chaos to be the study of the quantum-mechanical behavior implied by a Hamiltonian that when treated purely classically exhibits chaos. One then looks for the signature of the classical chaos in the properties of the quantum system. Another approach[3] is to attempt to reinterpret the classical ideas of trajectories and Liapunov exponents in a quantum-mechanical setting. In this approach, the space of expectation values for all of the quantum operators is studied. Trajectories created by the time evolution of the expectation values can be analyzed for positive Liapunov exponents, just as in the classical-mechanical setting. This approach was originally[4] applied over a decade ago to the study of two-level quantum systems interacting with a resonant electromagnetic field in a laser cavity. Subsequently, the mechanism[3,5] underlying the observed chaos in this system was discovered. It turned out that in this case, it was virtual transitions that created periodic modulations of an underlying pendulum dynamics that were responsible for the chaos. This case enhances our perspective because virtual transitions have no classical correspondence, and we may conclude that this system exhibits quantum chaos (positive Liapunov exponents for the trajectories of expectation values) without there being any classical correspondence. In this paper, however, we wish to study the correspondence limit for a system which does have both a classical and a quantal manifestation, and we want to do it from the perspective of expectation value trajectories.

The system to be studied in this paper is the periodically kicked pendulum.[6] It has been chosen because of its simplicity. Even so, we shall see that its analysis is by no means trivial. It is a close cousin of the periodically kicked harmonic oscillator, which when confined to a torus, classically yields the Arnol'd cat map.[7,8] Very recently,[9] it has been claimed that the correspondence limit fails for the quantized version of this model system. Our kicked pendulum exhibits the correspondence limit for one region of parameter space, whereas the same derivation fails for another region. These regions correspond to no chaos or very weak chaos and strong chaos, respectively, when the system is treated classically.

The paper is divided into several sections. In Sec. II the dynamical details, both classically and quantally, are given. The dynamics is reduced to a discrete mapping in both cases. Our mappings are for just prior to the nth kick to just prior to the $(n+1)$th kick. This is the standard choice[6] for the classical picture, but curiously, the choice previously used[6] for the quantal picture was the mapping from just after a kick to just after the next kick. To study the correspondence limit, we, of course, had to make the same choice for both cases. In Sec. III we derive the fundamental tool for the analysis of the correspondence limit: the Ehrenfest theorem for the mappings. Since the Ehrenfest theorem is so illuminating in the usual quantal-classical correspondence context, we thought it would be useful for the mappings as well. It is. There is one subtlety, however. The angle variable for the pendulum has a finite domain $[0,2\pi]$. This means there are boundary-value terms in the Ehrenfest formulation, that are usually absent when a dynamical coordinate has an infinite domain. We exhibit this fact first for the free rotor, before showing it for the kicked pendulum. In Sec. IV we show that the boundary-value terms are

indeed correct, by analyzing a disjoint, exhaustive decomposition of them in simple physical terms. In Sec. V we analyze the application of the idea of a minimum uncertainty wave packet to this problem. We do so because this is how the correspondence limit is usually achieved in the context of the Ehrenfest formulation. The finite domain for θ once again creates a difficulty which we overcome. Instead of a simple Gaussian wave packet, a series of Gaussians is required to achieve a minimum uncertainty and to simultaneously respect the 2π periodicity in the θ dependence of this quantum system. We show that the Gaussian structure of the minimum uncertainty wave packet is preserved under the quantum mapping provided that its variance is sufficiently small, that a classical amount of action ($\gg\hbar$) is initially given to the kicked pendulum, and that $\omega_0 T \ll 1$. This preservation persists for a time which grows longer as $\hbar\to 0$. In Sec. VI we analyze in detail the correspondence limit. We find it to be a double limit taken in a proper order. First $\hbar\to 0$, and then the variance of the Gaussian wave packet goes to zero. Moreover, if we denote the variance by σ, then σ goes to zero like $\hbar^{1/3}$ guarantees that the quantum map will produce expectation value trajectories which shadow the classical map trajectories with an error that is vanishing, for a time that is growing infinite in the limit. The constraint $\omega_0 T \ll 1$ restricts the behavior of the classical map to stable, nonchaotic or to very weakly chaotic trajectories. For $\omega_0 T \geq 1$, the classical map can be strongly chaotic, but then the same derivation fails.

We present a detailed account of the correspondence limit for a dynamic system that can exhibit chaos. While the methods used reflect the particular structure of this special model (many Bessel functions are used), the guiding philosophy behind the methodology should prove fruitful generally.

II. DYNAMICS OF THE KICKED PENDULUM

The Hamiltonian for the periodically kicked pendulum is

$$H=\frac{p_\theta^2}{2ml^2}-ml^2\omega_0^2(\cos\theta)\delta_P(t/T)\ , \tag{1}$$

in which the periodic delta function δ_P is given by

$$\delta_P(t/T)=\sum_{j=-\infty}^{\infty}\delta(j-t/T)$$
$$=1+2\sum_{n=1}^{\infty}\cos(2n\pi t/T)\ . \tag{2}$$

T is the time between kicks, ω_0 is the small amplitude frequency, l is the pendulum length, and m is its mass.

Hamilton's equations of motion are simply

$$\dot p_\theta=-ml^2\omega_0^2(\sin\theta)\delta_P(t/T)\ , \tag{3}$$

$$\dot\theta\equiv\frac{p_\theta}{ml^2}\ . \tag{4}$$

We are interested in the change in the values of p_θ and θ from just before the nth kick to just before the $(n+1)$th kick. Straightforward integration produces the classical mapping[6]

$$p_{n+1}=p_n-ml^2\omega_0^2 T\sin\theta_n\ , \tag{5}$$

$$\theta_{n+1}=\theta_n+p_{n+1}T/ml^2\ . \tag{6}$$

Quantum mechanically, the kicked pendulum is described by the Schrödinger equation

$$i\hbar\frac{\partial}{\partial t}\psi=-\frac{\hbar^2}{2ml^2}\frac{\partial^2}{\partial\theta^2}\psi-ml^2\omega_0^2(\cos\theta)\delta_P(t/T)\psi\ . \tag{7}$$

This implies that there is an essentially discontinuous change in ψ across a δ-function kick, given by[6]

$$\psi^+=\psi^-\exp\left[i\frac{ml^2\omega_0^2 T}{\hbar}\cos\theta\right]\ , \tag{8}$$

where ψ^- denotes ψ just before a kick, and ψ^+ denotes ψ just after the kick. We will denote the recurring quantity in the exponent by

$$\kappa\equiv\frac{ml^2\omega_0^2 T}{\hbar}\ . \tag{9}$$

We may also expand ψ in terms of free rotor wave functions:

$$\psi(\theta,t)=\frac{1}{\sqrt{2\pi}}\sum_{n=-\infty}^{\infty}A_n(t)e^{in\theta}\ . \tag{10}$$

From just before the nth kick to just after it, we have

$$\psi(\theta,(nT)^+)=\frac{1}{\sqrt{2\pi}}\sum_{q=-\infty}^{\infty}A_q((nT)^-)e^{i\kappa\cos\theta}e^{iq\theta}\ . \tag{11}$$

Using identity (A1) from the Appendix, this becomes

$$\psi(\theta,(nT)^+)$$
$$=\frac{1}{\sqrt{2\pi}}\sum_{q=-\infty}^{\infty}A_q((nT)^-)\sum_{s=-\infty}^{\infty}i^s J_s(\kappa)e^{i(q+s)\theta}\ . \tag{12}$$

The time evolution from $(nT)^+$ to $[(n+1)T]^-$ is the evolution of a free rotor. Each free rotor eigenstate, $(1/\sqrt{2\pi})e^{in\theta}$, evolves as

$$(1/\sqrt{2\pi})e^{in\theta}\exp(-itE_n/\hbar)\ ,$$

where $E_n=n^2\hbar^2/2ml^2$. We will denote a second recurring quantity by

$$\tau\equiv\frac{\hbar T}{ml^2}\ . \tag{13}$$

Therefore we may write

$$\psi[\theta,((n+1)T)^-]=\frac{1}{\sqrt{2\pi}}\sum_{q=-\infty}^{\infty}A_q((nT)^-)\sum_{s=-\infty}^{\infty}i^s J_s(\kappa)e^{i(q+s)\theta}e^{-i(q+s)^2\tau/2}\ . \tag{14}$$

But we may also write

$$\psi[\theta,((n+1)T)^-]=\frac{1}{\sqrt{2\pi}}\sum_{r=-\infty}^{\infty}A_r[((n+1)T)^-]e^{ir\theta}\,. \tag{15}$$

These two equations yield the quantum mapping

$$A_r(n+1)=\sum_{q=-\infty}^{\infty}A_q(n)i^{r-q}J_{r-q}(\kappa)e^{-ir^2\tau/2}\,, \tag{16}$$

in which $A_r(n+1)$ is shorthand for $A_r[((n+1)T)^-]$.

III. EHRENFEST'S THEOREM

Ehrenfest's theorem relates to each other the expectation values of the quantum operators corresponding to the classical variables that appear in Hamilton's equations of motion. Ordinarily the derivation involves integration by parts with boundary-value terms which vanish. This is not the case for the kicked pendulum; the corresponding boundary terms do not vanish. To illustrate this special situation, we first consider the simple, free rotor with Hamiltonian

$$H=\frac{p_\theta^2}{2ml^2}\,. \tag{17}$$

The classical, Hamiltonian equations are

$$\dot{p}_\theta=0\,, \tag{18}$$

$$\dot{\theta}=\frac{p_\theta}{ml^2}\,. \tag{19}$$

The derivation of the Ehrenfest identities is as follows:

$$\begin{aligned}\langle\dot{p}_\theta\rangle&=\int_0^{2\pi}d\theta\left[\left(\frac{\partial}{\partial t}\psi^*\right)p_\theta\psi+\psi^*p_\theta\frac{\partial}{\partial t}\psi\right]\\&=\frac{i}{\hbar}\int_0^{2\pi}d\theta[(H\psi^*)p_\theta\psi-\psi^*p_\theta H\psi]\\&=\frac{i}{\hbar}\int_0^{2\pi}d\theta\,\psi^*[H,p_\theta]\psi\\&=\frac{i}{\hbar}\int_0^{2\pi}d\theta\,\psi^*0\psi\\&=0\end{aligned} \tag{20}$$

and

$$\begin{aligned}\langle\dot{\theta}\rangle&=\int_0^{2\pi}d\theta\left[\left(\frac{\partial}{\partial t}\psi^*\right)\theta\psi+\psi^*\theta\frac{\partial}{\partial t}\psi\right]\\&=\frac{i}{\hbar}\int_0^{2\pi}d\theta[(H\psi^*)\theta\psi-\psi^*\theta H\psi]\\&=\frac{i}{\hbar}\int_0^{2\pi}d\theta\,\psi^*[H,\theta]\psi+\frac{i\hbar\pi}{ml^2}\left[\psi^*\frac{\partial\psi}{\partial\theta}-\psi\frac{\partial\psi^*}{\partial\theta}\right]\Bigg|_{\theta=2\pi}\\&=\frac{\langle p_\theta\rangle}{ml^2}+\frac{i\hbar\pi}{ml^2}\left[\psi^*\frac{\partial\psi}{\partial\theta}-\psi\frac{\partial\psi^*}{\partial\theta}\right]\Bigg|_{\theta=2\pi}\,.\end{aligned} \tag{21}$$

In both (20) and (21), it is the third equality on the right-hand side that requires integration by parts in order to manifest the Hamiltonian character of H. In (20), nothing special happens because all other factors in the integrand are 2π periodic, but in (21), the factor θ is not 2π periodic, causing the boundary-value terms. Their essential importance is easily checked by considering Ehrenfest's identities [(20) and (21)] for the time-evolving pure state

$$\psi=\frac{1}{\sqrt{2\pi}}\exp\left[in\theta-i\frac{\hbar n^2}{2ml^2}t\right]\,. \tag{22}$$

The non-2π-periodicity of θ causes more complicated boundary-value terms to appear in the Ehrenfest identities for the kicked pendulum. In addition, we will not exhibit Ehrenfest's theorem for the differential equations, but instead derive it for the maps. Using the notation in (15) and (16), we may write

$$\begin{aligned}\langle\theta(n)\rangle&=\frac{1}{2\pi}\int_0^{2\pi}d\theta\sum_{r=-\infty}^{\infty}\sum_{s=-\infty}^{\infty}A_r^*(n)A_s(n)e^{-ir\theta}\theta e^{is\theta}\\&=\pi+\sum_{r\neq s=-\infty}^{\infty}\frac{A_r^*(n)A_s(n)}{i(s-r)}\end{aligned} \tag{23}$$

and

$$\begin{aligned}\langle p_\theta(n)\rangle&=\frac{1}{2\pi}\int_0^{2\pi}d\theta\sum_{r,s=-\infty}^{\infty}A_r^*(n)A_s(n)e^{-ir\theta}p_\theta e^{is\theta}\\&=\sum_{s=-\infty}^{\infty}\hbar sA_s^*(n)A_s(n)\,.\end{aligned} \tag{24}$$

Now, using the quantum mapping (16), we may also write

$$\begin{aligned}\langle p_\theta(n+1)\rangle&=\sum_{q=-\infty}^{\infty}\hbar qA_q^*(n+1)A_q(n+1)\\&=\sum_{q=-\infty}^{\infty}\hbar q\sum_{r=-\infty}^{\infty}\sum_{s=-\infty}^{\infty}A_r^*(n)(-i)^{q-r}A_s(n)i^{q-s}J_{q-r}(\kappa)J_{q-s}(\kappa)\\&=\sum_{r,s=-\infty}^{\infty}i^{r-s}\sum_{q=-\infty}^{\infty}\hbar qJ_{q-r}(\kappa)J_{q-s}(\kappa)A_r^*(n)A_s(n)\,.\end{aligned} \tag{25}$$

Using identity (A5) from the Appendix, this becomes

$$\begin{aligned}\langle p_\theta(n+1)\rangle&=\sum_{r,s=-\infty}^{\infty}i^{r-s}\hbar[\tfrac{1}{2}\kappa(\delta_{r-s,1}+\delta_{r-s,-1})+r\delta_{rs}]A_r^*(n)A_s(n)\\&=\sum_{r=-\infty}^{\infty}\left[\hbar rA_r^*(n)A_r(n)+\frac{\hbar\kappa}{2}i[A_r^*(n)A_{r-1}(n)-A_r^*(n)A_{r+1}(n)]\right]\,.\end{aligned} \tag{26}$$

Now,

$$\langle \sin\theta(n)\rangle = \frac{1}{2\pi}\int_0^{2\pi} d\theta \sum_{r,s=-\infty}^{\infty} A_r^*(n)A_s(n)e^{-ir\theta}(\sin\theta)e^{is\theta}$$

$$= \sum_{r,s=-\infty}^{\infty} A_r^*(n)A_s(n)\frac{1}{2\pi}\int_0^{2\pi} d\theta \frac{1}{2i}(e^{-ir\theta+is\theta+i\theta} - e^{-ir\theta+is\theta-i\theta})$$

$$= \sum_{r,s=-\infty}^{\infty} A_r^*(n)A_s(n)\frac{1}{2i}(\delta_{r-s,1}-\delta_{r-s,-1})$$

$$= \frac{i}{2}\sum_{r=-\infty}^{\infty}[A_r^*(n)A_{r+1}(n) - A_r^*(n)A_{r-1}(n)] . \tag{27}$$

Using this and (24) in (26) yields the first half of Ehrenfest's theorem for the maps:

$$\langle p_\theta(n+1)\rangle = \langle p_\theta(n)\rangle - \hbar\kappa\langle \sin\theta(n)\rangle . \tag{28}$$

Again using the quantum mapping (16), we may also write

$$\langle \theta(n+1)\rangle = \frac{1}{2\pi}\sum_{p,q=-\infty}^{\infty} A_p^*(n+1)A_q(n+1)\int_0^{2\pi} d\theta\, e^{-i(p-q)\theta}\theta$$

$$= \frac{1}{2\pi}\sum_{p,q=-\infty}^{\infty}\sum_{r,s=-\infty}^{\infty} A_s^*(n)A_r(n)(-i)^{p-s}i^{q-r}J_{p-s}(\kappa)J_{q-r}(\kappa)\exp\left[i\frac{\tau}{2}(p^2-q^2)\right]\int_0^{2\pi} d\theta\, e^{-i(p-q)\theta}\theta$$

$$= \sum_{r,s=-\infty}^{\infty} A_s^*(n)A_r(n)\frac{1}{2\pi}\int_0^{2\pi} d\theta\,\theta\left[\sum_{p=-\infty}^{\infty}(-i)^{p-s}J_{p-s}(\kappa)\exp\left[i\frac{\tau}{2}p^2 - ip\theta\right]\right]$$

$$\times\left[\sum_{q=-\infty}^{\infty}(i)^{q-r}J_{q-r}(\kappa)\exp\left[-i\frac{\tau}{2}q^2+iq\theta\right]\right] . \tag{29a}$$

From (A1), we get

$$\sum_{q=-\infty}^{\infty} i^{q-r}J_{q-r}(\kappa)\exp\left[-i\frac{\tau}{2}q^2+iq\theta\right] = \sum_{k=-\infty}^{\infty} i^k J_k(\kappa)\exp\left[-i\frac{\tau}{2}(k+r)^2+i(k+r)\theta\right]$$

$$= \sum_{k=-\infty}^{\infty} i^k J_k(\kappa)\exp\left[ik(\theta-r\tau)-i\frac{\tau}{2}k^2\right]\exp\left[ir\theta-i\frac{\tau}{2}r^2\right]$$

$$= \exp\left[ir\theta-i\frac{\tau}{2}r^2\right]\exp\left[i\frac{\tau}{2}\frac{\partial^2}{\partial\theta^2}\right]\sum_{k=-\infty}^{\infty} i^k J_k(\kappa)e^{ik(\theta-r\tau)}$$

$$= \exp\left[ir\theta-i\frac{\tau}{2}r^2\right]\exp\left[i\frac{\tau}{2}\frac{\partial^2}{\partial\theta^2}\right]\exp[i\kappa\cos(\theta-r\tau)] \tag{29b}$$

and by complex conjugation

$$\sum_{p=-\infty}^{\infty}(-i)^{p-s}J_{p-s}(\kappa)\exp\left[i\frac{\tau}{2}p^2-ip\theta\right] = \exp\left[-is\theta+i\frac{\tau}{2}s^2\right]\exp\left[-i\frac{\tau}{2}\frac{\partial^2}{\partial\theta^2}\right]\exp[-i\kappa\cos(\theta-s\tau)] . \tag{29c}$$

When these identities are inserted into (29a), we get

$$\langle \theta(n+1)\rangle = \sum_{r,s=-\infty}^{\infty} A_s^*(n)A_r(n)\frac{1}{2\pi}\int_0^{2\pi} d\theta\,\theta\exp\left[-is\theta+i\frac{\tau}{2}s^2\right]\left[\exp\left[-i\frac{\tau}{2}\frac{\partial^2}{\partial\theta^2}\right]\exp[-i\kappa\cos(\theta-s\tau)]\right]$$

$$\times\exp\left[ir\theta-i\frac{\tau}{2}r^2\right]\left[\exp\left[i\frac{\tau}{2}\frac{\partial^2}{\partial\theta^2}\right]\exp[i\kappa\cos(\theta-r\tau)]\right] . \tag{30}$$

Using identity (A6) from the Appendix, we see that

$$\exp\left[-is\theta+i\frac{\tau}{2}s^2\right]\exp\left[-i\frac{\tau}{2}\frac{\partial^2}{\partial\theta^2}\right]\exp[-i\kappa\cos(\theta-s\tau)]$$

$$=\exp\left[-i\frac{\tau}{2}\frac{\partial^2}{\partial\theta^2}\right]\exp\left[-is\theta+i\frac{\tau}{2}s^2\right]\exp\left[s\tau\frac{\partial}{\partial\theta}\right]\exp\left[-is^2\frac{\tau}{2}\right]\exp[-i\kappa\cos(\theta-s\tau)]$$

$$=\exp\left[-i\frac{\tau}{2}\frac{\partial^2}{\partial\theta^2}\right]e^{-is\theta}\exp(-i\kappa\cos\theta) \tag{31}$$

and that

$$\exp\left[ir\theta-i\frac{\tau}{2}r^2\right]\exp\left[i\frac{\tau}{2}\frac{\partial^2}{\partial\theta^2}\right]\exp[i\kappa\cos(\theta-r\tau)]$$

$$=\exp\left[i\frac{\tau}{2}\frac{\partial^2}{\partial\theta^2}\right]\exp\left[ir\theta-i\frac{\tau}{2}r^2\right]\exp\left[r\tau\frac{\partial}{\partial\theta}\right]\exp\left[ir^2\frac{\tau}{2}\right]\exp[i\kappa\cos(\theta-r\tau)]$$

$$=\exp\left[i\frac{\tau}{2}\frac{\partial^2}{\partial\theta^2}\right]e^{ir\theta}\exp(i\kappa\cos\theta)\ . \tag{32}$$

When these transformations are inserted into (30), we obtain

$$\langle\theta(n+1)\rangle=\sum_{r,s=-\infty}^{\infty}A_s^*(n)A_r(n)\frac{1}{2\pi}\int_0^{2\pi}d\theta\,\theta\left[\exp\left[-i\frac{\tau}{2}\frac{\partial^2}{\partial\theta^2}\right]e^{-is\theta}\exp(-i\kappa\cos\theta)\right]$$
$$\times\left[\exp\left[i\frac{\tau}{2}\frac{\partial^2}{\partial\theta^2}\right]e^{ir\theta}\exp(i\kappa\cos\theta)\right]\ . \tag{33}$$

It is desired to evaluate this expression using integration by parts (repeatedly), but the non-2π-periodicity of the factor θ prevents this from being straightforward. Nevertheless, the following, extended argument achieves the goal.

Let us rewrite the θ integral of (33) in the form

$$\frac{1}{2\pi}\int_0^{2\pi}d\theta\,\theta f(\theta)\exp\left[i\frac{\tau}{2}\frac{\partial^2}{\partial\theta^2}\right]g(\theta)\equiv\left\langle\theta f\exp\left[i\frac{\tau}{2}\frac{\partial^2}{\partial\theta^2}\right]g\right\rangle\ , \tag{34a}$$

where

$$f(\theta)=\exp\left[-i\frac{\tau}{2}\frac{\partial^2}{\partial\theta^2}\right]e^{-is\theta}e^{-i\kappa\cos\theta},\quad g(\theta)=e^{ir\theta}e^{i\kappa\cos\theta}\ .$$

Therefore

$$\left\langle\theta f\exp\left[i\frac{\tau}{2}\frac{\partial^2}{\partial\theta^2}\right]g\right\rangle=\sum_{n=0}^{\infty}\frac{[i(\tau/2)]^n}{n!}\left\langle\theta f\frac{\partial^{2n}}{\partial\theta^{2n}}g\right\rangle\ . \tag{34b}$$

The $n=0$ term is trivial. For $n\neq0$, integration by parts justifies

$$\left\langle\theta f\frac{\partial^{2n}}{\partial\theta^{2n}}g\right\rangle=\left\langle g\frac{\partial^{2n}}{\partial\theta^{2n}}(\theta f)\right\rangle+\frac{1}{2\pi}\sum_{m=0}^{2n-1}(-1)^m\left[\frac{\partial^m}{\partial\theta^m}(\theta f)\right]\left[\frac{\partial^{2n-1-m}}{\partial\theta^{2n-1-m}}g\right]\Bigg|_0^{2\pi}\ . \tag{34c}$$

Since both f and g are 2π periodic,

$$\left[\frac{\partial^m}{\partial\theta^m}(\theta f)\right]\left[\frac{\partial^{2n-1-m}}{\partial\theta^{2n-1-m}}g\right]\Bigg|_0^{2\pi}=\theta\left[\frac{\partial^m}{\partial\theta^m}f\right]\left[\frac{\partial^{2n-1-m}}{\partial\theta^{2n-1-m}}g\right]\Bigg|_0^{2\pi}=2\pi\left[\frac{\partial^m}{\partial\theta^m}f\right]\left[\frac{\partial^{2n-1-m}}{\partial\theta^{2n-1-m}}g\right]\Bigg|_{\theta=2\pi}\ . \tag{34d}$$

Therefore

$$\left\langle\theta f\exp\left[i\frac{\tau}{2}\frac{\partial^2}{\partial\theta^2}\right]g\right\rangle=\left\langle g\exp\left[i\frac{\tau}{2}\frac{\partial^2}{\partial\theta^2}\right](\theta f)\right\rangle+\sum_{n=1}^{\infty}\frac{[i(\tau/2)]^n}{n!}\sum_{m=0}^{2n-1}(-1)^m\left[\frac{\partial^m}{\partial\theta^m}f\right]\left[\frac{\partial^{2n-1-m}}{\partial\theta^{2n-1-m}}g\right]\Bigg|_{\theta=2\pi}\ . \tag{35a}$$

Now,

$$f=\exp\left[-i\frac{\tau}{2}\frac{\partial^2}{\partial\theta^2}\right]e^{-is\theta}\sum_{l=-\infty}^{\infty}(-i)^lJ_l(\kappa)e^{-il\theta}=\sum_{l=-\infty}^{\infty}(-i)^lJ_l(\kappa)\exp\left[i\frac{\tau}{2}(s+l)^2-i(s+l)\theta\right]\ . \tag{35b}$$

Therefore

$$\left[\frac{\partial^m}{\partial\theta^m}f\right]\Bigg|_{\theta=2\pi}=\sum_{l=-\infty}^{\infty}(-i)^l J_l(\kappa)\exp\left[i\frac{\tau}{2}(s+l)^2\right][-i(s+l)]^m . \tag{35c}$$

Similarly,

$$g=e^{ir\theta}e^{i\kappa\cos\theta}=\sum_{k=-\infty}^{\infty}i^k J_k(\kappa)e^{i(r+k)\theta} \tag{35d}$$

so that

$$\frac{\partial^{2n-1-m}}{\partial\theta^{2n-1-m}}g\Bigg|_{\theta=2\pi}=\sum_{k=-\infty}^{\infty}i^k J_k(\kappa)[i(r+k)]^{2n-1-m} . \tag{35e}$$

Thus

$$\begin{aligned}
&\sum_{n=1}^{\infty}\frac{\left[i\frac{\tau}{2}\right]^n}{n!}\sum_{m=0}^{2n-1}(-1)^m\left[\frac{\partial^m}{\partial\theta^m}f\right]\left[\frac{\partial^{2n-1-m}}{\partial\theta^{2n-1-m}}g\right]\Bigg|_{\theta=2\pi}\\
&=\sum_{n=1}^{\infty}\frac{\left[i\frac{\tau}{2}\right]^n}{n!}\sum_{m=0}^{2n-1}(-1)^m\sum_{l,k=-\infty}^{\infty}i^{(k-l)}J_k(\kappa)J_l(\kappa)\exp\left[i\frac{\tau}{2}(s+l)^2\right][-i(s+l)]^m[i(r+k)]^{2n-1-m}\\
&=\sum_{l,k=-\infty}^{\infty}i^{(k-l)}J_k(\kappa)J_l(\kappa)\exp\left[i\frac{\tau}{2}(s+l)^2\right]\sum_{n=1}^{\infty}\frac{\left[-i\frac{\tau}{2}(r+k)^2\right]^n}{n!}\left[\frac{-i}{r+k}\right]\sum_{m=0}^{2n-1}\left[\frac{s+l}{r+k}\right]^m\\
&=\sum_{l,k=-\infty}^{\infty}i^{(k-l)}J_k(\kappa)J_l(\kappa)\exp\left[i\frac{\tau}{2}(s+l)^2\right]\sum_{n=1}^{\infty}\frac{\left[-i\frac{\tau}{2}(r+k)^2\right]^n}{n!}\left[\frac{-i}{r+k}\right]\frac{1-[(s+l)/(r+k)]^{2n}}{1-[(s+l)/(r+k)]}\\
&=\sum_{l,k=-\infty}^{\infty}i^{(k-l)}J_k(\kappa)J_l(\kappa)i\frac{1-\exp\{i(\tau/2)[(s+l)^2-(r+k)^2]\}}{(r+k)-(s+l)} .
\end{aligned} \tag{36a}$$

Equation (35a) is now expressible as

$$\left\langle\theta f\exp\left[i\frac{\tau}{2}\frac{\partial^2}{\partial\theta^2}\right]g\right\rangle=\left\langle g\exp\left[i\frac{\tau}{2}\frac{\partial^2}{\partial\theta^2}\right](\theta f)\right\rangle+\sum_{l,k=-\infty}^{\infty}i^{(k-l)}J_k(\kappa)J_l(\kappa)i\frac{1-\exp\{i(\tau/2)[(s+l)^2-(r+k)^2]\}}{(r+k)-(s+l)} . \tag{36b}$$

The first term on the right-hand side contains the factor

$$\exp\left[i\frac{\tau}{2}\frac{\partial^2}{\partial\theta^2}\right]\theta\exp\left[-i\frac{\tau}{2}\frac{\partial^2}{\partial\theta^2}\right]=\theta+i\tau\frac{\partial}{\partial\theta} \tag{36c}$$

as is well known from a commutator series expansion of the left-hand side. We are now prepared to return to (33), which becomes

$$\begin{aligned}
\langle\theta(n+1)\rangle=\sum_{r,s=-\infty}^{\infty}A_s^*(n)A_r(n)\Bigg[&\frac{1}{2\pi}\int_0^{2\pi}d\theta\,e^{ir\theta}\exp(i\kappa\cos\theta)\left[\theta+i\tau\frac{\partial}{\partial\theta}\right]e^{-is\theta}\exp(-i\kappa\cos\theta)\\
&+\sum_{l,k=-\infty}^{\infty}i^{(k-l)}J_k(\kappa)J_l(\kappa)i\frac{1-\exp\{i(\tau/2)[(s+l)^2-(r+k)^2]\}}{(r+k)-(s+l)}\Bigg] .
\end{aligned} \tag{37a}$$

The θ term reduces to $\langle\theta(n)\rangle$. The $i\tau(\partial/\partial\theta)$ term simplifies by noting that

$$\begin{aligned}
\frac{1}{2\pi}\int_0^{2\pi}d\theta\,e^{ir\theta}e^{i\kappa\cos\theta}i\tau\frac{\partial}{\partial\theta}e^{-is\theta}e^{-i\kappa\cos\theta}&=\frac{1}{2\pi}\int_0^{2\pi}d\theta\,e^{ir\theta}e^{i\kappa\cos\theta}(\tau s e^{-is\theta-i\kappa\cos\theta}-\tau\kappa\sin\theta e^{-is\theta-i\kappa\cos\theta})\\
&=\tau s\delta_{r,s}-\tau\kappa\frac{1}{2i}(\delta_{r-s,-1}-\delta_{r-s,1}) .
\end{aligned} \tag{37b}$$

In (37a), these terms become

$$\sum_{r,s=-\infty}^{\infty} A_s^*(n)A_r(n)\left[\tau s\delta_{r,s}-\tau\kappa\frac{1}{2i}(\delta_{r-s,-1}-\delta_{r-s,1})\right]=\frac{\tau}{\hbar}(\langle p_\theta(n)\rangle-\hbar\kappa\langle\sin\theta(n)\rangle)\ . \tag{38}$$

The final result is the second half of Ehrenfest's theorem for the maps:

$$\langle\theta(n+1)\rangle=\langle\theta(n)\rangle+\frac{\tau}{\hbar}\langle p_\theta(n+1)\rangle+\sum_{r,s=-\infty}^{\infty}A_s^*(n)A_r(n)\sum_{k,l=-\infty}^{\infty}J_k(\kappa)J_l(\kappa)i\frac{1-\exp\{i(\tau/2)[(s+l)^2-(r+k^2)]\}}{(r+k)-(s+l)}\ , \tag{39}$$

wherein we have used (28) to simplify (38).

Using (9) and (13), we can rewrite the classical mapping in the form

$$p_{n+1}=p_n-\hbar\kappa\sin\theta_n\ , \tag{40}$$

$$\theta_{n+1}=\theta_n+\frac{\tau}{\hbar}p_{n+1}\ , \tag{41}$$

which is to be compared with the quantum mapping, in the Ehrenfest formulation, given by (28) and (39). We see the presence of the boundary-value terms which result from the non-2π-periodicity of θ. In a study of the correspondence limit, we must see how these boundary terms disappear, and how the expectation values go over into the classical variables.

IV. ANALYSIS OF THE BOUNDARY-VALUE TERMS

It will be useful below to have a deeper appreciation of the content of the boundary-value terms in (39). By analyzing them in detail, we also confirm their validity.

Using expression (23) and the quantum mapping (16), we may perform a direct evaluation of $\langle\theta(n+1)\rangle$, which may be rendered:

$$\begin{aligned}\langle\theta(n+1)\rangle&=\pi+\sum_{r\neq s=-\infty}^{\infty}\frac{A_s^*(n+1)A_r(n+1)}{i(r-s)}\\&=\pi+\sum_{r\neq s=-\infty}^{\infty}\sum_{p,q=-\infty}^{\infty}i^{r-q-(s-p)}A_p^*(n)A_q(n)J_{r-q}(\kappa)J_{s-p}(\kappa)\exp\left[i\frac{\tau}{2}(s^2-r^2)\right]\frac{1}{i(r-s)}\ .\end{aligned} \tag{42}$$

This is to be compared with the boundary-value terms in (39). The comparison is facilitated by changing dummy indices in (39). First change (r,s) into (q,p) so that the boundary term becomes

$$\begin{aligned}&\sum_{p,q=-\infty}^{\infty}A_p^*(n)A_q(n)\sum_{k,l=-\infty}^{\infty}i^{k-l}J_k(\kappa)J_l(\kappa)i\frac{1-\exp\{i(\tau/2)[(s+l)^2-(r+k^2)]\}}{(r+k)-(s+l)}\\&\qquad=\sum_{p,q=-\infty}^{\infty}A_p^*(n)A_q(n)\sum_{r,s=-\infty}^{\infty}i^{r-q-(s-p)}J_{r-q}(\kappa)J_{s-p}(\kappa)i\frac{1-\exp\{i(\tau/2)[s^2-r^2]\}}{r-s}\ ,\end{aligned} \tag{43}$$

wherein the right-hand side comes from the additional change of (k,l) into $(r-q,s-p)$. Both (42) and (43) contain

$$\sum_{p,q=-\infty}^{\infty}A_p^*(n)A_q(n)$$

and

$$i^{r-q-(s-p)}J_{r-q}(\kappa)J_{s-p}(\kappa)\ .$$

The $r-s$ summation in (43) may be broken up into three pieces:

$$\begin{aligned}&\sum_{r,s=-\infty}^{\infty}i^{r-q-(s-p)}J_{r-q}(\kappa)J_{s-p}(\kappa)i\frac{1-\exp[i(\tau/2)(s^2-r^2)]}{r-s}\\&=\sum_{r\neq s=-\infty}^{\infty}i^{r-q-(s-p)}J_{r-q}(\kappa)J_{s-p}(\kappa)\exp\left[i\frac{\tau}{2}(s^2-r^2)\right]\frac{i}{s-r}\\&\quad-\sum_{r\neq s=-\infty}^{\infty}i^{r-q-(s-p)}J_{r-q}(\kappa)J_{s-p}(\kappa)\frac{i}{s-r}+\sum_{k=-\infty}^{\infty}i^{p-q}J_{k-q}(\kappa)J_{k-p}(\kappa)(-\tau\kappa)\ .\end{aligned} \tag{44}$$

The first term of the right-hand side of (44) matches the direct evaluation expression in (42). From (25) we see that the third term will generate $-(\tau/\hbar)\langle p_\theta(n+1)\rangle$ in (43). The second term may be evaluated by noting that

$$\frac{1}{2\pi}\int_0^{2\pi} d\theta\,\theta e^{-i(s-r)\theta}=\frac{i}{s-r}\ .$$

Therefore

$$-\sum_{r\neq s=-\infty}^{\infty} i^{r-q-(s-p)}J_{r-q}(\kappa)J_{s-p}(\kappa)\frac{i}{s-r}$$

$$=-\frac{1}{2\pi}\int_0^{2\pi} d\theta\,\theta\sum_{r\neq s=-\infty}^{\infty} i^{r-q-(s-p)}J_{r-q}(\kappa)J_{s-p}(\kappa)e^{-i(s-r)\theta}$$

$$=-\frac{1}{2\pi}\int_0^{2\pi} d\theta\,\theta\left[\sum_{r,s=-\infty}^{\infty} i^{r-q-(s-p)}J_{r-q}(\kappa)J_{s-p}(\kappa)e^{-i(s-r)\theta}-\delta_{pq}\right]$$

$$=\pi\delta_{pq}-\frac{1}{2\pi}\int_0^{2\pi} d\theta\,\theta\left[\sum_{r=-\infty}^{\infty} i^{r-q}J_{r-q}(\kappa)e^{ir\theta}\right]\left[\sum_{s=-\infty}^{\infty} i^{p-s}J_{s-p}(\kappa)e^{-is\theta}\right]$$

$$=\pi\delta_{pq}-\frac{1}{2\pi}\int_0^{2\pi} d\theta\,\theta e^{iq\theta}e^{i\kappa\cos\theta}e^{-ip\theta}e^{-i\kappa\cos\theta}=\pi\delta_{pq}-\frac{1}{2\pi}\int_0^{2\pi} d\theta\,\theta e^{i(q-p)\theta}\ ,$$

wherein (A1) has been used again. When this is inserted into (43), we finally obtain $\pi-\langle\theta(n)\rangle$. Thus, when pose the boundary-value terms in (39) into the three portions exhibited in (44), we find

$$\langle\theta(n+1)\rangle=\langle\theta(n)\rangle+\frac{\tau}{\hbar}\langle p_\theta(n+1)\rangle$$
$$+\sum_{p,q=-\infty}^{\infty}\sum_{r\neq s=-\infty}^{\infty} i^{r-q-(s-p)}A_p^*(n)A_q(n)J_{r-q}(\kappa)J_{s-p}(\kappa)\frac{\exp[i(\tau/2)(s^2-r^2)]}{i(r-s)}$$
$$+\pi-\langle\theta(n)\rangle-\frac{\tau}{\hbar}\langle p_\theta(n+1)\rangle\ ,$$

which is identical with (42).

In addition, we have checked (28) and (39) by numerical computation and direct comparison with computations based on the quantum map (16).

V. TIME EVOLUTION OF MINIMUM UNCERTAINTY WAVE PACKET

If θ were on the infinite interval, then a simple Gaussian wave function would provide the minimum uncertainty wave packet. However, θ is restricted to the finite interval $[0,2\pi]$ and ψ must be 2π periodic. We know from the theory of diffusion that a simple Gaussian on an infinite interval becomes a series of Gaussians on a finite interval with absorbing boundaries. Therefore we try

$$\psi(\theta,0)\sim\sum_{l=-\infty}^{\infty}(2\pi\sigma^2)^{-1/4}\exp\left[-\frac{(a-\theta+2\pi l)^2}{4\sigma^2}\right]e^{ib\theta}\ , \tag{48}$$

where b is an integer. If σ is sufficiently small, this wave function is a very sharply peaked Gaussian around a in the interval $[0,2\pi]$. In any case, it festly 2π periodic.

For very small σ,

$$\langle\theta\rangle\sim\int_0^{2\pi} d\theta\,\theta\frac{1}{(2\pi\sigma^2)^{1/2}}\exp\left[-\frac{(a-\theta)^2}{2\sigma^2}\right]\sim a$$

and

$$\langle\Delta\theta^2\rangle\sim\sigma^2\ ,$$

where $\Delta\theta=\theta-\langle\theta\rangle$. Similarly,

$$\langle p_\theta\rangle\sim i\hbar\int_0^{2\pi} d\theta\,\theta\frac{1}{(2\pi\sigma^2)^{1/2}}\exp\left[-\frac{(a-\theta)^2}{2\sigma^2}\right]\times\left[ib-\frac{(\theta-a)}{2\sigma^2}\right]$$
$$\sim\hbar b$$

and

$$\langle\Delta p_\theta^2\rangle\sim-\hbar^2\int_0^{2\pi} d\theta\,\theta\frac{1}{(2\pi\sigma^2)^{1/2}}\exp\left[-\frac{(a-\theta)^2}{2\sigma^2}\right]\left[\left[ib-\frac{(\theta-a)}{2\sigma^2}\right]^2-\frac{1}{2\sigma^2}\right]-\hbar^2b^2$$

$$\sim-\hbar^2\left[\frac{\sigma^2}{4\sigma^4}-\frac{1}{2\sigma^2}\right]=\frac{\hbar^2}{4\sigma^2}\ .$$

Therefore

$$(\langle \Delta\theta^2 \rangle)^{1/2}(\langle \Delta p_\theta^2 \rangle)^{1/2} = \frac{\hbar}{2} , \tag{53}$$

confirming that we have a minimum uncertainty wave packet.

The wave-packet nature of (48) is clearer if we write

$$\psi(\theta,0) = \frac{1}{\sqrt{2\pi}} \sum_{n=-\infty}^{\infty} A_n(0) e^{in\theta} . \tag{54}$$

Therefore

$$\begin{aligned} A_n(0) &= \int_0^{2\pi} d\theta \frac{1}{\sqrt{2\pi}} e^{-in\theta} \psi(\theta,0) \\ &\sim \int_0^{2\pi} d\theta \frac{1}{\sqrt{2\pi}} e^{-in\theta} (2\pi\sigma^2)^{-1/4} \\ &\quad \times \exp\left[-\frac{(a-\theta)^2}{4\sigma^2} \right] e^{ib\theta} \\ &\sim \frac{1}{\sqrt{2\pi}} e^{i(b-n)a} (2\pi\sigma^2)^{1/4} e^{-\sigma^2(b-n)^2} \\ &= \left[\frac{\pi}{2\sigma^2} \right]^{-1/4} e^{iba} e^{-ina} e^{-\sigma^2(b-n)^2} \end{aligned} \tag{55}$$

for sufficiently small σ. In (48) we see the Gaussianness in the θ dependence, whereas in (55) we see it in the n dependence.

The fundamental question is the following: how does the minimum uncertainty wave packet evolve in time? It is easiest to explore this question through the evolution of the A_n's, beginning with (55).

From the quantum map (16) we have

$$A_m(1) = \sum_{r=-\infty}^{\infty} A_r(0) i^{m-r} J_{m-r}(\kappa) e^{-im^2\tau/2} . \tag{56}$$

Use the integral representation

$$J_{m-r}(\kappa) = \frac{1}{2\pi} \int_{-\pi}^{\pi} d\phi\, e^{-i(m-r)\phi + i\kappa\sin\phi} \quad \text{for } m-r \geq 0 \tag{57a}$$

and

$$J_{m-r}(\kappa) = (-1)^{r-m} \frac{1}{2\pi} \int_{-\pi}^{\pi} d\phi\, e^{-i(r-m)\phi + i\kappa\sin\phi} \quad \text{for } m-r \leq 0 \tag{57b}$$

and (55) to write

$$\begin{aligned} A_m(1) &= \frac{1}{2\pi} \int_{-\pi}^{\pi} d\phi\, e^{i\kappa\sin\phi} \left[\frac{\pi}{2\sigma^2} \right]^{-1/4} e^{-im^2\tau/2} \left[\sum_{r=-\infty}^{m} e^{i(b-r)a} e^{-\sigma^2(b-r)^2} i^{m-r} e^{-i(m-r)\phi} \right. \\ &\qquad \left. + \sum_{r=m+1}^{\infty} (-1)^{r-m} e^{i(b-r)a} e^{-\sigma^2(b-r)^2} i^{m-r} e^{-i(r-m)\phi} \right] \\ &= \frac{1}{2\pi} \int_{-\pi}^{\pi} d\phi\, e^{i\kappa\sin\phi} \left[\frac{\pi}{2\sigma^2} \right]^{-1/4} e^{-im^2\tau/2} \left[\sum_{s=-\infty}^{m-b} e^{-isa} e^{-\sigma^2 s^2} i^{m-b-s} e^{-i(m-b-s)\phi} \right. \\ &\qquad \left. + \sum_{s=m+1-b}^{\infty} (-1)^{s+b-m} e^{-isa} e^{-\sigma^2 s^2} i^{m-b-s} e^{-i(s+b-m)\phi} \right] , \end{aligned} \tag{58}$$

wherein the substitution $s = r - b$ was made. For sufficiently small σ, we may convert the summations into integrals. We do this by setting $x = \sigma s$ and let $dx = \sigma$ correspond to the interval from $s-1$ to s. Thus we may write

$$\begin{aligned} \sum_{s=-\infty}^{m-b} e^{-\sigma^2 s^2} e^{is(\phi-a)} i^{-s} &= \sum_{s=-\infty}^{m-b} \sigma \frac{\sqrt{\pi}}{\sigma} \frac{e^{-\sigma^2 s^2}}{\sqrt{\pi}} \exp\left[i\sigma s \frac{\phi - a + (\pi/2) \mp \pi}{\sigma} \right] \\ &= \frac{\sqrt{\pi}}{\sigma} \int_{-\infty}^{(m-b)/\sigma} dx \frac{e^{-x^2}}{\sqrt{\pi}} \exp\left[ix \frac{\phi - a + (\pi/2) \mp \pi}{\sigma} \right] , \end{aligned} \tag{59a}$$

where we used $i = \exp[-i(\pi/2) \pm i\pi]$, and also

$$\begin{aligned} \sum_{s=m+1-b}^{\infty} e^{-\sigma^2 s^2} e^{-is(\phi+a)} (-1)^s i^{-s} &= \sum_{s=m+1-b}^{\infty} \sigma \frac{\sqrt{\pi}}{\sigma} \frac{e^{-\sigma^2 s^2}}{\sqrt{\pi}} \exp\left[-i\sigma s \frac{\phi + a - (\tau/2) \pm \pi - \pi}{\sigma} \right] \\ &= \frac{\sqrt{\pi}}{\sigma} \int_{(m-b)/\sigma}^{\infty} dx \frac{e^{-x^2}}{\sqrt{\pi}} \exp\left[-ix \frac{\phi + a - (\pi/2) \pm \pi - \pi}{\sigma} \right] , \end{aligned} \tag{59b}$$

where we have also used $-1 = e^{i\pi}$. Notice that the lower limit of the last integral is $(m-b)/\sigma$ and not $(m+1-b)/\sigma$ because the differential dx matches the interval from $m-b$ to $m+1-b$. We may now express $A_m(1)$ as

$$A_m(1)=\frac{1}{2\pi}\int_{-\pi}^{\pi}d\phi\, e^{i\kappa\sin\phi}\left[\frac{\pi}{2\sigma^2}\right]^{-1/4}e^{-im^2\tau/2}\frac{\sqrt{\pi}}{\sigma}$$
$$\times\left[\int_{-\infty}^{(m-b)/\sigma}dx\frac{e^{-x^2}}{\sqrt{\pi}}\exp\left[ix\frac{\phi-a+(\pi/2)\mp\pi}{\sigma}\right]i^{m-b}e^{-i(m-b)}\right.$$
$$\left.+\int_{(m-b)/\sigma}^{\infty}dx\frac{e^{-x^2}}{\sqrt{\pi}}\exp\left[-ix\frac{\phi+a-(\pi/2)\pm\pi-\pi}{\sigma}\right]i^{m-b}(-1)^{m-b}e^{-i(b-m)\phi}\right]. \tag{60}$$

Three cases must be considered: $m>b$, $m<b$, and $m=b$. For sufficiently small σ, the upper limit of the first x integral and the lower limit of the second x integral may be replaced by ∞, $-\infty$, and 0 for $m>b$, $m<b$, and $m=b$, respectively. This means that for $m>b$, only the first integral contributes, that for $m<b$, only the second contributes, and for $m=b$ both integrals contribute. Therefore we obtain for $m>b$:

$$A_m(1)=\left[\frac{\pi}{2\sigma^2}\right]^{-1/4}e^{-im^2\tau/2}i^{m-b}\int_{-\pi}^{\pi}d\phi\, e^{i\kappa(\sin\phi)-i(m-b)\phi}\frac{\exp\left[-\frac{[\phi-a+(\pi/2)\mp\pi]^2}{4\sigma^2}\right]}{(4\pi\sigma^2)^{1/2}}, \tag{61a}$$

for $m<b$:

$$A_m(1)=\left[\frac{\pi}{2\sigma^2}\right]^{-1/4}e^{-im^2\tau/2}(-i)^{m-b}\int_{-\pi}^{\pi}d\phi\, e^{i\kappa(\sin\phi)-i(b-m)\phi}\frac{\exp\left[-\frac{[\phi+a-(\pi/2)\pm\pi-\pi]^2}{4\sigma^2}\right]}{(4\pi\sigma^2)^{1/2}}, \tag{61b}$$

and for $m=b$:

$$A_m(1)=\left[\frac{\pi}{2\sigma^2}\right]^{-1/4}e^{-ib^2\tau/2}\frac{1}{2}\int_{-\pi}^{\pi}d\phi\, e^{i\kappa(\sin\phi)}\left\{\frac{\exp\left[-\frac{[\phi-a+(\pi/2)\mp\pi]^2}{4\sigma^2}\right]}{(4\pi\sigma^2)^{1/2}}\right.$$
$$\times\left[1-i\frac{\phi-a+(\pi/2)\mp\pi}{\sqrt{\pi}\sigma}{}_1F_1\left[\frac{1}{2};\frac{3}{2};\frac{[\phi-a+(\pi/2)\mp\pi]^2}{4\sigma^2}\right]\right]$$
$$+\frac{\exp\left[-\frac{[\phi+a-(\pi/2)\pm\pi-\pi]^2}{4\sigma^2}\right]}{(4\pi\sigma^2)^{1/2}}$$
$$\left.\times\left[1-i\frac{\phi+a-(\pi/2)\pm\pi-\pi}{\sqrt{\pi}\sigma}\times{}_1F_1\left[\frac{1}{2};\frac{3}{2};\frac{[\phi+a-(\pi/2)\pm\pi-\pi]^2}{4\sigma^2}\right]\right]\right\}, \tag{61c}$$

in which ${}_1F_1$ is a degenerate hypergeometric function. In order to execute the remaining ϕ integrations we again use the fact that for sufficiently small σ, the Gaussian integrands are very sharply peaked. In (61a) and in the first term on the right-hand side of (61c) we change variables to $\eta=\phi-a+(\pi/2)\mp\pi$, whereas in (61b) and in the second term on the right-hand side of (61c) we change variables to $\eta=\phi+a-(\pi/2)\pm\pi-\pi$. Now each Gaussian is centered around $\eta=0$. However, the limits of integrations have shifted. The results of these changes are for $m>b$:

$$A_m(1)=\left[\frac{\pi}{2\sigma^2}\right]^{-1/4}e^{-im^2\tau/2}i^{m-b}\int_{-a-(\pi/2)\mp\pi}^{-a+(3\pi/2)\mp\pi}d\eta\exp\left\{i\kappa\left[\sin\left[\eta+a-\frac{\pi}{2}\pm\pi\right]\right]\right.$$
$$\left.-i(m-b)\left[\eta+a-\frac{\pi}{2}\pm\pi\right]\right\}\frac{\exp(-\eta^2/4\sigma^2)}{(4\pi\sigma^2)^{1/2}}, \tag{62a}$$

for $m<b$:

$$A_m(1)=\left[\frac{\pi}{2\sigma^2}\right]^{-1/4}e^{-im^2\tau/2}(-i)^{m-b}$$
$$\times\int_{a-(3\pi/2)\pm\pi-\pi}^{a+(\pi/2)\pm\pi-\pi}d\eta\exp\left\{i\kappa\left[\sin\left[\eta-a+\frac{\pi}{2}\mp\pi+\pi\right]\right]-i(b-m)\left[\eta-a+\frac{\pi}{2}\mp\pi+\pi\right]\right\}\frac{\exp(-\eta^2/4\sigma^2)}{(4\pi\sigma^2)^{1/2}}, \tag{62b}$$

and for $m=b$:

$$A_m(1)=\left[\frac{\pi}{2\sigma^2}\right]^{-1/4} e^{-ib^2\tau/2}\,{}_1\!/_2$$
$$\times\left[\int_{-a-(\pi/2)\mp\pi}^{-a+(3\pi/2)\mp\pi} d\eta\exp\left\{i\kappa\left[\sin\left[\eta+a-\frac{\pi}{2}\pm\pi\right]\right]\right\}\frac{\exp(-\eta^2/4\sigma^2)}{(4\pi\sigma^2)^{1/2}}\left[1-i\frac{\eta}{\sqrt{\pi}\sigma}\,{}_1F_1\left[\frac{1}{2};\frac{3}{2};\frac{\eta^2}{4\sigma^2}\right]\right]\right.$$
$$\left.+\int_{a-(3\pi/2)\pm\pi-\pi}^{a+(\pi/2)\pm\pi-\pi} d\eta\exp\left\{i\kappa\left[\sin\left[\eta-a+\frac{\pi}{2}\mp\pi+\pi\right]\right]\right\}\frac{\exp(-\eta^2/4\sigma^2)}{(4\pi\sigma^2)^{1/2}}\right.$$
$$\left.\times\left[1-i\frac{\eta}{\sqrt{\pi}\sigma}\,{}_1F_1\left[\frac{1}{2};\frac{3}{2};\frac{\eta^2}{4\sigma^2}\right]\right]\right]. \tag{62c}$$

Now, observe that

$$e^{-i(m-b)[\eta+a-(\pi/2)\pm\pi]}=e^{-i(m-b)\eta}e^{-i(m-b)a}(-i)^{m-b} \tag{63a}$$

and that

$$e^{-i(b-m)[\eta-a+(\pi/2)\mp\pi+\pi]}=e^{-i(b-m)\eta}e^{-i(m-b)a}i^{m-b}\,. \tag{63b}$$

We will also employ the Taylor expansions

$$\sin\left[\eta+a-\frac{\pi}{2}\pm\pi\right]=\sin\left[a-\frac{\pi}{2}\pm\pi\right]+\eta\cos\left[a-\frac{\pi}{2}\pm\pi\right]-\tfrac{1}{2}\eta^2\sin\left[a-\frac{\pi}{2}\pm\pi\right]+O(\eta^3)$$
$$=(\cos a)-\eta(\sin a)-\tfrac{1}{2}\eta^2(\cos a)+O(\eta^3) \tag{64a}$$

and

$$\sin\left[\eta-a+\frac{\pi}{2}\mp\pi+\pi\right]=\sin\left[-a+\frac{\pi}{2}\mp\pi+\pi\right]+\eta\cos\left[-a+\frac{\pi}{2}\mp\pi+\pi\right]-\tfrac{1}{2}\eta^2\sin\left[a+\frac{\pi}{2}\mp\pi+\pi\right]+O(\eta^3)$$
$$=(\cos a)+\eta(\sin a)-\tfrac{1}{2}\eta^2(\cos a)+O(\eta^3)\,. \tag{64b}$$

We are now in a position to determine whether to use the upper or lower sign in each of these expressions, which till now have carried this ambiguity along. The objective is to span $\eta=0$. In (62a) and in the corresponding integral in (62c), the upper sign is used for $a\in[0,\pi/2]$ and the lower sign is used for $a\in[\pi/2,2\pi]$, whereas in (62b) and in the corresponding integral in (62c), the upper sign is used for $a\in[0,3\pi/2]$ and the lower sign is used for $a\in[3\pi/2,2\pi]$. The smallness of σ implies that once we have spanned $\eta=0$, we can replace the upper and lower limits of integration by $+\infty$ and $-\infty$, respectively, to a very high degree of approximate accuracy (to be discussed in greater detail later). The result, for all three cases, is

$$A_m(1)=\left[\frac{\pi}{2\sigma^2}\right]^{-1/4} e^{-im^2\tau/2}e^{-i(m-b)a+i\kappa\cos a}\exp\left[-\tfrac{1}{2}(\kappa\sin a+m-b)^2\left[\frac{1}{2\sigma^2}+i\kappa\cos a\right]^{-1}\right][(1+2i\kappa\sigma^2\cos a)^{-1}]^{1/2}\,, \tag{65a}$$

provided $\kappa\sigma^3\ll 1$. This provision is required in order to ignore the $O(\eta^3)$ terms in (64a) and (64b). However, we find that the order η^2 terms in (64a) and (64b) change the variance in $\exp(-\eta^2/4\sigma^2)$, which is $2\sigma^2$, into $(1/2\sigma^2+i\kappa\cos a)^{-1}$. Our use of the sharply peakedness of the Gaussian requires the further provision that $\kappa\sigma^2\ll 1$, in order that we can safely ignore the increase in the variance that is created by the imaginary term $i\kappa\cos a$. If $\kappa\sigma^2\ll 1$, then the condition $\kappa\sigma^3\ll 1$ is certainly guaranteed since σ is so small. We will, therefore, assume that $\kappa\sigma^2\ll 1$ in order to write

$$A_m(1)=\left[\frac{\pi}{2\sigma^2}\right]^{-1/4} e^{i\kappa\cos a}e^{i(b-m)a}e^{-im^2\tau/2}$$
$$\times e^{-\sigma^2[b-\kappa(\sin a)-m]^2}\,. \tag{65b}$$

Note that if we combine the notation used in (49) and (51) with that used in (40) and (41), the classical map, we may write

$$b_{n+1}=b_n-\kappa\sin a_n\,, \tag{66a}$$

$$a_{n+1}=a_n+b_{n+1}\tau\,, \tag{66b}$$

so that, in particular, we would have

$$b_1=b-\kappa\sin a\,, \tag{67}$$

$$a_1=a+b_1\tau\,. \tag{68}$$

We see the combination (67) in (65b), but not the combination (68). This is because there are two m^2 factors in (65b) and we must combine them (by "completing the square") before we see everything in proper form. After a bit of tedious algebra, (65b) transforms exactly into

$$A_m(1)=\left[\frac{\pi}{2\sigma^2}\right]^{-1/4} e^{i\kappa\cos a}e^{iba}\exp\left[\left[\frac{b-\kappa\sin a}{1+\tau^2/4\sigma^4}\right]^2\left[i\frac{\tau}{2}-\frac{\tau^2}{2\sigma^2}-\frac{\tau^4}{16\sigma^6}\right]\right]$$
$$\times\exp\left[-im\left[a+\frac{\tau(b-\kappa\sin a)}{1-i\tau/2\sigma^2}\right]\right]\exp\left[-(\sigma^2+i\tau/2)\left[m-\frac{(b-\kappa\sin a)}{1+\tau^2/4\sigma^4}\right]^2\right]. \tag{69}$$

Let us suppose that not only is σ very small but that $\tau/\sigma^2\ll 1$ as well. We will discuss the physical meaning of this supposition in detail, below. Keeping terms to first order in τ/σ^2 yields

$$A_m(1)=\left[\frac{\pi}{2\sigma^2}\right]^{-1/4} e^{i[\kappa\cos a+ba+(\tau/2)(b-\kappa\sin a)^2]}e^{-im[a+\tau(b-\kappa\sin a)]}e^{-(\sigma^2+i\tau/2)[m-(b-\kappa\sin a)]^2}. \tag{70}$$

This is to be compared with $A_n(0)$ of (55). There are four changes created by the map. The phase factor e^{iba} in (55) is more complicated in (70). We show below that this phase factor has no effect on θ or p_θ expectation values. The e^{-ina} factor in (55) has become $e^{-im[a+\tau(b-\kappa\sin a)]}$ in (70). This exhibits the classical map (68) of the angle. The factor $e^{-\sigma^2(b-n)^2}$ of (55) has become $e^{-(\sigma^2+i\tau/2)[m-(b-\kappa\sin a)]^2}$ of (70). This exhibits the classical map (67) of the momentum, and a change in the variance from σ^2 to $\sigma^2+i\tau/2$. This last change is identical to what happens to the variance for a free particle Gaussian wave packet, and as in that case, may be reinterpreted by reverting to $\psi(\theta,1)$, as we must do for the phase factor discussion.

The key point is that if $\sigma\ll 1$, $\kappa\sigma^2\ll 1$, *and* $\tau/\sigma^2\ll 1$, then the form of the minimum uncertainty wave-packet coefficients (55) is preserved, except for a slight increase in the variance. Obviously, this feature will persist for many iterations of the map until the variance has grown too much. The time for this to happen will be of order σ^2/τ. More will be said about this later.

Many of the discussion points we have deferred till later hinge on the structure of $\psi(\theta,1)$ which we obtain from (70) by the inverse process used in (55):

$$\psi(\theta,1)=\frac{1}{\sqrt{2\pi}}\sum_{m=-\infty}^{\infty}A_m(1)e^{im\theta}$$
$$=\frac{1}{\sqrt{2\pi}}\sum_{m=-\infty}^{\infty}\left[\frac{\pi}{2\sigma^2}\right]^{-1/4}e^{i[\kappa\cos a+ba+(\tau/2)(b-\kappa\sin a)^2]}e^{im\{\theta-[a+\tau(b-\kappa\sin a)]\}}e^{-(\sigma^2+i\tau/2)[m-(b-\kappa\sin a)]^2}$$
$$=\frac{1}{\sqrt{2\pi}}\sum_{m=-\infty}^{\infty}\left[\frac{\pi}{2\sigma^2}\right]^{-1/4}e^{i\gamma}e^{im(\theta-\alpha)}e^{-(\sigma^2+i\tau/2)(m-\beta)^2}, \tag{71}$$

wherein the last line defines α, β, and γ for ease of computation. Therefore we get

$$\psi(\theta,1)\cong\frac{1}{\sqrt{2\pi}}\left[\frac{\pi}{2\sigma^2}\right]^{-1/4}\left[\frac{\pi}{\sigma^2+i\tau/2}\right]^{1/2}e^{i\gamma}\int_{-\infty}^{\infty}dx\,e^{ix(\theta-\alpha)/(\sigma^2+i\tau/2)^{1/2}}\frac{e^{-[x-(\sigma^2+i\tau/2)^{1/2}\beta]^2}}{\sqrt{\pi}}$$
$$=(2\pi)^{-1/4}\frac{\sigma^{1/2}}{(\sigma^2+i\tau/2)^{1/2}}e^{i\gamma}e^{i\beta(\theta-\alpha)}\exp\left[-\frac{1}{4}\frac{(\theta-\alpha)^2}{\sigma^2+i\tau/2}\right]. \tag{72}$$

Thus

$$|\psi(\theta,1)|^2=\frac{1}{\sqrt{2\pi}}\frac{\sigma}{(\sigma^4+\tau^2/4)^{1/2}}$$
$$\times\exp\left[-\tfrac{1}{2}(\theta-\alpha)^2\frac{\sigma^2}{\sigma^4+\tau^2/4}\right] \tag{73}$$

as compared with [remember: $\alpha=a+\tau(b-\kappa\sin a)$]

$$|\psi(\theta,0)|^2=\frac{1}{(2\pi\sigma^2)^{1/2}}\exp\left[-\tfrac{1}{2}(\theta-a)^2\frac{1}{\sigma^2}\right]. \tag{74}$$

For sufficiently small σ, we see that the overwhelmingly dominant Gaussian in (48), centered at a, has moved its center to $a+\tau(b-\kappa\sin a)$, the classical map shift, and that the variance has grown from σ^2 to $\sigma^2(1+\tau^2/4\sigma^4)$. As far as expectation values of θ or its powers are concerned, the phase factor, $\gamma=\kappa\cos a+ba+(\tau/2)(b-\kappa\sin a)^2$, which was just ba in (55), is of no consequence.

Equations (55) and (70) can be used to write

$$|A_n(0)|^2=\left[\frac{\pi}{2\sigma^2}\right]^{-1/2}e^{-2\sigma^2(b-n)^2} \tag{75}$$

and

$$|A_m(1)|^2=\left[\frac{\pi}{2\sigma^2}\right]^{-1/2}e^{-2\sigma^2[m-(b-\kappa\sin a)]^2}, \tag{76}$$

which shows that the momentum probability distribution is also a normalized Gaussian. According to (24), the expectation values of p_θ and its powers depend on these squared moduli, and are, therefore, independent of the phase factors. Finally, note that because the phase factor has no index dependence (n or m), it cannot even affect cross correlations between θ and p_θ or their powers.

By repeating the mapping, the structure of (70) remains invariant. The a's and b's evolve according to (66a) and (66b), the phase gets more complicated—but remains inconsequential, and the variance grows through the factor $\sigma^2+Ni\tau/2$ where N is the number of iterations of the map. This makes the variance in $|\psi(\theta,N)|^2$ equal to $\sigma^2(1+N^2\tau^2/4\sigma^4)$, so that we get a factor of 2 increase in σ^2 when

$$N_2=\frac{2\sigma^2}{\tau} . \tag{77}$$

This is a large number when the condition $\tau/\sigma^2\ll 1$ is satisfied. Recall that σ measures the variance around $\langle\theta\rangle$. It is dimensionless. Let us take it to be 10^{-8}. This is very small. Nevertheless, p_θ is an angular momentum, which means its units are the same as those for $\hbar$, i.e., action. The variance around $\langle p_\theta\rangle$ was found to be $\hbar/2\sigma$. For $\sigma=10^{-8}$, this is $10^{-27}/(2\times10^{-8})$ erg sec$=5\times10^{-20}$ erg sec. Now, for a typical small molecule in thermal equilibrium at room temperature, the value for $\langle p_\theta\rangle$ is of order 10^{-26} erg sec. Thus a variance of 10^{-19} erg sec is very large from a molecular perspective, i.e., a quantum perspective, but from a classical viewpoint, the size of $\langle p_\theta\rangle$ is of order 1 erg sec. That is to say, classically we would deal with an object measured by grams and centimeters on a time scale measured in seconds. Consequently, if the b in (51) is a classical b, then it is of order 10^{27}, which makes a variance of 10^{-19} erg sec very small indeed (compared with $hb=10^{-27}\times10^{27}$ erg sec). Similarly, the definition of τ, (13), for a classical pendulum, being kicked classically, would involve factors of τ/ml^2 of order 1 (erg sec)$^{-1}$. Thus τ would have the dimensionless value 10^{-27}. Therefore, with $\sigma=10^{-8}$, we find $\tau/\sigma^2=10^{-27}/10^{-16}=10^{-11}\ll1$, which implies that $N_2=2\sigma^2/\tau=2\times10^{11}$. Since each map iteration corresponds with a kick, the time over which N_2 kicks take place is N_2T, i.e., of order 10^{11} sec$\sim$30 000 years! Note that this result is inversely proportional to $\hbar$.

We have checked the propagation of the Gaussian form of the wave packet by numerical computation. Needless to say, we found it much easier to use rather smaller values of the exponents for the various parameters. We chose $b=10^6$, $\hbar=10^{-6}$, $\tau=10^{-6}$, $\kappa=10^2$, and $\sigma=10^{-2}$. These choices imply $N_2=200$. With 14 digits of accuracy, computing on a Cyber 855, we verified the repeated propagation of Eq. (70). This numerical confirmation of our formulas provides a great deal of confidence in the approximations used.

VI. THE CORRESPONDENCE LIMIT

The correspondence limit is some appropriate limit in which the Ehrenfest formulation of the quantum map, Eqs. (28) and (39), is indistinguishable from the classical map, Eqs. (40) and (41). We have already seen that for very small σ, the initial expectation values for θ and p_θ can match the classical values a and b, respectively, and that after one iteration of the map the new expectation values match the classical iterates [Eqs. (66)–(68)]. In fact, the invariance of the Gaussian wave packet under the mapping (for very small σ, $\kappa\sigma^2\ll1$, and for $\tau/\sigma^2\ll1$) suggests that this "correspondence" will continue. Of course, the variance is slowly growing during this process, and we used this fact to deduce the N_2 bound on the number of iterations allowed before the variance doubles to $2\sigma^2$. This is not the only relevant consideration for the correspondence limit. The quantum mapping in the Ehrenfest formulation, Eq. (28), involves the nonlinear expectation value: $\langle\sin\theta(n)\rangle$. For the classical mapping correspondence, $\langle\sin\theta(n)\rangle$ must be compared with $\sin\langle\theta(n)\rangle$, i.e., the expectation of a nonlinear function must be compared to the nonlinear function of the expectation. Only if these two quantities are very close in value can the correspondence hold.

Looking back at (73), and recalling the ensuing discussion, we may conclude that for $N<N_2$ (and $\sigma\ll1$, $\kappa\sigma^2\ll1$, and $\tau/\sigma^2\ll1$):

$$|\psi(\theta,N)|^2=\frac{1}{\sqrt{2\pi}}\frac{1}{(\sigma^2+N^2\tau^2/4\sigma^2)^{1/2}}\times\exp\left[-\tfrac{1}{2}(\theta-\alpha_N)^2\frac{\sigma^2}{\sigma^4+N^2\tau^2/4}\right], \tag{78}$$

where α_N is the Nth classical iterate of θ starting from $\theta=a$ initially. Now, the key is that this θ distribution is Gaussian. Therefore

$$\begin{aligned}\langle\sin\theta(N)\rangle&=\frac{1}{2i}\left[\langle e^{i\theta(N)}\rangle-\langle e^{-i\theta(N)}\rangle\right]\\&=\frac{1}{2i}\left[e^{i\alpha_N}e^{-(1/2)(\sigma^2+N^2\tau^2/4\sigma^2)}-e^{-i\alpha_N}e^{-(1/2)(\sigma^2+N^2\tau^2/4\sigma^2)}\right]\\&=\sin\alpha_N e^{-(1/2)(\sigma^2+N^2\tau^2/4\sigma^2)} .\end{aligned} \tag{79}$$

Moreover, (78) implies, consistent with all of the previous discussion, that $\alpha_N=\langle\theta(N)\rangle$. Therefore, even if $N=N_2$, $\langle\sin\theta(N)\rangle$ and $\sin\langle\theta(N)\rangle$ differ by a factor of only $(1-e^{-\sigma^2})$ which for $\sigma\ll1$ is very accurately approximated by σ^2, i.e.,

$$\frac{|\langle\sin\theta(N_2)\rangle-\sin\langle\theta(N_2)\rangle|}{\langle\sin\theta(N_2)\rangle}=\sigma^2\ll1 . \tag{80}$$

In Sec. V we used the value $\sigma=10^{-8}$, which in that context implied $N_2=2\times10^{11}$. In that number of iterations, the error given in (80) will have grown to $2\times10^{11}\times10^{-16}=2\times10^{-5}$, which may still be considered quite acceptable accuracy from a numerical point of view, and is certainly unnoticed graphically. In our numerical computations, this error became 2×10^{-2}.

No other nonlinear terms appear in the Ehrenfest formulation of the quantum mapping, Eqs. (28) and (39). However, there is still the question of the behavior of the boundary-value terms for $\sigma\ll1$ and $\tau/\sigma^2\ll1$. There

are two approaches to this question: a direct evaluation, and an indirect evaluation. The direct evaluation utilizes the asymptotic expressions for Bessel functions:

$$J_{\pm\nu}(\kappa)\cong\left[\frac{2}{\pi\kappa}\right]^{1/2}\left[\cos\left[\kappa\mp\frac{\pi}{2}\nu-\frac{\pi}{4}\right]+O\left[\frac{1}{\kappa}\right]\right] \tag{81}$$

for very large κ.

From (9), it is seen that κ is inversely proportional to $\hbar$. Thus, in the correspondence limit, as $\hbar\to 0$, κ becomes enormous. Moreover, from (16) we also see that

$$\kappa\tau=\omega_0^2T^2\ . \tag{82}$$

If we choose values of ω_0 and T so that ω_0T is of order unity, then κ and τ are essentially reciprocals of each other. The parameter values chosen in Sec. V that made $\tau\sim 10^{-27}$ will now make $\kappa\sim 10^{27}$. Thus κ is very large indeed. This means that to very high accuracy, (81) may be used to replace the Bessel functions in (39) by their asymptotic cosines. It turns out that when the factor i^{k-l} in (39) is replaced by $e^{i(\pi/2)(k-l)}$, and one repeatedly uses the $(k,l)\leftrightarrow(-k,-l)$ dummy index exchange, along with the integer character of l and k, the k,l summation identically vanishes. A few key steps are given in the following lines:

$$\begin{aligned}S&\equiv\sum_{k,l=-\infty}^{\infty}i^{k-l}J_k(\kappa)J_l(\kappa)i\\&\quad\times\frac{1-\exp\{i(\tau/2)[(s+l)^2-(r+k)^2]\}}{(r+k)-(s+l)}\\&=\sum_{k,l=-\infty}^{\infty}i^{k-r-(l-s)}J_{k-r}(\kappa)J_{l-s}(\kappa)i\\&\quad\times\frac{1-\exp\{i(\tau/2)[(l^2-k^2)\}}{k-l}\end{aligned} \tag{83}$$

because of the index change: $(k,l)\to(k-r,l-s)$. Now, use (81) to write

$$\begin{aligned}S&\cong i^{s-r}\sum_{k,l=-\infty}^{\infty}i^{k-l}\frac{2}{\pi\kappa}\cos\left[\kappa-\frac{\pi}{2}(k-r)-\frac{\pi}{4}\right]\cos\left[\kappa-\frac{\pi}{2}(l-s)-\frac{\pi}{4}\right]\frac{e^{i(\tau/2)(l^2-k^2)}-1}{l-k}\\&=i^{s-r}\sum_{k,l=-\infty}^{\infty}\frac{1}{\pi\kappa}\left[\sin\left[2\kappa-\frac{\pi}{2}(k+l)\right]\cos\left[\frac{\pi}{2}(r+s)\right]+\cos\left[2\kappa-\frac{\pi}{2}(k+l)\right]\sin\left[\frac{\pi}{2}(r+s)\right]\right.\\&\quad\left.+\cos\left[\frac{\pi}{2}(l-k)\right]\cos\left[\frac{\pi}{2}(r-s)\right]-\sin\left[\frac{\pi}{2}(l-k)\right]\sin\left[\frac{\pi}{2}(r-s)\right]\right]e^{i(\pi/2)(k-l)}\frac{e^{i(\tau/2)(l^2-k^2)}-1}{l-k}\ ,\end{aligned} \tag{84}$$

wherein the last expression follows from application of elementary trigonometric identities. Now, $(k,l)\leftrightarrow(-k,-l)$, and the fact that $\sin(n\pi)=0$ for any integer n, may be used to show that $S=0$.

On the one hand, this is very satisfying. In the correspondence limit (i.e., $\hbar\to 0$) $\kappa\to\infty$ and $S\equiv 0$. However, one should now look at the first correction to (81) to see how large this boundary-value term really is as the limit is approached. This means we should use

$$\begin{aligned}J_{\pm\nu}(\kappa)\cong\left[\frac{2}{\pi\kappa}\right]^{1/2}&\left[\cos\left[\kappa\mp\frac{\pi}{2}\nu-\frac{\pi}{4}\right]\right.\\&-\frac{\nu^2-\frac{1}{4}}{2\kappa}\sin\left[\kappa\mp\frac{\pi}{2}\nu-\frac{\pi}{4}\right]\\&\left.+O\left[\frac{1}{\kappa^2}\right]\right]\ .\end{aligned} \tag{85}$$

When this is used instead of (81), the k,l summations are very much more difficult and no simple expressions are obtained. All we can say is that the next corrections to $S\equiv 0$ are each of order $1/\kappa^2$, but the k,l summation is doubly infinite, so this is of no real help. Further work on the direct evaluation method may well prove fruitful, and there is no reason to expect a surprise.

The indirect approach obviates the need to properly conclude the preceding approach. The size of the boundary-value term in (39) can also be approached by estimating the size of $\langle\theta(n+1)\rangle-\langle\theta(n)\rangle-(\tau/\hbar)\langle p_\theta(n+1)\rangle$. But from what we have already seen, if we keep the number of iterations $n<N_2$, then the Gaussian, minimum uncertainty wave packet evolves in time preserving its Gaussian form (provided $\sigma\ll 1$ and $\tau/\sigma^2\ll 1$), and we find

$$\langle\theta(n+1)\rangle=a_{n+1}\ , \tag{86}$$

$$\langle\theta(n)\rangle=a_n\ , \tag{87}$$

$$\langle p_\theta(n+1)\rangle=\hbar b_{n+1}\ , \tag{88}$$

which satisfy the classical mapping, Eqs. (66a) and (66b). It would appear that $\langle\theta(n+1)\rangle-\langle\theta(n)\rangle-(\tau/\hbar)\langle p_\theta\langle n+1\rangle\rangle=0$. However, both (49) and (51) remind us that these identities are approximate because of the approximation in doing the integrals:

$$\begin{aligned}\int_0^{2\pi}d\theta\frac{1}{(2\pi\sigma^2)^{1/2}}\exp\left[-\frac{(\theta-a)^2}{2\sigma^2}\right]\cdots\\\to\int_{-\infty}^{\infty}d\theta\frac{1}{(2\pi\sigma^2)^{1/2}}\exp\left[-\frac{(\theta-a)^2}{2\sigma^2}\right]\cdots\ .\end{aligned} \tag{89}$$

Therefore identities (86)–(88) are approximate and a detailed inspection of the approximation in (89) brings in error functions, which for $\sigma\ll 1$, introduces a measure of the error made by the approximation. This error is obtained by noticing

$$\int_0^{2\pi} d\theta \frac{1}{(2\pi\sigma^2)^{1/2}} \exp\left[-\frac{(\theta-a)^2}{2\sigma^2}\right] \cdots = \int_{-a}^{2\pi-a} dx \frac{1}{(2\pi\sigma^2)^{1/2}} e^{-x^2/2\sigma^2} \cdots$$

$$= \frac{1}{\sqrt{\pi}} \int_{-a/\sqrt{2}\sigma}^{(2\pi-a)/\sqrt{2}\sigma} dt\, e^{-t^2} \cdots$$

$$= \frac{1}{\sqrt{\pi}} \int_{-\infty}^{\infty} dt\, e^{-t^2} \cdots - \frac{1}{\sqrt{\pi}} \int_{(2\pi-a)/\sqrt{2}\sigma}^{\infty} dt\, e^{-t^2} \cdots$$

$$- \frac{1}{\sqrt{\pi}} \int_{-\infty}^{-a/\sqrt{2}\sigma} dt\, e^{-t^2} \cdots . \tag{90}$$

Now, provided that whatever the integrand factor represented by $\cdots$ happens to be, that it is not growing exponentially with t^2 (it is not for either θ or p_θ), then the two negative corrections may be estimated by the asymptotic formulas for the complementary error function, and are $\exp[-(2\pi-a)^2/2\sigma^2]$ and $\exp(-a^2/2\sigma^2)$, respectively. These are extremely small for $\sigma \ll 1$, except when a is extraordinarily close (within σ) to either 0 or 2π. Even for the classical map, these are unusual θ values since the θ variable evolves mod2π. In conclusion, we see that while the boundary-value term in (39) cannot be precisely zero, it is extremely small for $\sigma \ll 1$.

We have now exhausted the considerations associated with the correspondence limit which takes (28) and (39) into (40) and (41). Two limits are required, and their order is crucial. We must have $\sigma \ll 1$ and $\tau/\sigma^2 \ll 1$, $\tau/\sigma^2 \to 0$ must precede $\sigma \to 0$. $\tau \to 0$ is the same as $\hbar \to 0$ if all other physical parameters (m, l, ω_0, T) are fixed. As $\tau/\sigma^2 \to 0$, $N_2 \to \infty$. This may be phrased in the following form: as $\hbar \to 0$, the length of time for which the Ehrenfest formulation of the quantum map shadows the classical map with an error of order $\sigma^2 N_2$ is $N_2 T$. The quantity $\sigma^2 N_2$ occurred in the $\langle \sin\theta(N) \rangle$ analysis [see Eq. (80)]. Therefore we want

$$\tau/\sigma^2 \to 0 \quad (N_2 \to \infty) , \tag{91}$$

$$\sigma \to 0 , \tag{92}$$

$$\sigma^2 N_2 \to 0 , \tag{93}$$

as a succession of limits in the order given. These multiple desires may be achieved easily by the following scaling argument. We already have $\tau \sim \hbar$. Suppose $\sigma \sim \hbar^\epsilon$, such that $\epsilon > 0$, which guarantees (92). Limits (91) and (93) require, respectively,

$$1-2\epsilon > 0 \quad \text{and} \quad 4\epsilon - 1 > 0 , \tag{94}$$

which is satisfied by

$$\tfrac{1}{2} > \epsilon > \tfrac{1}{4} . \tag{95}$$

Therefore the error $\sigma^2 N_2$ goes to zero as the length of time $N_2 T$ goes to infinity in the correspondence limit.

However, our analysis also requires $\kappa\sigma^2 \ll 1$ in order that the Gaussian wave packet propagates in time as a Gaussian wave packet. Equation (82) tells us that $\kappa\sigma^2 \ll 1$ and $\tau/\sigma^2 \ll 1$ require

$$\omega_0 T \ll 1 . \tag{96}$$

For the classical map, it is known[6] that the time evolution is predominantly nonchaotic or very weakly chaotic in this parameter regime. Thus we have shown the validity of the correspondence limit (both with formulas and by numerical computation) only for the situation wherein the classical map is not chaotic or only very weakly chaotic. In addition, the details of the analysis in Sec. V clearly show that for $\omega_0 T = 1$, say, so that $\kappa\sigma^2 \gg 1$, the straightforward Gaussian integration we employed is invalid. This means that the minimum uncertainty wave packet does not propagate as such, even for a single iteration of the maps. We were also able to confirm this numerically. In short, the same derivation fails to hold for parameter values for which the classical map can produce strong chaos.

In a sequel to this paper, we will present our numerical evidence for the assertion that the quantum time evolution and the classical time evolution are different when the parameter values correspond with strong classical chaos.

VII. CONCLUDING REMARKS

The preceding study shows how the trajectories (mappings) of quantum expectation values can mimic the corresponding classical trajectories, and under what conditions. The correspondence limit is an ordered, double limit and the error in the mimicry gets smaller for longer times as the limit is approached. However, this correspondence limit holds only for parameter values for which the classical map produces no chaos or is only very weakly chaotic. For parameter values for which the classical map can be strongly chaotic, the same derivation fails, because the Gaussian, minimum uncertainty wave packet does not propagate as such. Instead, the quantum time evolution and the classical time evolution are different for initial starting conditions for which a minimum uncertainty wave packet has been constructed so that its expectation values match the classical initial conditions. Which time evolution is physically correct? Is the quantum time evolution also chaotic in its own way? These are questions we are actively pursuing with numerical computation.

It has been argued that because the Schrödinger equation is linear, it is not possible for quantum mechanics to exhibit chaos, a putative hallmark of nonlinearity. However, even for a classically chaotic system, it is possible to describe the classical mechanics of the phase-space trajectories by the Liouville equation for the trajectory distri-

bution function. The Liouville equation is linear and "lives" in a Hilbert space, in parallel with the Schrödinger equation. The Liouville equation always possesses a special solution which is a Dirac δ function distribution which precisely follows the classical trajectory emanating from a precise initial phase-space point. Thus, initially nearby Liouville distributions can exponentiate apart just like their corresponding classical trajectories. There is no conflict with the linearity of the Liouville equation, but there is the necessity that it possess a properly continuous eigenspectrum in the chaotic case. The same holds for the Schrödinger equation. If the Hamiltonian given in (1) has a continuous spectrum when treated quantum mechanically, then chaos is possible in the pure quantum mechanics. Since this Hamiltonian is time dependent it could well produce a continuous spectrum, but the spectral analysis is very difficult. It is perhaps noteworthy to remark that the Dirac δ function solution to Liouville's equation is an unstable solution for a chaotic trajectory. Since quantum mechanics implies that precise initial conditions for the classical trajectories are a physical impossibility, then an initial Dirac δ function for Liouville's equation is an idealization. Even the quantum uncertainty initially ($\hbar > 0$) will require the initial δ function to be replaced by a broader distribution, which the instability will cause to eventually grow to the order of the size of the available phase space.

When studying pure quantum chaos through expectation value trajectories, one generally will not have a minimum uncertainty wave packet, and each set of initial expectation values will correspond with a bundle of trajectories corresponding with all the different wave functions which have identical initial expectation values, but different subsequent time evolutions. For chaos we expect to see a positive Liapunov exponent for the separation of initially, closely adjacent expectation values for two sets of initial conditions, irrespectively of which pair of representative wave functions is chosen from the two bundles. This remains to be studied. It is also of interest to study the separation (or nonseparation) of two wave functions from the same bundle. We are in the midst of such studies (numerical) and hope to report our findings in the near future.

ACKNOWLEDGMENTS

This work was supported by National Science Foundation Grant No. PHY-8902549. We are indebted to Joseph Ford for numerous illuminating discussions.

APPENDIX

We have

$$e^{i\kappa\cos\theta} = \sum_{s=-\infty}^{\infty} i^s J_s(\kappa) e^{is\theta} , \tag{A1}$$

where J_s is a Bessel function.[10] Look at

$$\sum_{q=-\infty}^{\infty} qJ_{q-r}(\kappa)J_{q-s}(\kappa) = \sum_{k=-\infty}^{\infty} kJ_k(\kappa)J_{k+\nu}(\kappa) + r\sum_{k=-\infty}^{\infty} J_k(\kappa)J_{k+\nu}(\kappa) , \tag{A2}$$

where $k = q - r$ and $\nu = r - s$. Both series on the right-hand side may be evaluated using the Bessel function "summation theorem":[11]

$$e^{i\nu\psi}J_\nu(mR) = \sum_{k=-\infty}^{\infty} J_k(m\rho)J_{k+\nu}(mr)e^{ik\phi} ,$$

where

$$e^{2i\psi} = \frac{r-\rho e^{-i\phi}}{r-\rho e^{i\phi}} \quad \text{for } 0 < \psi \le \frac{\pi}{2}$$

and

$$R = (r^2+\rho^2-2r\rho\cos\phi)^{1/2} .$$

For $\rho = r$ and $\phi = 0$, $R = 0$, and

$$e^{2i\psi} = \left.\frac{1-e^{-i\phi}}{1-e^{i\phi}}\right|_{\phi=0} = -1 ,$$

which implies $\psi = \pi/2$. Therefore the summation theorem reduces to

$$e^{i\nu(\pi/2)}J_\nu(0) = \sum_{k=-\infty}^{\infty} J_k(\kappa)J_{k+\nu}(\kappa) .$$

For $\nu \ge 1$, $J_\nu(0) = 0$, and $J_0(0) = 1$. This implies

$$\sum_{k=-\infty}^{\infty} J_k(\kappa)J_{k+\nu}(\kappa) = \delta_{\nu,0} . \tag{A3}$$

The summation theorem may be used to write

$$\sum_{k=-\infty}^{\infty} kJ_k(\kappa)J_{k+\nu}(\kappa) = -i\frac{d}{d\phi}\sum_{k=-\infty}^{\infty} J_k(\kappa)J_{k+\nu}(\kappa)e^{ik\phi}\big|_{\phi=0} = -i\frac{d}{d\phi}[e^{i\nu\psi}J_\nu(\kappa\sqrt{2-2\cos\phi})]\big|_{\phi=0} .$$

First note that

$$-i\frac{d}{d\phi}J_\nu(\kappa\sqrt{2-2\cos\phi})\big|_{\phi=0} = J'_\nu(0)\kappa\tfrac{1}{2}(2-2\cos\phi)^{-1/2}2\sin\phi\big|_{\phi=0} = J'_\nu(0)\kappa\left.\frac{\sin\phi}{2\sin(\phi/2)}\right|_{\phi=0} = J'_\nu(0)\kappa$$

and that[12]

$$J'_\nu(0) = \tfrac{1}{2}[J_{\nu-1}(0) - J_{\nu+1}(0)] = \tfrac{1}{2}\delta_{\nu,1} - \tfrac{1}{2}\delta_{\nu,-1} .$$

Therefore

$$-i\frac{d}{d\phi}[e^{i\nu\psi}J_\nu(\kappa\sqrt{2-2\cos\phi})]\Big|_{\phi=0}$$
$$=-i\exp\left[i\nu\frac{\pi}{2}\right](\tfrac{1}{2}\delta_{\nu,1}-\tfrac{1}{2}\delta_{\nu,-1})_\kappa$$
$$-iJ_\nu(0)\frac{d}{d\phi}e^{i\nu\psi}\Big|_{\phi=0}.$$

However, $J_\nu(0)=\delta_{\nu,0}$ and

$$\frac{d}{d\phi}e^{i\nu\psi}\Big|_{\phi=0}=i\nu\exp\left[i\nu\frac{\pi}{2}\right]\frac{d\psi}{d\phi}\Big|_{\phi=0}.$$

But, $e^{2i\psi}=(1-e^{-i\phi})/(1-e^{i\phi})$ implies

$$2ie^{2i\psi}\frac{d\psi}{d\phi}\Big|_{\phi=0}=\frac{ie^{-i\phi}+ie^{i\phi}-2i}{(1-e^{i\phi})^2}\Big|_{\phi=0}=i.$$

Therefore

$$2i\exp\left[2i\frac{\pi}{2}\right]\frac{d\psi}{d\phi}\Big|_{\phi=0}=i$$

or

$$\frac{d\psi}{d\phi}\Big|_{\phi=0}=-\tfrac{1}{2}.$$

Consequently, we arrive at

$$-iJ_\nu(0)\frac{d}{d\phi}e^{i\nu\psi}\Big|_{\phi=0}=0,$$

and conclude that

$$-i\frac{d}{d\phi}[e^{i\nu\psi}J_\nu(\kappa\sqrt{2-2\cos\phi})]\Big|_{\phi=0}=\frac{\kappa}{2}(\delta_{\nu,1}+\delta_{\nu,-1})$$

and obtain

$$\sum_{k=-\infty}^{\infty}kJ_k(\kappa)J_{k+\nu}(\kappa)=\tfrac{1}{2}\kappa(\delta_{\nu,1}+\delta_{\nu,-1}). \tag{A4}$$

Put together, identities (A2)–(A4) yield

$$\sum_{q=-\infty}^{\infty}qJ_{q-r}(\kappa)J_{q-s}(\kappa)=\tfrac{1}{2}\kappa(\delta_{r-s,1}+\delta_{r-s,-1})+r\delta_{rs}. \tag{A5}$$

The proof for the well-known identity

$$e^{\alpha\theta}e^{\beta(\partial/\partial\theta)}=e^{\beta(\partial/\partial\theta)}e^{\alpha\theta}e^{-\alpha\beta}$$

may be generalized without great difficulty to produce the identity

$$e^{\alpha\theta}e^{\beta(\partial^2/\partial\theta^2)}=e^{\beta(\partial^2/\partial\theta^2)}e^{\alpha\theta}e^{-2\alpha\beta(\partial/\partial\theta)}e^{-\alpha^2\beta}. \tag{A6}$$

[1]A. J. Lichtenberg and M. A. Lieberman, *Regular and Stochastic Motion* (Springer-Verlag, New York, 1983), Chap. 5.

[2]R. Jensen, in *The Ubiquity of Chaos,* edited by S. Krasner (American Association for the Advancement of Science, Washington, DC, in press).

[3]R. F. Fox, in *The Ubiquity of Chaos,* edited by S. Krasner (American Association for the Advancement of Science, Washington, DC, in press).

[4]P. I. Belobrov, G. M. Zaslavskii, and G. Kh. Tartakovskii, Zh. Eksp. Theor. Fiz. **71**, 1799 (1976) [Sov. Phys.—JETP **44**, 945 (1977)].

[5]R. F. Fox and J. C. Eidson, Phys. Rev. A **36**, 4321 (1987).

[6]G. Casati, B. V. Chirikov, F. M. Izraliev, and J. Ford, in *Stochastic Behavior in Classical and Quantum Hamiltonian Systems,* Vol. 93 of *Lecture Notes in Physics,* edited by G. Casati and J. Ford (Springer, Berlin, 1979).

[7]V. I. Arnol'd and A. Avez, *Ergodic Problems of Classical Mechanics* (Benjamin, New York, 1968).

[8]J. H. Hannay and M. V. Berry, Physica **1D**, 267 (1980).

[9]J. Ford, G. Mantica, and G. H. Ristow (unpublished).

[10]I. S. Gradshteyn and I. M. Ryzhik, *Table of Integrals Series and Products,* 4th ed. (Academic, New York, 1965), formula 8.511(4).

[11]I. S. Gradshteyn and I. M. Ryzhik, Ref. 10, formula 8.530(2).

[12]I. S. Gradshteyn and I. M. Ryzhik, Ref. 10, formula 8.471(2).

Master equation for the logistic map

Ronald F. Fox
School of Physics, Georgia Institute of Technology, Atlanta, Georgia 30332
(Received 9 April 1990)

A master equation is constructed that provides a stochastic description underlying the logistic map. In an appropriate macroscopic limit, the underlying master map (equation) yields the logistic map. It also describes intrinsic fluctuations associated with the logistic map. When the logistic map parameters are chosen so that the map produces a chaotic trajectory, the variance of the associated fluctuations diverges. This means that the distribution function determined by the master map becomes very broad and that the logistic map no longer results from averaging with respect to the master map distribution function. Numerical examples of this behavior and its interpretation are discussed.

I. INTRODUCTION

There is a long tradition behind the description of macroscopic dissipative processes by phenomenological equations, e.g., hydrodynamics, electrical circuits, and mass action chemical reactions. It is now widely appreciated[1–8] that a complete macroscopic description of these processes must include intrinsic molecular fluctuations as well as the deterministic macrovariables, both of which reflect underlying microscopic dynamics.[1,2,8] Indeed, these fluctuations provide the basis for our understanding of light scattering,[9] electrical noise, and other noise measurements for macroscopic systems.[10] Recently, the effect of dynamical chaos on these ideas was explored in detailed and general ways.[11]

A general approach to the effect of chaos on macrovariable fluctuations is provided by the master equation idea.[10–20] Given a macrovariable dynamics, a master equation is constructed such that an appropriate macroscopic limit yields the macrovariable dynamics as well as a description of the fluctuations. The construction process involves the underlying physics.[8] For chemical reactions it is very well established how this construction works,[8,10,16,17] but for hydrodynamics it is not so straightforward, so that, to date, there is no single master equation for all fluid density regimes.[10,13–15]

The purpose of this paper is to exhibit the effect of chaos on the description of intrinsic fluctuations in a very simple setting, the logistic map. The fluctuations described in this paper are intrinsic fluctuations and must be carefully distinguished from externally introduced fluctuations. A number of authors have explored the consequences of introduced external fluctuations on the behavior of the chaotic systems. See, for example, Refs. 21–24. Below we will address the appropriateness of these earlier studies in the context established here (and in Ref. 11) that results from the interplay of chaos and intrinsic fluctuations on the description of chaotic dynamics.

In classical physics, chaos is characterized by sensitive dependence of trajectories on initial conditions.[25] This idea is made quantitative by the Liapunov exponent.[25] A positive Liapunov exponent implies chaos. As was shown elsewhere,[11,25,26] the value of the Liapunov exponent is related to the Jacobi matrix for the macrovariable dynamics, and the Jacobi matrix also determines the time evolution of the fluctuations.[11] The salient consequence recently discovered[11] is that a positive Liapunov exponent (chaos) for the macrovariable dynamics implies a divergence of the covariance matrix for the fluctuations. Moreover, this circumstance implies that the macroscopic limit procedure breaks down so that the macrovariable equations no longer follow from the underlying master equation.[11] Instead, the distribution function determined by the master equation becomes very broad and the dynamical description is only correctly given entirely at the master equation level. Clearly, it is inappropriate to introduce external fluctuations[21–24] into macrovariable equations that are no longer valid; instead, external fluctuations will have to be introduced into the master equation level of description.

Because relatively few scientist are fluent in master equation ideas, this paper has been written to present a very simple example of the essential ideas and their consequences. This objective is realized by constructing a master map (equation) for the logistic map. We have chosen the logistic-map paradigm because it is virtually the simplest example possible and because of its fundamental and historical significance with respect to chaos.[27]

In Sec. II, a master map for the logistic map is constructed. In Sec. III, the Liapunov exponent concept is developed for both the logistic map and the master map. In Sec. IV, the breakdown of the macroscopic limit is presented, along with an account of the numerical evidence. In Sec. V, concluding remarks are offered.

II. LOGISTIC MAP AND MASTER MAP

The logistic map is given by[27]

$$x_{n+1}=4\lambda x_n(1-x_n)\ , \tag{1}$$

in which the x's are mapped from the unit interval onto the unit interval and the tunable parameter λ is taken from the unit interval as well. It is now well understood[27]

that for $\lambda < 0.25$ the logistic map has a globally stable fixed-point attractor at $x=0$; for $0.25 < \lambda < 0.75$, $x=0$ becomes unstable and $x = 1 - 1/4\lambda$ becomes the globally stable fixed-point attractor; and for $0.75 < \lambda$, there are no fixed-point attractors. Instead, a sequence of bifurcations yielding 2^k cycles ensues up to about $\lambda = 0.892\,48\ldots$. Beyond this value there are regions of chaos interspersed with windows of all possible cycles not expressible as 2^k. At $\lambda = 1$, the chaotic attractor covers the entire unit interval.

For the sake of the presentation in this paper, we take the perspective[11] that Eq. (1) is a macrovariable map. This means that we are thinking of the x's as describing a macroscopic amount of something (rescaled to the unit interval). In fact, in the original context of population biology, the x's represented populations of a species from generation to generation. Therefore we expect intrinsic fluctuations to be associated with the macrovariable x that represent variations induced at the level of individual organisms. We may achieve a more refined description by introducing a master map (equation) that describes the process at the more microscopic level of individuals and yields the logistic map as its moment map in the macroscopic limit.

The master map is constructed as follows. We first rewrite Eq. (1) on the real numbers between 0 and N:

$$y_{n+1} = 4\lambda y_n (N - y_n)/N \ . \tag{2}$$

This map takes real numbers from the interval 0 to N onto the same interval. Clearly, in the limit $N \to \infty$, $y_n/N \to x_n$. This limit is what we will call the macroscopic limit. Next, we introduce the probability distribution for the population in the nth generation $W(q,n)$, in which q only takes on integer values from 0 to N. The restriction of the argument of W to the integers introduces an effective noise level of size $1/N$. Of course, as $N \to \infty$, this noise vanishes. The master map determines how the probability distribution changes from generation to generation. With this simple example, we are attempting to exhibit a more general phenomenon[11] that occurs in real physical systems, e.g., chemical reactions. For them, the underlying physics determines the form of the master equation, whereas in this simple example we are free to choose any one of many possible constructions since we are dealing with a paradigm and not with a real process.

Initially, we construct it in the following simple way:

$$W(q,n+1) = \int_0^N dq' \delta_N(q - 4\lambda q'(N-q')/N) W(q',n) \ , \tag{3}$$

in which $\delta_N(\ )$ is not precisely a Dirac delta function, but instead picks out the largest integer value q contained in $4\lambda q'(N-q')/N$, and, therefore, has some dispersion of order $1/N$. A computer program realization of this mapping may be found in the Appendix.

In the literature,[22,23] this equation is known as the noisy Frobenius-Perron equation and has been introduced in the context of adding external noise to the logistic map. Consequently, it would appear as though the two problems of intrinsic noise and external noise reduce to an identical analysis. There are two important reasons why this is not so, however. The first reason is that the particular master map picked in Eq. (3) is quite arbitrary, i.e., many master maps can be constructed that reduce to the logistic map in the macroscopic limit ($N \to \infty$), and the one we have picked is the same as the noisy Frobenius-Perron equation by accident. The expression $4\lambda q'(N-q')/N$ in Eq. (3) can be augmented by any function of q' of an order higher than N^{-1} and there will accrue no difference in the macroscopic limit. Had I chosen such an expression at the outset, there would be no cause for confusion with the noisy Frobenius-Perron equation. The second reason is deeper. As is shown below and elsewhere,[11] the consequence of chaos on the macroscopic limit is to invalidate the logistic map as a stable contracted description of the behavior of the underlying master map. This consequence is caused by the intrinsic noise, the variance of which becomes enormous. The addition of external noise cannot be made at the level of the logistic map in this situation, as it is in Ref. 22 and 23, but must be made at the master map level instead.

III. LIAPUNOV EXPONENTS

For the logistic map, the Liapunov exponent Λ may be computed from the formula[28]

$$\Lambda = \lim_{n \to \infty} \frac{1}{n} \sum_{i=1}^{n} \ln \left| \frac{df}{dy_i} \right| \ , \tag{4}$$

where f is given by

$$f = 4\lambda y (N-y)/N \ . \tag{5}$$

The quantity df/dy_i is the Jacobi matrix for a one-dimensional map. For a map in r dimensions, the Jacobi matrix is $r \times r$ dimensional. If we represent the r variables of an r-dimensional map by $\mathbf{z}$, then the Jacobi matrix $\mathbf{J}$ determines how a small deviation from $\mathbf{z}$ will map:

$$\Delta \mathbf{z}(n+1) = \mathbf{J}(n) \Delta \mathbf{z}(n) \ . \tag{6}$$

If we have some way of averaging over these deviations, e.g., there is an underlying master map probability distribution, then the covariance of the fluctuations (deviations) defined by

$$C_{ij} = \langle \Delta z_i \Delta z_j \rangle \tag{7}$$

satisfies the mapping[26]

$$\mathbf{C}(n+1) = \mathbf{J}(n) \mathbf{C}(n) \mathbf{J}^{\dagger}(n) \ , \tag{8}$$

in which $\mathbf{J}^{\dagger}$ is the adjoint of $\mathbf{J}$. We have shown how to define a Liapunov exponent for this covariance equation[11,26] and have proven the identity that for the one-dimensional case it has exactly twice the value determined from Eq. (4). This factor-of-2 relationship also holds in r dimensions.[11,26]

The impact of this identity is that the covariance of the fluctuations becomes very large when the Liapunov exponent is positive. For the present situation in which we have a one-dimensional map, the covariance matrix simply degenerates into the variance for the fluctuation (deviation) for y_n, i.e., Δy_n, which satisfies the degenerate

version of Eq. (6):

$$\Delta y_{n+1}=\frac{df}{dy_n}\Delta y_n \ . \tag{9}$$

If we now use the master map probability distribution to determine the averaged variance, i.e., $\langle \Delta y_n \Delta y_n \rangle$, then we see that df/dy_n determines both the Liapunov exponent for the logistic map [Eq. (4)] and the growth of the variance [Eq. (9)].

The dual role of the Jacobi matrix in these considerations is crucial and occurs in a much broader class of systems than represented by the simple example in this paper.[11]

IV. MASTER MAP → LOGISTIC-MAP TRANSITION

We will now describe the consequences of the preceding results. The reader may wish to avail himself/herself of the advantages of following our remarks with a computer simulation. In this way the reader can see firsthand the numerical evidence we ourselves have seen for the remarks that follow (see also the figures in Ref. 23). The program in the Appendix will provide assistance.

Succinctly put, we find that when the Liapunov exponent is not positive, it is always possible to choose N sufficiently large that the distribution function determined by the master map follows the logistic map's output with a very sharp distribution. However, when the Liapunov exponent for the logistic map is positive, no matter how large an N is chosen, the distribution function determined by the master map becomes very broad and after only a few iterations neither its mean nor its maximum bear any relationship to the output of the logistic map. In the first case, i.e., nonpositive Liapunov exponent, averaging over the distribution function will produce a mean value for y which is precisely equal to the output of the logistic map in the macroscopic limit. This is a consequence of averaging Eq. (2) and finding that the right-hand side, the average of a nonlinear expression, can be replaced with very high accuracy by the nonlinear expression of the average

$$\langle y_{n+1}\rangle=4\lambda\langle y_n(N-y_n)\rangle/N=4\lambda\langle y_n\rangle(N-\langle y_n\rangle)/N \ . \tag{10}$$

It is this replacement that breaks down in the second case, i.e., positive Liapunov exponent, for which the distribution is too broad,

$$4\lambda\langle y_n(N-y_n)\rangle/N\neq 4\lambda\langle y_n\rangle(N-\langle y_n\rangle)/N \ . \tag{11}$$

The following remarks elaborate the content of the preceding paragraph in much more detail. Because there are so many special cases, some involving complicated transient behavior, far too many figures would have been required for this paper. The reader may reproduce those cases of interest to him on a computer. Our remarks are presented in the order of increasing complexity. In each case, unless stated otherwise, all of the initial probability is placed in bin no. 25, i.e., $W(25,1)=1$.

(1) $N=100$, $\lambda=0.3$. The logistic map output approaches the attractor at $x=\frac{1}{6}$. The distribution function stays sharp and follows the logistic map output with a precision of $\frac{1}{100}$.

(2) $N=400$, $\lambda=0.3$. This is the same as case (1), except the precision is now $\frac{1}{400}$.

(3) $N=100$, $\lambda=0.8$. The logistic map output approaches the two-cycle (0.513 045, 0.799 455). The distribution function stays sharp and follows the logistic map output with a precision of $\frac{1}{100}$. This means that the distribution function also describes a two-cycle.

(4) $N=400$ $\lambda=0.8$. This is the same as case (3), except the precision is now $\frac{1}{400}$.

(5) $N=100$, $\lambda=0.865$. The logistic map output approaches the four-cycle (0.413 233, 0.838 951, 0.467 488, 0.861 343). The distribution function stays sharp and follows the logistic-map output with a precision of $\frac{1}{100}$. This means that the distribution function also describes a four-cycle. The distribution is sharper around the two larger cycle values than it is around the two smaller values. If we reduce the bin subdivision parameter from 50 to 10, then the results are qualitatively the same although somewhat less smooth.

(6) $N=400$, $\lambda=0.865$. This is the same as case (5), except the precision is now $\frac{1}{400}$.

(7) $N=100$, $\lambda=0.886$. The logistic-map output approaches the eight-cycle (0.3642, 0.8206, 0.5216, 0.8843, 0.3625, 0.8190, 0.5254, 0.8837). The approach to this eight-cycle takes several hundred iterations before the fourth digit of accuracy is obtained. This contrasts markedly with the preceding examples. The $\frac{1}{100}$ precision of the master map produces a distribution function that cannot follow this eight-cycle. Instead, the distribution settles down on a four-cycle associated with the values (0.36, 0.82, 0.52, 0.88). While the distribution is still quite sharp around the two larger values, it is rather broad around the two lower values and is in fact bimodal around both 0.36 and 0.52. Thus, if we were to use the average of y determined by this distribution function, it would describe a four-cycle that is not identical with any four-cycle of the logistic map for any value of λ. This consequence of the noise in the master map output can be eliminated by reducing the noise level by increasing N (see below). It is also noteworthy that the apparent four-cycle reached by the master map distribution function is reached in relatively few iterations, i.e., in much less than 100 iterations.

(8) $N=400$, $\lambda=0.886$. This is the same as case (7), except the precision is now $\frac{1}{400}$. This precision is still not good enough because a precision of at least $\frac{1}{1000}$ is needed in order to distinguish each separate eight-cycle point.

(9) $N=4000$, $\lambda=0.886$. Now the precision is high enough for the distribution function to follow the logistic-map output. The time required by the computer, however, has grown enormous.

(10) $N=400$, $\lambda=0.886$, $W(208,1)=1$. This time we have started the master map distribution function with all of its probability on one of the eight-cycle points (0.5216, $400\times 0.5216=208.64$). We must also initialize the logistic map with $y=208$. The behavior of the master map distribution function is now dramatically different. It can follow the eight-cycle accurately. For

the large cycle values (0.88) it is extremely sharp, and it is somewhat less sharp for the smallest values (0.36), but for the intermediate values (0.52) it is rather broad. Nevertheless, the distribution function is clearly peaked at 0.5216 and 0.5254, respectively, in spite of the fact that its rather broad structures for these two-cycle points overlap greatly. By contrasting the results for cases (7)–(10), we see that the outcome depends crucially on the initial conditions. It is clear that a trajectory with a transient will create a growth in the master map distribution function that will persist even after a stationary state has been reached, whereas the absence of such a transient permits the master map distribution function to follow the logistic map even when the noise level would indicate that there is insufficient precision. Even though by starting on one of the eight-cycle points, the probability distribution follows the logistic-map output, averages with respect to this distribution do not satisfy Eq. (10). It is simply the peaks of the distribution that follow the logistic-map output. The averages satisfy Eq. (11) for $N=400$. By increasing N, Eq. (10) is approached more and more accurately.

(11) $N=100$, $\lambda=0.9$. The value of λ implies chaos for the logistic map. The Liapunov exponent for this λ is 0.183. Scrutiny of an attractor plot for the logistic map[29] shows that the attractor for $\lambda=0.9$ is made up of two disjoint regions. One region covers the x interval from about 0.3 to about 0.6 whereas the other region covers the x interval from about 0.8 to about 0.9. The invariant measure on these regions is not uniform.[29,30] The logistic-map output quickly reaches the attractor and then jumps about chaotically on the attractor. The master map distribution function, however spreads out on the two attractor regions and alternately hops from one to the other. After only a few dozen iterations, the distribution function reaches a steady two-cycle behavior. This two-cycle is between two broad subdistributions. Any average over this behavior would look like a two-cycle. Equation (11) is strongly the case. Most remarkable of all, however, is the fact that the union of the two subdistributions very closely matches the invariant measure for the logistic map attractor. By increasing N, this match gets better. Thus we see that the master map's probability distribution may be identified with a noisy average of the invariant measure for the deterministic logistic map.

(12) $N=100$, $\lambda=0.95$. The value of λ implies chaos for the logistic map. The Liapunov exponent for this lambda is 0.435. Scrutiny of an attractor plot for the logistic map[29] shows that the attractor for $\lambda=0.95$ is now made up of just one region. Once again the master map probability distribution quickly approaches a steady distribution that closely matches the invariant measure for the logistic map with $\lambda=0.95$. Since the Liapunov exponent here is bigger than in case (11), the steady distribution is reached correspondingly more quickly. Again, by increasing N, the correspondence with the invariant measure is improved. Because there is now only one region covered by the very broad distribution function, or by the invariant measure for that matter, an average over the master map distribution function yields a simple fixed value that bears no resemblance to the chaotic trajectory of the logistic map.

(13) $N=100$, $\lambda=0.96$. This value of λ produces a three-cycle for the logistic map (0.1494, 0.4879, 0.9594). This is in one of the periodic windows of the attractor plot.[29] The corresponding Liapunov exponent is -0.0044. This is clearly not chaotic. However, the transient for the approach to the three-cycle causes the master map distribution to grow very broad before the three-cycle attractor is reached. Consequently, the distribution ends up steady and broad and looking very much like the invariant measure for a chaotic λ just below 0.96. Because there is again only one region covered by the very broad distribution function, an average over the master map distribution function yields a simple fixed value that bears no resemblance to the three-cycle trajectory of the logistic map.

(14) $N=300$, $\lambda=0.96$, $W(146,1)=1$. This is the same as case (13) except that the initialization of both the master map and the logistic map has been switched to a three-cycle point (0.4879). The distribution function now attempts to follow the logistic map's three-cycle and does so quite sharply for over a dozen internations, but by iteration 15 it has developed a broad background. Nevertheless, a steady distribution is not the outcome as it was in case (13). A three-cycle distribution results in which each of the three subdistributions has three peaks and a broad background spanning the space between the peaks. The peak corresponding to the cycle point of the logistic map is the largest in each case, and accounts for 99% of the total probability, whereas the background accounts for less than 0.1% of the probability, while the two lesser peaks make up the remainder, about 1%. This three-cycle distribution is reached in about two dozen iterations.

(15) $N=100$, $\lambda=1$. For the logistic map, this is the strongest chaos with a Liapunov exponent of 0.693. The master map probability distribution rapidly spreads over the entire unit interval and assumes a form very similar to the invariant measure for the logistic map.[29,30] Because the entire unit interval is covered by the distribution function, an average over the master map distribution function yields a simple fixed value that bears no resemblance to the chaotic trajectory of the logistic map. By increasing N, the correspondence between the probability distribution for the master map and the invariant measure for the logistic map gets better.

V. CONCLUDING REMARKS

These examples demonstrate how very different the logistic map and the master map behave. When λ is less than 0.892 48. . . , the Liapunov exponent for the logistic map is less than zero and the master map can produce a distribution function that follows the behavior of the logistic map as accurately as desired provided N is taken sufficiently large. Indeed, in the macroscopic limit they have identical behavior. In practice, however, N may have to be enormous in order to have the master map distribution follow a 2^k cycle with $k>5$. For λ greater than

0.892 48. . . , chaos ensues for most λ values. For the chaotic λ's, the master map distribution grows broad and no longer follows the behavior of the logistic map. In fact, it goes rapidly to a steady distribution (or to a low cycle distribution of subdistributions). This steady distribution has a very accurate resemblance to the invariant measure on the attractor for the logistic map. It is made more accurate by increasing N, which is tantamount to decreasing the noise. For λ values corresponding with periodic windows, the Liapunov exponent is again less than zero. Nevertheless, points not on the periodic attractors tend to exponentiate part until their iterates reach the periodic attractors. The master map distribution function in this situation depends strongly on the initial conditions. A trajectory with a transient will result in a broad and steady distribution. By starting on a cycle point, however, a periodic distribution will result that follows the logistic map and also possesses a low level but broad background.

The point of this paper is to take the view that this simple paradigm represents physical reality as regards the relationship between a macrovariable description and an underlying microscopic or master equation description.[11,26] In this view, the master map is viewed as physical reality whereas the logistic map is viewed as a contracted description created by averaging with respect to the master map's distribution function. As long as the distribution is sharply peaked, Eq. (10) may be expected to hold and one can have faith in the contracted description. But when the distribution is not sharply peaked, Eq. (11) must hold instead and the contraction is no longer valid. This circumstance occurs whenever the contracted description (the logistic map) predicts chaos, because of the connection of the Liapunov exponent to the Jacobi matrix and the connection of the Jacobi matrix to the covariance of the fluctuations.[11,26] Therefore, under these circumstances, the only recourse is to abandon the logistic map and to use the master map instead. This consequence is of special significance when it comes to introducing external fluctuations into consideration.[21–24] Since the logistic map is no longer valid, external fluctuations must be introduced into the master map in order to properly see their effects. The chaos of the logistic map is a mathematical artifact of an equation that no longer has physical significance. It is, nevertheless, significant that the invariant measure for the chaotic attractor produced by the logistic map is so similar to the stationary probability distribution produced by the master map, in the low noise limit. This fact is readily explained by looking at the equation for the invariant measure on the logistic map's attractor (the Frobenius-Perron equation):[23,28]

$$P(x)=\int_0^1 dz\,\delta(x-4\lambda z(1-z))P(z)\,, \tag{12}$$

in which the kernel, $\delta(\ )$, is a genuine Dirac delta function [cf. Eq. (3)]. Clearly, the invariant probability distribution determined by Eq. (3) is equivalent to P in the macroscopic limit. The importance of these thoughts in realistic physical contexts has been explored elsewhere.[11,26,31]

ACKNOWLEDGMENTS

This work was supported by National Science Foundation Grant No. PHY89-02549.

APPENDIX

This program produces a plot of the master map distribution function. In fact, it yields the scaled logarithm of the distribution because the distribution function ranges over many orders of magnitude, but it can easily be modified to yield the distribution function directly if desired. It also plots the position of the output from the logistic map as a pair of points just below and above the distribution function plot. This makes it easy to compare the two types of output. We develop the program in the following simple steps. The restriction of q to the integers may remind one of maps on the integers,[32] but here this restriction only occurs in the master map:

```
FOR q =0 to N
    IF W(q,N,1)>0 then
        FOR m =0 to N
            IF m =INT[4λq(N−q)/N] then
                LET W(m,n+1,2)=W(m,n,2)+W(q,n,1)
            END IF
        NEXT m
    END IF
NEXT q .                                        (A1)
```

In this mapping, a third variable, taking on the values 1 or 2, has been introduced into W. After completing the FOR-NEXT cycle above, the W values are updated for another cycle of Eq. (A1) by the FOR-NEXT cycle below:

```
FOR q =0 to N
    LET W(q,n+1,1)=W(q,n+1,2)
    LET W(q,n+1,2)=0
NEXT q .                                        (A2)
```

This master map does not achieve our desired result very effectively. In fact, it produces a probability distribution that follows the modified, diophantine logistic map,

$$y_{n+1}=\text{INT}\,(4\lambda y_n(N-y_n)/N)\,, \tag{A3}$$

precisely if $W(q,0,1)=1$ when the initial value of y for Eq. (A3) is $y_0=q$. Since we really want to follow Eq. (2) with a master map and not Eq. (A3), we must make our master map a bit more complicated. The desired result is achieved by subdividing the integer interval between q and $q+1$ into a large number of equal subintervals and distributing the probability uniformly among them before mapping the probability into the next generation. This is achieved by the following mapping:

```
FOR q=0 to N-1
  IF W(q,n,1)>0 then
   FOR m=0 to N
     FOR j=1 to 50
       IF m=INT {4λ(q+j/50)[N-(q+j/50)]/N} then
         LET W(m,n+1,2)=W(m,n,2)+W(q,n,1)/50
       END IF
     NEXT j
   NEXT m
  END IF
NEXT q
LET q=N
IF W(N,n,1)>0 then
  LET W(0,n+1,2)=W(0,n,2)+W(N,n,1)
END IF .                                                    (A4)
```

This FOR-NEXT cycle must be followed by Eq. (A2). In this example, 50 subdivisions have been invoked. It should be clear that in the macroscopic limit this fine subdivision will have no effect on the logistic-map limit. However, it will just as clearly affect the fluctuations because probability in the integer interval from q to $q+1$ will now potentially end up in more than one integer valued probability bin, $W(m,n+1,2)$. In this way, the master map follows the behavior of of the logistic map, Eq. (2), with a noise level of $1/N$. A version of the entire program, written in the true-basic language of Kemeny and Kurtz,[33] follows for a Macintosh II computer.

```
REM LOGISTIC MAP MASTER MAP
SET WINDOW 0,640,0,460
DIM W(0 to 10000,2)
PRINT "What is N?"
INPUT N
PRINT "What is lambda?"
INPUT lambda
LET i=0
LET s=0
MAT REDIM W(0 to N,2)
LET W(25,1)=1
LET y=25
DO
   FOR q=0 to N-1
  IF W(q,1)>0 then
    FOR m=0 to N
      FOR j=1 to 50
        IF m=INT {4*lambda*(q+j/50)*[N-(q+j/50)]/N} then
          LET W(m,2)=W(m,2)+W(q,1)/50
```

```
        END IF
      NEXT j
    NEXT m
  END IF
NEXT q
LET q=N
IF W(N,1)>0 then
 LET W(0,2)=W(0,2)+W(N,1)
END IF
LET y=4*lambda*y*(N-y)/N
LET i=i+1
CLEAR
FOR m=0 to N
  PLOT 100+m,300+10*log[W(m,2)+1e-50]
  LET s=s+W(m,2)
NEXT m
PLOT 100+y,50
PLOT 100+y,350
PRINT i,"sum=";s,"lambda=";lambda,"N=";N
PRINT y
FOR m=0 to N
 LET W(m,1)=W(m,2)
 LET W(m,2)=0
NEXT m
LET s=0
LOOP
END
```

In this program, the initial probability is entirely put into bin no. 25. This is an arbitrary choice. The subdivision by 50 is also aribtrary. Becuase the mapping is now embedded in a DO-LOOP, we no longer need the reference to n and $n+1$ inside W. The variable s checks the normalization requirement after each mapping interation.

---

[1]G. E. Uhlenbeck and G. W. Ford, *Lectures in Statistical Mechanics* (American Mathematical Society, Providence, 1963).

[2]H. Mori, Prog. Theor. Phys. **33**, 423 (1965).

[3]P. Langevin, C. R. Acad. Sci. Paris **146**, 530 (1908).

[4]G. E. Uhlenbeck and L. S. Ornstein, Phys. Rev. **36**, 823 (1930).

[5]M. C. Wang and G. E. Uhlenbeck, Rev. Mod. Phys. **17**, 323 (1945).

[6]L. Onsager and S. Machlup, Phys. Rev. **91**, 1512 (1953).

[7]R. F. Fox and G. E. Uhlenbeck, Phys. Fluids **13**, 1893 (1970); **13**, 2881 (1970).

[8]J. E. Keizer, *Statistical Thermodynamics of Nonequilibrium Processes* (Springer-Verlag, New York, 1987).

[9]B. J. Berne and R. Pecora, *Dynamic Light Scattering* (Wiley, New York, 1976).

[10]N. G. van Kampen, *Stochastic Processes in Physics and Chemistry* (North-Holland, Amsterdam, 1981).

[11]R. F. Fox, Phys. Rev. A **41**, 2969 (1990).

[12]A. Nordsieck, W. E. Lamb, and G. E. Uhlenbeck, Physica (Utrecht) **7**, 344 (1940).

[13]A. J. F. Siegert, Phys. Rev. **76**, 1708 (1949).

[14]H. P. McKean, J. Comb. Theory **2**, 358 (1976).

[15]J. Logan and M. Kac, Phys. Rev. A **13**, 458 (1976).
[16]D. A. McQuarrie, J. Appl. Prob. **4**, 413 (1967).
[17]T. G. Kurtz, J. Appl. Prob. **7**, 49 (1970); **8**, 344 (1971).
[18]N. G. van Kampen, Can. J. Phys. **39**, 551 (1961).
[19]R. Kubo, K. Matsuo, and K. Kitahara, J. Stat. Phys. **9**, 51 (1973).
[20]R. F. Fox, J. Chem. Phys. **70**, 4660 (1979).
[21]J. P. Crutchfield and B. A. Huberman, Phys. Lett. **77A**, 407 (1980).
[22]M. J. Feigenbaum and B. Hasslacher, Phys. Rev. Lett. **49**, 605 (1982).
[23]J. P. Crutchfield and N. Packard, Physcia D **7**, 201 (1983); see also J. P. Crutchfield, J. D. Farmer, and B. A. Huberman, Phys. Rep. **92**, 45 (1982).
[24]S. J. Linz and M. Lucke, Phys. Rev. A **33**, 2694 (1986).
[25]A. J. Lichtenberg and M. A. Lieberman, *Regular and Stochastic Motion* (Springer-Verlag, New York, 1983), Sec. 5.2b.
[26]R. F. Fox and J. E. Kiezer, Phys. Rev. Lett. **64**, 249 (1990), and unpublished.
[27]M. J. Fiegenbaum, Physica D **7**, 16 (1983).
[28]R. Shaw, Z. Naturforsch. **36A**, 80 (1981).
[29]J. Eidson, S. Flynn, C. Holm, D. Weeks, and R. F. Fox, Phys. Rev. A **33**, 2809 (1986).
[30]A. J. Lichtenberg and M. A. Lieberman, Ref. 25, Sec. 7.2c.
[31]R. F. Fox and B. L. Lan, Phys. Rev. A **41**, 2952 (1990).
[32]B. A. Huberman and W. F. Wolff, Phys. Rev. A **32**, 3768 (1985).
[33]J. G. Kemeny and T. E. Kurtz, *True Basic: The Structured Language for the Future, Reference Manual* (True BASIC, Inc., Hanover, 1988).

AMPLIFICATION OF INTRINSIC FLUCTUATIONS BY CHAOTIC DYNAMICS IN PHYSICAL SYSTEMS

by

Ronald F. Fox
School of Physics
Georgia Institute of Technology
Atlanta, Georgia
30332

and

Joel Keizer
Institute of Theoretical Dynamics
and
Department of Chemistry
University of California
Davis, California
95616

PACS # 05.40.+j, 05.45.+b

ABSTRACT

A quantitative method for the treatment of large scale intrinsic fluctuations amplified by chaotic trajectories in macrovariable physical systems is presented. Paradigmatic results for the Rossler model and preliminary computational results for chaotic Josephson junctions and for chaotic multi-mode Nd:YAG lasers are described. These studies are directed towards identification of a real physical system in which experimental confirmation may be realized. The probability distribution on the intrinsic-noise-modified, chaotic attractor is identified as a likely candidate for comparison of experiment and theory.

I. Introduction

In several recent papers[1,2,3,4], we showed that chaotic dynamics can cause macroscopic growth of intrinsic fluctuations in a macrovariable system. Implications of this effect were suggested for systems as diverse as chemical, hydrodynamic, electronic, and quantum. In this paper, we propose a highly accurate approach to the theoretical description of such large scale fluctuations. Our proposal is based upon a limit theorem for Markov chains proved by T. G. Kurtz[5,6] in 1975, long before its relevance for chaotic dynamics could be appreciated.

That chaotic dynamics and the growth of intrinsic fluctuations are related to each other is a consequence of each being fundamentally tied to a dynamical quantity called the Jacobi matrix[2]. A quantitative characterization of chaos is provided by the largest Liapunov exponent, which when positive, implies chaos[7]. The computation of the largest Liapunov exponent directly utilizes the instantaneous values of the Jacobi matrix[8]. Similarly, the growth of the intrinsic fluctuations is made quantitative by following the time evolution of the covariance matrix[9,10]. Again, the computation of the covariance matrix evolution directly utilizes the instantaneous values of the Jacobi matrix[2]. This dual role of the Jacobi matrix and the consequence that intrinsic fluctuations become very large in a chaotically dynamic system was apparently noticed for the first time only recently[1,2,4].

In order to make this connection explicit, imagine a macrovariable system described by N macrovariables $M_i(t)$ for i=1,2,...N satisfying N coupled, nonlinear, ordinary, differential equations:

$$\frac{d}{dt} M_i(t)=F_i(M(t)) \qquad (1)$$

in which the F_i's are N, generally nonlinear functions of the M_k's. The Jacobi matrix, $J_{ik}(t)$, is defined[7] by

$$J_{ik}(t) = \frac{\partial F_i}{\partial M_k(t)} \tag{2}$$

for each instant of time. It has been shown that the largest Liapunov exponent for this dynamics, λ, is given by[8]:

$$\lambda = \underset{t\to\infty}{\text{limit}} \frac{1}{2t} \ln(\text{Trace } [\mathbf{J}^\dagger(t)\mathbf{J}(t)]) \tag{3}$$

in which $\mathbf{J}^\dagger(t)$ is the adjoint of $\mathbf{J}(t)$. On the other hand, it has also been established that if (1) is the macroscopic limit of an embedding (see below) master equation (i.e. some "largeness parameter", say Ω, is allowed to go to an infinite limit), and if the scaled linearized deviations from the deterministic solutions to (1) are denoted by $\mu_i(t)=\Omega^{1/2}\Delta M_i(t)$ (where $\Delta M_i(t)$ is the unscaled deviation), and if the covariance matrix for these deviations (fluctuations) is denoted by $C_{ik}(t)=\langle\mu_i(t)\mu_k(t)\rangle$ where $\langle\ldots\rangle$ denotes averaging with respect to the master equation's probability distribution, then $C_{ik}(t)$ satisfies:

$$\frac{d}{dt} C_{ik}(t) = J_{ij}(t)C_{jk}(t) + C_{ij}(t)J_{kj}(t) + R_{ik}(t) \tag{4}$$

in which $R_{ik}(t)$ is explicitly determined from the master equation. The exponential divergence of fluctuations in the limit of large Ω is reflected in the fact that Eq (3) is also valid if $\mathbf{C}^\dagger(t)$ and $\mathbf{C}(t)$ are substituted in place of $\mathbf{J}^\dagger(t)$ and $\mathbf{J}(t)$ on the right-hand side[1,4].

The covariance matrix evolution equation involves a linearization of the macrovariable dynamics instantaneously in time. This, of course, produces the Jacobi matrix dependence, but it also means that once the fluctuations have grown even a little bit, the linearized equations lose their validity. In our earlier work[1,2,4] we stressed this point, and noted that while the covariance matrix evolution permitted computation of the largest Liapunov exponent, it

did not accurately describe the fluctuations once they grew to macroscopic size. In order to obtain the large scale fluctuations, a mesoscopic underpinning of the macrovariable equations is required[2,3]. One way to accomplish this is to embed the macrovariable equations in a mesoscopic master equation and deduce the time evolution of the underlying probability distribution. Given the master equation, which is not generally agreed upon for all interesting contexts (e.g. hydrodynamics[9]), one must solve it, albeit numerically. This last task is formidable for multivariable systems and has prompted us to look for alternative approaches.

One alternative to solving the master equation for the probability distribution is to implement the process described by the master equation as a stochastic process[9]. This requires performing many realizations of the stochastic process in order to build up the equivalent probability distribution. A theorem due to Kurtz[5,6] is closely related to this approach and establishes a highly accurate approximation to the stochastic process needed. Because the implementation of Kurtz's theorem for this purpose looks very much like merely adding extrinsic fluctuations to the macrovariable equations, we will attempt to distinguish clearly the important differences.

Kurtz's theorem may be implemented either as a stochastic process or as an equivalent Fokker-Planck equation. In the latter guise it is a so-called nonlinear Fokker-Planck equation that is used[11]. In other contexts, objections to such an equation have been voiced[12]. The chief objection is that the averaged quantities determined by a nonlinear Fokker-Planck equation do not satisfy the macrovariable equations because averages of nonlinear expressions are not equal to identical nonlinear expressions of the averages. However, this is precisely the circumstance that is relevant when intrinsic fluctuations grow to large scale. Thus, we again find it necessary to contrast what is done here with earlier applications of some closely related methods. Context will prove to be the crucial distinguishing element.

The remainder of this paper is divided into three sections. In section II, we define a variety of kinds of noise or fluctuations. We do this because earlier work[13] does not distinguish the many types of noise discussed here and the same words we use are used with different meaning in these earlier papers. In section III, we discuss the transition from a mesoscopic picture to a macrovariable dynamics. Both the traditional view[11] of this transition and Kurtz's theorem[5,6] will be presented. Certain technical matters regarding the application of Kurtz's theorem to our problems will be addressed. In section IV, we conclude the paper with three examples. The Rossler model[14] is used as a paradigm for the description of the growth of fluctuations on a chaotic trajectory. We establish the probability distribution on an attractor as a good candidate for the comparison of experiment and theory. The amplification of intrinsic noise on chaotic trajectories produces a probability distribution noticeably different from the corresponding, noise-free invariant measure. Preliminary results from a detailed theoretical study of fluctuations in a chaotic Josephson junction[15] are presented. Similar results, with the possibilty of future experimental confirmation, for a chaotic multi-mode Nd:YAG laser[16] are outlined. These examples provide insight into the methods and their consequences.

II. Noises

In order to minimize misunderstanding, we will distinguish among several distinct types of noise[13,17]. In the vast literature covering noise in physical systems, words such as "noise", "fluctuations", and "random" have been applied to processes of rather different origin. In some cases the established usage is so ingrained that alternative usage is easily misconstrued. To define our usage here as clearly as possible, five classes of "noise" are distinguished:

1) instrumental,

2) initial data,

3) external reservoir,

4) intrinsic molecular,

5) deterministic chaos.

Instrumental noise is the systematic noise associated with making observations, either in real experiments or in numerical simulations. It is the noise associated with the limits of resolution in the observation procedure. If, for example, σ is the standard deviation for the limit of resolution, no observation will resolve quantities below the σ scale. At the same time, observations will also be no worse than the scale set by σ. This feature is in marked contrast to what will be seen regarding intrinsic fluctuations, below.

Uncertainties in the precision of the initial data introduces another kind of noise. One must consider what happens to an ensemble of initial states each of which is consistent with the limited precision of the initial data. If the dynamics is dissipative and involves an attractor, then the ensemble of initial data will end up as an ensemble distributed over the attractor. For an ergodic attractor, this final ensemble will be an invariant distribution quite

independent of its initial properties. Therefore, properties of the stationary ergodic attractor really don't depend on the initial data noise.

Identifiable physical systems are isolated from the rest of the world by container boundaries. These container walls are in contact with the rest of the world. In this way, every system is coupled to a heat bath, or a pressure reservoir, etc.. This introduces another kind of noise that we will call extrinsic noise. It is essentially independent of the nature of the system, depending instead on how the system is isolated from the rest of the world. In mathematical modeling, this type of noise is introduced by simply adding noise terms to the deterministic equations. The noise properties are introduced through various parameters that are fundamentally independent of the system and the system state. Most earlier studies of the interaction of noise and chaos concerns this sort of extrinsic noise[13,17].

The type of noise upon which we focus attention in this paper is intrinsic molecular noise. By this expression we refer to the molecular composition of real physical systems that are otherwise described by macrovariable equations. The macrovariables refer to macroscopic amounts of matter, and, therefore, represent some sort of averaging over an underlying microscopic, or perhaps mesoscopic, description[9]. Consequently, associated with each macrovariable is an intrinsic fluctuation of molecular origin. Frequently, these fluctuations are ignored and only the macrovariables are studied. However, light scattering[18] from a hydrodynamic system can be accounted for quantitatively only by working out the dynamics of the fluctuations as well as the macrovariables. Near full equilibrium or near a stable steady state, the fluctuations in no way affect the macrovariable dynamics. For chaotic macrovariable dynamics, however, we have shown that the intrinsic fluctuations are amplified to macroscopic size so that the macrovariable description might be markedly modified. The central purpose of this paper is to present a procedure for an accurate quantitative treatment of chaotic dynamics

including amplified intrinsic fluctuations. This treatment of chaotic, intrinsic fluctuations does not appear in any of the earlier literature.

The reader should not confuse our object of study, namely the amplification of intrinsic fluctuations by chaotic dynamics, with a prevalent usage in the literature wherein wild macrovariable trajectories of chaotic dynamics are themselves referred to as "enhanced fluctuations". This latter usage is consistent with the notion of "deterministic randomness" that also has wide currency. These usages ignore intrinsic molecular fluctuations and refer only to the chaotic macrovariable trajectories as noise. In this light, it is significant that recent research[19] has begun to emphasize the ordered structure of chaotic macrovariable trajectories by showing how to systematically approximate them in terms of unstable periodic orbits. These researches are shifting the emphasis from "deterministic randomness" to "ordered chaos". Perhaps this shift will help to eliminate confusion between the wild, chaotic macrovariable trajectories and amplification of intrinsic noise.

III. Mesoscopic to Macroscopic Transition

The macroscopic description[9,11] of physical systems, e.g. hydrodynamics and chemical reactions, involves macrovariable equations in which the dependent variables refer to quantities representing averages over the properties of many constituent molecules. When intrinsic fluctuations are totally ignored, a deterministic description is obtained, usually in the form of ordinary or partial differential equations with precise initial and/or boundary conditions. Measurements on such systems often involve scattering probes, e.g. light scattering, that necessitate a quantitative treatment[18] of the intrinsic fluctuations since the scattering is determined by fluctuation correlations. This leads to a stochastic adjunct to the macrovariable description.

There are several ways to obtain a quantitative description of the intrinsic fluctuations. For the linear regime near full equilibrium or near a stable steady state, the Onsager theory has been generalized[20] so that the fluctuation equations may be written down directly from the macrovariable equations through imposition of the fluctuation-dissipation relation which connects the strength of the fluctuations to the magnitude of associated dissipative parameters. For example, in hydrodynamics, the magnitude of the velocity field fluctuations is determined by the viscosity. In order to treat the fluctuations in the dynamical regime further away from full equilibrium or a stable steady state, where nonlinearities may be important, it is necessary to go beyond just the fluctuation-dissipation relation and to obtain a fuller treatment of the dynamics of the intrinsic fluctuations[9]. While some special cases have been successfully treated by kinetic theory[21], a more general approach is that of the master equation[9,11]. This approach is a mesoscopic description that provides the time evolution of the entire probability distribution for the intrinsic fluctuations and subsumes all of their properties including the fluctuation-dissipation relation.

For spatially homogeneous chemical reactions, the master equation approach is well developed[22]. In fact, several quite rigorous limit theorem[23] results, also due to Kurtz, have been obtained in this case. For hydrodynamics[9,11], however, a generally accepted master equation for all fluid densities does not exist yet, although in the dilute fluid regime, Boltzmann's equation can be thought of as serving the purpose. Therefore, some of what we have to say about master equations can already be realized in certain contexts, whereas in other contexts, the master equation itself is still to be constructed. Nevertheless, after reviewing the properties of the master equation to macrovariable equation transition, we will present a new approach[5,6] to large scale fluctuations that does not require the master equation description per se, even though this alternative is also mesoscopic.

Equation (1) represents a typical macrovariable equation in the form of an ordinary differential equation. Without loss of generality, we will restrict our remarks in this paper to such equations because most partial differential equations can be recast as ordinary differential equations either through expansions in Fourier modes or by discretizing space. In fact, the typical nonlinear partial differential equation must be treated numerically, in which case one or the other of these treatments is required. The objective of the master equation treatment associated with equation (1) is two-fold. First, the master equation must imply equation (1) in the macroscopic limit for which some scaling parameter, Ω say, is made infinitely large[11]. Second, this same limit must yield the equation for the intrinsic fluctuations associated with the macrovariables by the master equation. The proper physical interpretation of these relations is that the fundamental physics is given by the master equation and both the deterministic macrovariable equations and the fluctuation equations are approximate representations of the information contained in the master equation, the approximation being the better as $\Omega \to \infty$.

The form of the general master equation associated with equation (1) is [11,22]:

$$\frac{\partial}{\partial t}P(\mathbf{m},t)= \int d^N m'(W(\mathbf{m},\mathbf{m}')P(\mathbf{m}',t)-W(\mathbf{m}',\mathbf{m})P(\mathbf{m},t)) \qquad (5)$$

in which $P(\mathbf{m},t)$ is the probability density for $\mathbf{M}(t)$ values, i.e. $P(\mathbf{m},t)d\mathbf{m}$ is the probability that the values of $\mathbf{M}(t)$ at time t are between $\mathbf{m}$ and $\mathbf{m}+d\mathbf{m}$, component by component; $W(\mathbf{m},\mathbf{m}')dt$ is the transition probability for $\mathbf{M}(t)$ values to change from $\mathbf{m}'$ to $\mathbf{m}$ in dt; and $W(\mathbf{m},\mathbf{m}')$ is of order Ω for $|\mathbf{m}-\mathbf{m}'|$ of order $1/\Omega$. In the limit $\Omega\rightarrow\infty$, we identify the macrovariable as the average

$$\mathbf{M}(t) = <\mathbf{m}> = \int d^N m \ \mathbf{m} \ P(\mathbf{m},t) \qquad (6)$$

The transition moments[11] are defined by

$$K_i^{(1)}(\mathbf{m},t) = \int d^N m' \ (m'_i-m_i)W(\mathbf{m}',\mathbf{m}) \qquad (7)$$

$$K_{ij}^{(2)}(\mathbf{m},t) = \int d^N m' \ (m'_i-m_i)(m'_j-m_j)W(\mathbf{m}',\mathbf{m}) \qquad (8)$$

and so on. The Ω properties of W imply [23] that $K^{(1)}\approx O(1)$, $K^{(2)}\approx O(1/\Omega)$ and generally $K^{(n)}\approx O(1/\Omega^{n-1})$. Using these transition moments, the master equation may be rewritten in the equivalent Kramers-Moyal form[24,25]:

$$\frac{\partial}{\partial t}P(\mathbf{m},t) = \sum_{n=1}^{\infty} \frac{(-1)^n}{n!} \left(\prod_{j=1}^{n} \frac{\partial}{\partial m_{k_j}}\right) (K^{(n)}_{k_1 k_2 \ldots k_n}(\mathbf{m}) \ P(\mathbf{m},t)) \qquad (9)$$

With these properties, the macroscopic limit, i.e. $\Omega\rightarrow\infty$, implies[2]:

$$\frac{\partial}{\partial t}P_{\infty}(\mathbf{m},t) = -\frac{\partial}{\partial m_i}(K_i^{(1)\infty}(\mathbf{m})\, P_{\infty}(\mathbf{m},t)) \tag{10}$$

where the repeated indices in both (9) and (10) imply a summation and where the sub(super)-script ∞ denotes the macroscopic limit of the corresponding quantity. This partial differential equation is very special since its derivatives are all first order. This means that if the initial values for the $\mathbf{m}$ components are precisely given, i.e. $P_{\infty}(\mathbf{m},0) = \delta(\mathbf{m}-\mathbf{m}_o)$, then the solution to (10) is simply[2]:

$$P_{\infty}(\mathbf{m},t) = \delta(\mathbf{m}-\mathbf{m}(t)) \tag{11}$$

where $\mathbf{m}(t)$ satisfies the system of coupled ordinary differential equations

$$\frac{d}{dt}m_i(t) = K_i^{(1)\infty}(\mathbf{m}(t)) \tag{12}$$

Moreover, if we apply the averaging defined in (6), we obtain the equations

$$\frac{d}{dt}M_i(t) = \langle K_i^{(1)\infty}(\mathbf{m})\rangle = K_i^{(1)\infty}(\langle\mathbf{m}\rangle) = K_i^{(1)\infty}(\mathbf{M}(t)) \tag{13}$$

on account of the Dirac delta function solution (11). Thus $\mathbf{M}(t)$ is the same as $\mathbf{m}(t)$ since both solve the same equation with the same initial condition $\mathbf{m}(0) = \mathbf{M}(0) = \mathbf{m}_o$. Having constructed the master equation so that $K_i^{(1)\infty} = F_i$ for the F_i's of equation (1), we achieve an embedding of the macrovariable equations in the master equation description as the macroscopic limit.

We can also obtain a dynamical description of the intrinsic fluctuations with this master equation approach. Generally, the intrinsic fluctuations in the macrovariables scale[11] like $1/\Omega^{1/2}$. This means that they simply vanish in the macroscopic limit. In the spirit of the central limit theorem of probability theory[23], it is possible to

rescale the fluctuations so that their limiting behavior may be rigorously deduced. This is done by considering the deviations of the **m** components from the deterministic solution to the macroscopic limit equation (12). i.e. $\mathbf{m}(t)$, scaled with $\Omega^{-1/2}$:

$$\mathbf{m} = \mathbf{m}(t) + \Omega^{-1/2}\,\boldsymbol{\mu} \tag{14}$$

which defines the scaled intrinsic fluctuations $\boldsymbol{\mu}$. This scaling implies that as $\Omega\to\infty$, the $\boldsymbol{\mu}$ components are of order unity. We shift attention from the probability distribution $P(\mathbf{m},t)$ to the probability distribution for the scaled intrinsic fluctuations, $\Phi(\boldsymbol{\mu},t)$. It is then possible to show[2] that in the macroscopic limit (i.e. $\Omega\to\infty$), we obtain

$$\frac{\partial}{\partial t}\Phi = -\frac{\partial}{\partial \mu_i}\left(\frac{\partial}{\partial m_j}K_i^{(1)\infty}(\mathbf{m}(t))\;\mu_j\;\Phi\right) \tag{15}$$

$$+\frac{1}{2}\frac{\partial^2}{\partial\mu_i\partial\mu_j}\left(R_{ij}^{(2)}(\mathbf{m}(t))\;\Phi\right)$$

in which $R_{ij}^{(2)}$ is defined by

$$R_{ij}^{(2)} = \lim_{\Omega\to\infty}\Omega\,K_{ij}^{(2)}(\mathbf{m}(t)) \tag{16}$$

This is a Fokker-Planck equation for a non-stationary, Gaussian, Markov process. The non-stationarity results from the explicit dependence on $\mathbf{m}(t)$ in both $K_i^{(1)\infty}$ and $R^{(2)}$. Since this $\mathbf{m}(t)$ is found from (12), the deterministic macrovariable equations, we say that the intrinsic fluctuations "ride on the back" of the deterministic motion. We will refer to the rigorous proof of this result as "Kurtz's first theorem".

Several remarks are in order[2]. The time dependent coefficients of the first order μ-derivatives in (15) are precisely the components of the Jacobi matrix for the deterministic macrovariable equations (either (1) or (12)):

$$J_{ij}(t) = \frac{\partial}{\partial m_j} K_i^{(1)\infty} \tag{17}$$

Defining the covariance matrix for the intrinsic fluctuations by

$$C_{ik}(t) = \langle \mu_i(t)\mu_k(t) \rangle \cdot \tag{18}$$

where $\langle ... \rangle$ denotes averaging with respect to $\Phi(\boldsymbol{\mu},t)$, leads to the equation (derived from (15))

$$\frac{d}{dt} C_{ik}(t) = J_{ij}(t)C_{jk}(t) + C_{ij}(t)J_{kj}(t) + R_{ik}^{(2)}(t) \tag{19}$$

This is exactly (4) of the introduction ((17) is precisely (2) because of (6)), and shows how the Jacobi matrix for the deterministic motion arises in the dynamics of the intrinsic fluctuations. The following and final remark is the central issue of this paper. <u>If the deterministic motion is chaotic, then the Jacobi matrix will create an unbounded growth of the C_{ik} components</u>[2,4]. Since the derivation of (15), and hence of (19), assumes that the μ components remain of order unity, it would be inconsistent to use (19) when the fluctuations grow larger than this. As will be shown below, there exists an alternative treatment[5,6] for this case in which the intrinsic fluctuations can grow large.

One way to express the content of the limit theorem[2,3] reviewed above is to write:

$$\mathbf{M}(t) = \langle \mathbf{m} \rangle_t + O(1/\Omega^{1/2}) \tag{20}$$

in which $\langle ... \rangle_t$ is the average with respect to $P(\mathbf{m},t)$. This says that the deterministic equations' solution approximates the expected

values of the underlying mesoscopic master equation with an error of order $1/\Omega^{1/2}$, i.e. an error the size of the fluctuations. The proper interpretation of this result is that the more fundamental physical description is given by the master equation, whereas the deterministic macrovariable equation is an approximate description. In the macroscopic limit where intrinsic fluctuations may be ignored (provided that they don't grow large), it is far easier to use the macrovariable equations than to use the master equation. However, if the intrinsic fluctuations grow too large for this treatment to be valid (seen as chaos at the macrovariable level), then another limit theorem is available, "Kurtz's second theorem"[5,6]. Not only does Kurtz's second theorem allow one to handle the large intrinsic fluctuations, but it does so with even greater accuracy than expressed in (20). If we denote the solution to this alternative treatment, to be elucidated below, by $\mathbf{M}_f(t)$, then Kurtz's second theorem[5,6] implies:

$$\mathbf{M}_f(t) = \langle \mathbf{m} \rangle_t + O(\ln\Omega/\Omega) \tag{21}$$

$\mathbf{M}_f(t)$ combines both the macrovariable behavior and the large fluctuations and its probability distribution satisfies the Fokker-Planck equation

$$\frac{\partial}{\partial t} P_f(\mathbf{m},t) = - \frac{\partial}{\partial m_i}(K_i^{(1)\infty}(\mathbf{m})\ P_f(\mathbf{m},t)) \tag{22}$$

$$+\frac{1}{2}\frac{\partial^2}{\partial m_i \partial m_j}(K_{ij}^{(2)\infty}(\mathbf{m})\ P_f(\mathbf{m},t))$$

so that

$$\mathbf{M}_f(t) = \int d^N m\ \mathbf{m}\ P_f(\mathbf{m},t) \tag{23}$$

When this limit theorem was originally obtained[5,6], the chaotic amplification of intrinsic fluctuations was not yet clearly understood[9,10]. Since the typical applications involved near equilibrium states or stable steady states away from critical points, for which intrinsic fluctuations remained small, a vanishingly small difference in behavior resulted from using (22) instead of the more tractable (15). Thus, this treatment remained largely ignored. On occasion, however, an objection to (22) has been voiced[12] because the averaging defined by (23) implies

$$\frac{d}{dt}(M_f(t))_i = < K_i^{(1)\infty}(\mathbf{m}) > \neq K_i^{(1)\infty}(<\mathbf{m}>) \qquad (24)$$

since (22) does not have a Dirac delta function solution (cf. equations (10-13)). For intrinsic fluctuations that remain small, the difference between the two expressions on the right-hand side of (24) is only order $O(1/\Omega^{1/2})$, i.e. ignorable. For intrinsic fluctuations that grow large, this same inequality is a sign of the breakdown of the macrovariable limit altogether, as has been shown earlier[1,2]. Therefore, Eq(22) is perfectly suited to the situation we are confronting.

Because the direct solution to (22) numerically is demanding, we prefer to use a more tractable, equivalent[9] method, the nonlinear Langevin treatment. This is possible because to every probability distribution equation satisfying (22) there is associated a unique Langevin-like equation. However, great care is required in order to express the Langevin equivalent correctly since there are two valid, yet distinct, versions of stochastic calculus by which the equivalence can be realized, the Ito and the Stratonovich versions[26]. The proof of the limit theorem[5,6] that produces (22) makes use of Martingale properties[26] and in so doing arrives at (22) in the Ito context. Numerical realizations of Langevin equations in our hands are done *a la* Stratonovich[27] using the traditional Newtonian calculus. Therefore, we need to obtain the Stratonovich Langevin equation equivalent to the Ito probability distribution equation (22). This is

done as follows. Suppose $\mathbf{M}_f(t)$ satisfies the stochastic differential equation

$$\frac{d}{dt}(\mathbf{M}_f(t))_i = \alpha_i(\mathbf{M}_f(t)) + \beta_{ij}(t)\, g_j(t) \tag{25}$$

where the derivatives are to be manipulated according to the usual calculus and where the g_j's are statistically independent Gaussian white noises with zero means and covariances of unit strength, i.e.

$$\langle g_k(t) \rangle = 0 \tag{26}$$

$$\langle g_i(t) g_k(t') \rangle = \delta_{ik}\delta(t-t') \tag{27}$$

in which $\langle ... \rangle$ denotes averaging with respect to the g_k distributions. The Fokker-Planck equation satisfied by the Stratonovich stochastic process in Eq(25) is[26]

$$\frac{\partial}{\partial t}P_f(\mathbf{m},t) = -\frac{\partial}{\partial m_i}(\alpha_i(\mathbf{m})\, P_f(\mathbf{m},t)) + \frac{1}{2}\frac{\partial}{\partial m_i}\beta_{ik}(t)\,\frac{\partial}{\partial m_j}\beta_{jk}(t)\, P_f(\mathbf{m},t) \tag{28}$$

which may be rearranged as

$$\frac{\partial}{\partial t}P_f(\mathbf{m},t) = -\frac{\partial}{\partial m_i}(\alpha_i(\mathbf{m})\, P_f(\mathbf{m},t) + \frac{1}{2}(\frac{\partial}{\partial m_j}\beta_{ik}(t))\,\beta_{jk}(t)\, P_f(\mathbf{m},t)) \tag{29}$$

$$+\frac{1}{2}\frac{\partial^2}{\partial m_i \partial m_j}\beta_{ik}(t)\beta_{jk}(t)\, P_f(\mathbf{m},t)$$

In both (28) and (29) repeated indices are summed. To identify the correct α and β to be used in Eq(25), we need only compare Eqs(22) and (29). Since $K_{ij}^{(2)\infty}$ is a symmetric, non-negative matrix at each instant of time, the square-root of $K_{ij}^{(2)\infty}$ will also be symmetric and one finds that

$$\beta(t) = (K^{(2)\infty}(t))^{1/2} \tag{30}$$

$$\alpha_i(t) = K_i^{(1)\infty}(t) - \frac{1}{2}\left(\frac{\partial}{\partial m_j}\beta_{ik}(t)\right)\beta_{jk}(t) \qquad (31)$$

Generally, β is of order $1/\Omega^{1/2}$ so that α differs from $K_i^{(1)\infty}$ only to order $1/\Omega$ and this "Ito-Stratonovich shift" is ignorable[9], but when the intrinsic fluctuations are large, not only will this difference be important, but (25) will differ markedly from the purely deterministic macrovariable equation (12) (equivalently (1)).

There is an additional advantage to using equation (25) for the study of chaotically amplified intrinsic fluctuations. The only feature of the underlying mesoscopic master equation that remains in Eqs(25), (30) and (31) is the matrix $K_{ij}^{(2)\infty}$ (the vector $K_i^{(1)\infty}$ is predetermined by the macrovariable equations). Thus, we need not know the underlying master equation in full detail but only the second moment of the transition probability (see (8)). With physical insight, it may be possible to correctly guess $K_{ij}^{(2)\infty}$ without obtaining the full master equation. Hydrodynamics may be an example of this circumstance[9].

The description of large scale intrinsic fluctuations by equations (25-27,30,31) combines the macrovariable and the intrinsic fluctuation dynamics in one quantity, $\mathbf{M}_f(t)$, unlike the situation for small fluctuations wherein two sets of equations, equations (12) and (15), are obtained. The intrinsic fluctuations no longer "ride on the back" of the deterministic macrovariables and, indeed, no autonomous macrovariable equation exists (see (24)). When the intrinsic fluctuations grow large, the distribution function $P_f(\mathbf{m},t)$ becomes broadly spread out, unlike the extremely sharp distribution given by (11), which is only valid when the fluctuations remain small[9]. For this reason the concept of a deterministic macrovariable is lost. While one may still use (23) to define an

"average" value, there is no longer an autonomous dynamics for the $\mathbf{M}_f$ components because of the broadness of the P_f distribution[2].

The breakdown of the autonomous macrovariable equations associated with large scale intrinsic fluctuations forces a reassessment of the meaning of chaos in real physical systems. Conceptually, one must shift focus from the wild deterministic macrovariable trajectories to large scale intrinsic fluctuations. A variety of new characterizations need to be developed, and the examples that are presented in the next section are meant to indicate some possible avenues for this development. In each of the examples, we will use the approach represented by equation (25), since it is the most tractable and is also a highly accurate representation of the mesoscopic level of description.

One should not confuse this approach with previous work that treats the effects of <u>extrinsic</u> noise on macrovariable systems[13,17] using similar equations. In these treatments, some of which have the same form as (25), the α_i's are just the $K_i^{(1)\infty}$'s (i.e. the F_i's of equation (1)), and the β_{ik}'s are not connected to the state of the system, i.e. there is no "intrinsic fluctuation-dissipation relation" as in (30), because the fluctuations are <u>extrinsic</u> and not <u>intrinsic</u>. That is, the strength of the extrinsic noise does not depend on the state of the system. Moreover, if the intrinsic fluctuations have grown large scale, the breakdown of the autonomous macrovariable equations implies that extrinsic fluctuations should be introduced directly at the mesoscopic level, not at the deterministic macrovariable level, which is no longer valid.

All the preceding considerations must be qualified by the observation that the growth of intrinsic fluctuations depends upon two quantities, their rate of growth (this is related to the largest Liapunov exponent) and their initial size (this is determined by (30) at t=0). In the Josephson junction[15] example that follows, both of these quantities are "large", whereas in the laser[16] example both of these quantities are "small". In the Rossler[14] paradigm, we explore

both regimes and motivate our expectations for the real physical systems.

IV Examples

The purpose of these examples is two-fold. They make the general ideas concrete, and they help to make contact with real experiments. Ultimately, we wish to identify a real physical system on which quantitative measurements can be used to explore the amplification of intrinsic fluctuations. Significant progress in this direction is reported.

As our first example, which exhibits behavior like both of the following examples, we look at a purely mathematical model, the Rossler model[14,28]. This model was invented to show the minimal ordinary differential equation system that can have chaos. We have chosen it because of its great simplicity. The route to chaos in this model is period doubling of a limit cycle. The equations, in three independent variables, X, Y, and Z, are

$$\frac{d}{dt}X = -(Y + Z) \tag{32}$$

$$\frac{d}{dt}Y = X + \frac{1}{5}Y \tag{33}$$

$$\frac{d}{dt}Z = \frac{1}{5} + Z(X-\mu) \tag{34}$$

in which μ is an adjustable parameter. For μ=2.6, the asymptotic state is a simple limit cycle attractor. It has a period of about 5.8 time units. The unit of time is dimensionless, and power spectra show a fundamental at about 0.17 Hz (cycles per unit of dimensionless time). (In the literature[14], the unit of time is arbitrarily taken to be .01 sec, so that the fundamental becomes 17 Hz.) For μ=3.5, the limit cycle has bifurcated once, while for μ=4.1 it has done so twice. After this, much smaller changes in μ lead to increasing numbers of bifurcations until around μ=4.2 infinitely many have occurred and the motion becomes chaotic. For μ=4.23, the largest Liapunov exponent is λ=.014.

This system of equations does not describe a real physical system. Therefore, construction of an underlying master equation cannot benefit from physical insight into real molecular substructure. Nevertheless, for the sake of illustration, we can imagine that such an underlying, mesoscopic, molecular picture really does exist. This means that we must construct an underlying master equation for the Rossler model, based on an imagined underlying molecular basis. There are many ways to do this that yield the Rossler model in the macroscopic limit but produce different fluctuations. Whichever specific choice we make, we can circumvent the actual construction of the master equation by invoking Kurtz's second theorem. We do so by merely adding an intrinsic noise term to equation (34), say, in accord with Kurtz's second theorem as discussed in the previous section. While arbitrary for the Rossler model, this procedure serves to illustrate how noise amplification can be seen in models of real physical systems wherein the specification of the added noise is entirely determined by the nature of the physical system. The noise to be added to the Rossler model is Gaussian, white noise with state independent strength, so that no Ito-Stratonovich shift is required.

Note that what we are doing looks similar to what others have done to treat the addition of extrinsic noise to the Rossler model. However, the interpretation is significantly different. For extrinsic noise, X,Y,and Z retain their meaning and their values merely become noisy, but for intrinsic molecular noise, the underlying probability distribution implicitly in mind when we construct the mesoscopic description, either by a master equation are by Kurtz's second theorem, becomes broad because of chaos-amplification of noise, and X,Y, and Z cease to be meaningful variables. No autonomous dynamics exists for them. In other words, the macrovariable picture breaks down[2,4] and the mesoscopic description is required for a correct quantitative treatment.

Let us now return to our ad hoc mesoscopic treatment of the Rossler model. The observation of the amplification of intrinsic noise by chaotic trajectories is achieved in the following manner. First we

run equations (32-34) numerically and plot the attractor (after the transients have died away) in the X-Y plane (X along the horizontal axis and Y along the vertical axis). This is shown in figure 1 for $\mu=4.23$. Also shown is a horizontal line cutting the left-hand portion ($X<0$) of the attractor along $Y=0$. We numerically determine probability distribution (in the noise-free case, this is called the invariant measure) for X values. This is shown in figure 2. Next, we redo all of this with the noise present. As indicated above, this is done by using equations (32-33) as is and by adding Gaussian, white noise with zero mean, g, to (34), i.e.

$$\frac{d}{dt}Z = \frac{1}{5} + Z(X-\mu) + g \tag{35}$$

in which g has correlation formula

$$\langle g(t)g(t')\rangle = 2\sigma\delta(t-t') \tag{36}$$

in which σ is an adjustable noise strength. In a real physical model, this noise strength would be determined by the underlying physics through the master equation. For our illustrative purposes, it is adjustable so that we can explore how effects depend on its size. Figures 3 and 4 show the results paralleling figures 1 and 2 for $\mu=4.23$ and $\sigma=10^{-8}$. It is extremely difficult to discern any differences between figures 1 and 3, but there is very clear smoothing of the probability distribution of figure 2 in figure 4 as a result of intrinsic noise amplification. If, instead, our noise had been instrumental, then we would see it as a smoothing of figure 2 with a Gaussian smoothing function with standard deviation equal to $\sigma^{1/2}$, a magnitude of 10^{-4}, that would not produce a visually observable effect on figure 2. However, amplification of intrinsic noise produces the clearly observable effect seen in figure 4 and shows that the amplification is to macroscopic size (i.e. order unity). Figures 5 and 6 show what happens when $\sigma=10^{-6}$. Now both figures are visually effected, and the attractor shows only two bands instead of four. The attractor in figure 5 could be mistaken for the more chaotic, noise-free attractor

in figure 7 obtained for μ=4.3, but the corresponding invariant measure of figure 8 is easily distinguished from figure 6.

These cases clearly suggest that the way to observe the chaotic amplification of intrinsic noise is to contrast the resulting probability distribution with the noise-free invariant measure. Even when the corresponding attractor plots show no discernable differences, the differences in the probability distributions can be very marked. For big enough noise, even the attractor plots may become distinguishable. The following two examples illustrate this diagnostic approach in models of real physical systems.

The Josephson junction is a real, electronic, physical system in which conditions can be arranged so that it appears to exhibit chaos. A simple mathematical description of the phenomenon in terms of either a macrovariable current, or a macrovariable voltage (or associated phase), also can exhibit chaos. Incidentally, this is one of those examples, alluded to in the introduction, for which published accounts [15] refer to the chaos in the macrovariable time dependence as a "noise rise". This usage is not what we mean by "chaotically amplified intrinsic noise", and one must make an effort to avoid confusion.

The macrovariable model for superconductor-insulator-superconductor (SIS) Josephson junctions operated in the classical regime (i.e. $eI_oR < K_BT$, to be interpreted below) is[15]:

$$C\frac{dV}{dt} + \frac{V}{R} + I_o \sin\phi = I_{cd} + I_{rf} \sin\omega t \qquad (37)$$

in which ϕ is the macroscopic quantum phase of the supercurrent, C is the capacitance of the junction, R is its resistance, I_o is the critical current, I_{dc} is the applied d-c current, I_{rf} is the amplitude of the applied r-f current with frequency ω, and V is the junction voltage, related to ϕ by

$$V = \frac{\hbar}{2e}\frac{d\phi}{dt} \qquad (38)$$

in which $\hbar$ is Planck's constant (divided by 2π) and e is the charge of an electron. One may proceed with the two coupled equations (37-38), or convert to one second-order equation

$$\frac{\hbar}{2e}\frac{C}{I_o}\frac{d^2\phi}{dt^2}+\frac{\hbar}{2e}\frac{1}{I_oR}\frac{d\phi}{dt}+\sin\phi=\frac{I_{dc}}{I_o}+\frac{I_{rf}}{I_o}\sin\omega t \qquad (39)$$

This form of the equation suggests defining the junction frequency, ω_o, by

$$\omega_o=\left(\frac{\hbar C}{2eI_o}\right)^{-1/2} \qquad (40)$$

and the dimensionless time, τ, by

$$\tau=\omega_o t \qquad (41)$$

If we also introduce the McCumber parameter[29], $\beta_c=\frac{2eI_oR^2C}{\hbar}$, and the ratios $\rho=\frac{I_{dc}}{I_o}$ and $\rho_1=\frac{I_{rf}}{I_o}$, equation (39) becomes:

$$\frac{d^2\phi}{d\tau^2}+\frac{1}{\sqrt{\beta_c}}\frac{d\phi}{d\tau}+\sin\phi=\rho+\rho_1\sin\left(\frac{\omega}{\omega_o}\tau\right) \qquad (42)$$

which is the canonical form for the Josephson junction, and is seen to be the equation for a periodically perturbed, damped, planar pendulum[30], well known for its capacity to exhibit chaos.

This description of the junction is macroscopic, and the macrovariable current represents many Cooper electron pairs. Individual Cooper pair motions show up as intrinsic fluctuations in the macrovariable current. This is not unlike the picture of current fluctuations in a classical resistor[9], i.e. Johnson noise, except that the electrons are not paired, and in addition, Johnson noise occurs in a resistor in series with a voltage, whereas Josephson junction noise occurs with a resistor and a capacitor in parallel with the junction voltage.

In principle, we should now try to construct a master equation that has equation (42) as its macroscopic limit and contains the correct physics for the determination of $K^{(2)\infty}$. This is not an easy task. However, in other electronic circuits with a configuration of capacitor and resistance identical to that for Eq(37) (i.e. in parallel with the voltage), the determination of the strength of the fluctuations, through a master equation, has already been successfully obtained[9]. This allows us to use Kurtz's second theorem to obtain a stochastic realization of the mesoscopic description. The result is to add a stochastic term to the right-hand side of (37) of the form g f(t), where f is Gaussian, white noise with zero mean and

$$\langle f(t)f(t')\rangle = \delta(t-t') \tag{43}$$

$$g = (2K_B T/R)^{1/2} \tag{44}$$

in which K_B is Boltzmann's constant, T is the junction temperature, and R is the junction resistance. (Note that for Johnson noise, $g \sim R^{1/2}$ when quantities are expressed as functions of frequency instead of time.) This amounts to the addition of $\frac{g}{I_o}\omega_o{}^{1/2}\, f(\tau)$ to the right-hand side of (42), where

$$\langle f(\tau)f(\tau')\rangle = \delta(\tau-\tau') \tag{45}$$

Since the numerical integration of this non-integrable equation is easier to implement as two coupled first-order equations, we recast it as

$$\frac{d\phi}{d\tau} = v \tag{46}$$

$$\frac{dv}{dt} + \frac{1}{\sqrt{\beta_c}}\, v + \sin\phi = \rho + \rho_1 \sin\left(\frac{\omega}{\omega_o}\tau\right) + \left(2\frac{I_T}{I_o}\right)^{1/2}\beta_c{}^{-1/4} f(\tau) \tag{47}$$

where (46) defines the variable v, and in (47) we have introduced the "thermal current", I_T, defined by

$$I_T = \frac{2eK_BT}{h} \tag{48}$$

and have used the identity

$$\frac{g\omega_o^{1/2}}{I_o} = (2\frac{I_T}{I_o})^{1/2}\beta_c^{-1/4} \tag{49}$$

We see from (49) that the fluctuation-dissipation relation maintains its usual significance in this case because the mean square of the fluctuation has a strength proportional to both $2K_BT$ and $\beta_c^{-1/2}$. Moreover, it is inversely proportional to the system size, in this case I_o, which itself is proportional to the cross-sectional area of the junction. The cross-sectional area of the junction is the macroscopic parameter, i.e. Ω, characteristic of this system. A particularly nice feature of this example is that the fluctuation strength is independent of the state of the system (in so far as R is). This is why there is no "β-correction to α" (see equations (30-31)) in (47). Said another way, the Ito-Stratonovich distinction is irrelevant in this case.

We have done numerical studies of equations (42) and (46-47). The results will be reported in detail elsewhere[31]. Using physically derived parameters (β_c=4, ρ=0, ρ_1=.91, and $\frac{\omega}{\omega_o}$ =.5655), the scaled parameters in (47) are all roughly of order unity except for the noise strength given in (49). It works out to be of order 10^{-2}. There is no freedom here because this magnitude is determined by the fluctuation-dissipation relation expressed by (44) and depends on predetermined macroscopic parameters (i.e. T and R). This magnitude is relatively very large. For comparison, a typical hydrodynamics problem cast in dimensionless form such that the macrovariable magnitudes are order unity has a mean squared noise strength of order 10^{-10}. Moreover, the largest Liapunov exponent for (42) with the same parameters is λ=0.112, which implies a sizeable amplification of the intrinsic noise in only 10-100 dimensionless time units. This does show up in the attractor plots with the noise

compared with those with no noise (see figures 9 and 11). This is like the Rossler case of μ=4.23 with $\sigma=10^{-6}$. In addition, dramatic differences in the probability distributions are seen, as is shown in figures 10 and 12.

Recent studies of a class-B Nd:YAG laser containing a nonlinear intracavity crystal exhibited chaotic output intensity[16]. The dynamics was shown to be very well modeled by equations such as:

$$\tau_c \frac{dI_j}{dt} = (G_j - \alpha_j - g\varepsilon I_j - 2g\varepsilon \sum_{k\neq j}^{3} I_k)I_j \qquad (50)$$

$$\tau_f \frac{dG_j}{dt} = G_j^o - G_j(1 + \beta_j I_j + \sum_{k\neq j}^{3} \beta_{jk} I_k) \qquad (51)$$

for j,k = 1,2,3. These equations represent only one of many possible cases studied. In this case, three modes polarized in the same direction have intensities I_j and gains G_j for j = 1,2,3. In other cases, six, or even eight, modes are used and the equations are correspondingly enlarged. The cavity round trip time, τ_c, is set equal to .2 nsec, the flourescence time, τ_f, is set equal to 240μsec, the cavity losses, α_j, are set equal to .01, the nonlinear crystal coupling coefficient, ε, is set equal to $5x10^{-5}$, the self-saturations, β_k, are each set equal to 1, the cross-saturations, β_{ik}, are each set equal to .6, and the pump parameters, G_j^o, are each set equal to .04. The parameter g is a variable configuration parameter depending on the relative orientation of the laser and nonlinear crystals. For different choices (g is always in the interval [0,1]) stable, periodic, chaotic and intermittent output intensities are produced. The correspondence between the numerical simulation of equations (50-51) and real laser measurements for which all of the above parameters were determined is good in the periodic regime when the time course of the total intensity is compared. Spontaneous emission is the physical basis for intrinsic noise in this laser system (pump noise may also prove important but appears to be very small in this case), and in

other laser contexts[32] it has been very accurately simulated by adding Gaussian, white noise to equations that are the analogues to (50-51). We may do the same here, in the spirit of Kurtz's second theorem.

Chaos is confirmed for the equations by computing the Liapunov exponent which turns out to be $\lambda=4.6\times10^{4}$ sec^{-1} [33]. The magnitude of the white noise that should be used to model spontaneous emission is of order 10^{-8}. The probability distribution for the total intensity shows a significant effect in our preliminary studies, and this characterization is currently under investigation. A detailed account of the comparison of the theory with experiment is in preparation[33].

Generally, a numerical simulation of model equations will determine whether or not amplification of intrinsic noise will be significant. If the initial intrinsic noise level is n_o and the largest Liapunov exponent is λ, then the time required for the noise level to reach n is of the order of[4]:

$$t = \frac{1}{\lambda} \ln(\frac{n}{n_o}) \qquad (53)$$

It may take much longer because this value assumes pure exponential growth whereas after a certain noise level, nonlinearities will begin to suppress the noise growth.

Acknowledgments

This work was supported by National Science Foundation research grants PHY-9043227(RFF) and CHE 89-18422(JK) and Air Force grant AFOSR-90-0158(RFF). We thank Chris Bracikowski for sharing preliminary results from his ongoing study of laser chaos and John Wagner for his diligent work on the numerical calculations.

References

1) R.F. Fox and J. Keizer, Phys. Rev. Letts. **64**, 249 (1990).

2) R.F. Fox, Phys. Rev. **41A**, 2969 (1990).

3) R.F. Fox, Phys. Rev. **42A**, 1946 (1990).

4) J. Keizer, R.F. Fox and J.W. Tilden, "On the Growth of Molecular Fluctuations for Nonstationary Systems: Their Effect on Deterministic Chaos", submitted to Phys. Rev. A.

5) T.G. Kurtz, Math. Prog. Stud. **5**, 67 (1976).

6) T.G. Kurtz, Stoch. Proc. and their Appl. **6**, 223 (1978).

7) A.J. Lichtenberg and M.A. Lieberman, Regular and Stochastic Motion, (Springer-Verlag, New York, 1983), section 5.2b.

8) P. Berge, Y. Pomeau and C. Vidal, Order within Chaos, (John Wiley, New York, 1984), Appendix B, pp. 279-286.

9) J. Keizer, Statistical Thermodynamics of Nonequilibrium Processes, (Springer-Verlag, New York, 1987).

10) J. Keizer and J.W. Tilden, J. Chem. Phys. **93**, 2811 (1989).

11) N.G. van Kampen, Stochastic Processes in Physics and Chemistry, (North-Holland, Amsterdam, 1981), pp. 211-213, 272.

12)D.K.C. McDonald, Phil. Mag. **45**, 63 (1954);**45**, 345 (1954); Phys. Rev. **108**, 541 (1957).

13) J.P. Crutchfield, J.D. Farmer and B.A. Huberman, Phys. Repts. **92**, 45 (1982).

14) J.P. Crutchfield, J.D. Farmer, N. Packard, R. Shaw, G. Jones and R. Donnelly, Phys. Lett. **76A**, 1 (1980).

15) N.F. Pederson and A. Davidson, Appl. Phys. Lett. **39**, 830 (1981).

16) G.E. James, Models of Intracavity Frequency Doubled Lasers, Ph.D. dissertation, Georgia Institute of Technology (1990); G.E. James, E.M. Harrell and R. Roy, Phys. Rev. **41A**, 2778 (1990).

17) J.P. Crutchfield and N.H. Packard, Physica **7D**, 201 (1983).

18) B.J. Berne and R. Pecora, Dynamic Light Scattering, (John Wiley, New York, 1976).

19) P. Cvitanovic, "Chaos of Cyclists" in Noise and Chaos in Nonlinear Dynamical Systems, edited by F. Moss, L. Lugiato and W. Schleich, (Cambridge Univ. Press, Cambridge, 1990), pp. 270-288.

20) R.F. Fox, Phys. Repts. **48**, 179 (1978).

21) T.R. Kirkpatrick, E.G.D. Cohen and J.R. Dorfman, Phys. Rev. **26A**, 950 (1982); **26A**, 972 (1982).

22) D.A. McQuarrie, J. Appl. Prob. **4**, 413 (1967).

23) T.G. Kurtz, J. Appl. Prob. **7**, 49 (1970); **8**, 344 (1971).

24) H.A. Kramers, Physica **7**, 284 (1940).

25) J.E. Moyal, J. R. Stat. Soc. **B11**, 150 (1949).

26) L. Arnold, Stochastic Differential Equations, (John Wiley, New York, 1974).

27) R.F. Fox, J. Stat. Phys. **54**, 1353 (1989); **58**, 395 (1990).

28) O. Rossler, Phys. Letts. **57A**, 397 (1976).

29) D.E. McCumber, J. Appl. Phys. **39**, 3113 (1968).

30) J. Guckenheimer and P. Holmes, Nonlinear Oscillations, Dynamical Systems, and Bifurcations of Vector Fields, (Springer-Verlag, New York, 1983), section 4.6.

31) J. Keizer, R.F. Fox, and J. Wagner, manuscript in preparation.

32) M. Sargent III, M.O. Scully and W.E. Lamb Jr., Laser Physics, (Addison-Wesley, Reading, Massa., 1974), chapter XX.

33) C. Bracikowski, R.F. Fox and R. Roy, manuscript in preparation.

Figure Captions

Figure 1. X-Y plot of the Rossler attractor for μ=4.23 and σ=0.

Figure 2. Invariant measure for the attractor in figure 1 projected onto the negative X axis at Y=0. The vertical axis gives the percentage of crossing points in an X-axis bin. 1024 bins were used over the range of X values indicated in the figure.

Figure 3. X-Y plot of the Rossler attractor for μ=4.23 and $\sigma=10^{-8}$.

Figure 4. Probability distribution for the attractor in figure 3 projected onto the negative X axis at Y=0. All other aspects of the figure are the same as in figure 2.

Figure 5. X-Y plot of the Rossler attractor for μ=4.23 and $\sigma=10^{-6}$.

Figure 6. Probability distribution for the attractor in figure 5 projected onto the negative X axis at Y=0. All other aspects of the figure are the same as in figures 2 and 4.

Figure 7. X-Y plot of the Rossler attractor for μ=4.3 and σ=0.

Figure 8. Invariant measure for the attractor in figure 7 projected onto the negative X axis at Y=0. All other aspects of the figure are the same as in figures 2,4 and 6.

Figure 9. Invariant measure for the Josephson junction equations with no noise.

Figure 10. Projection of figure 9 along the v=0 axis yielding a the ϕ distribution.

Figure 11. Probability distribution for the Josephson junction with intrinsic noise.

Figure 12. Projection of figure 11 along the v=0 axis yielding a the ϕ distribution.

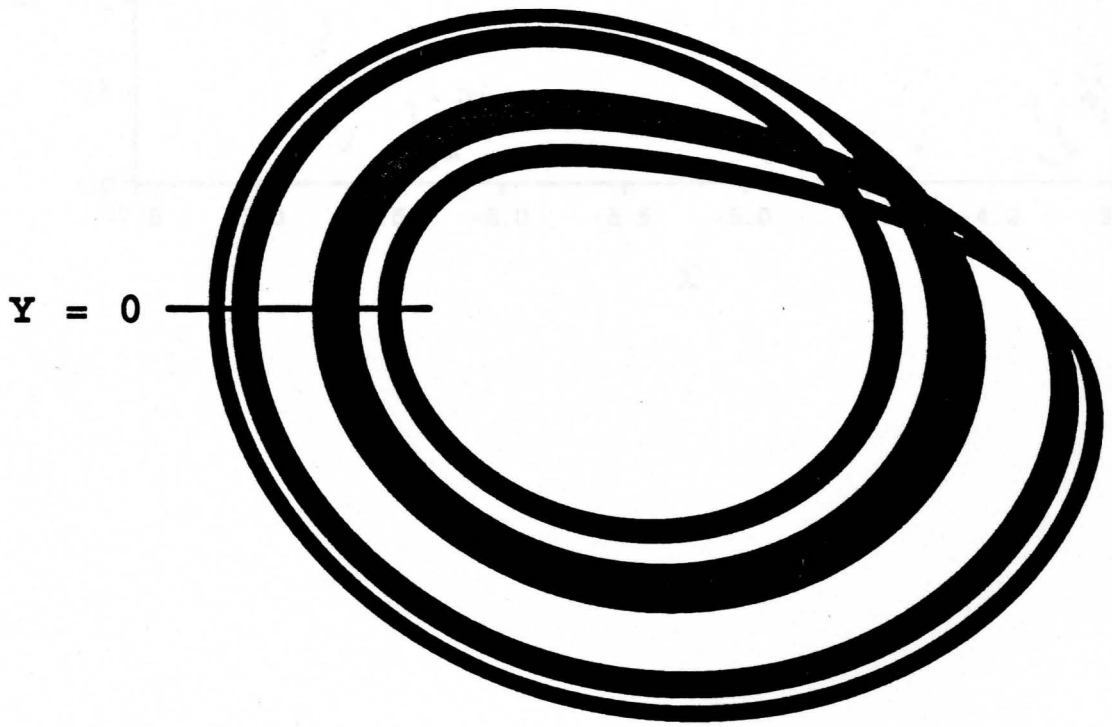

F. 1

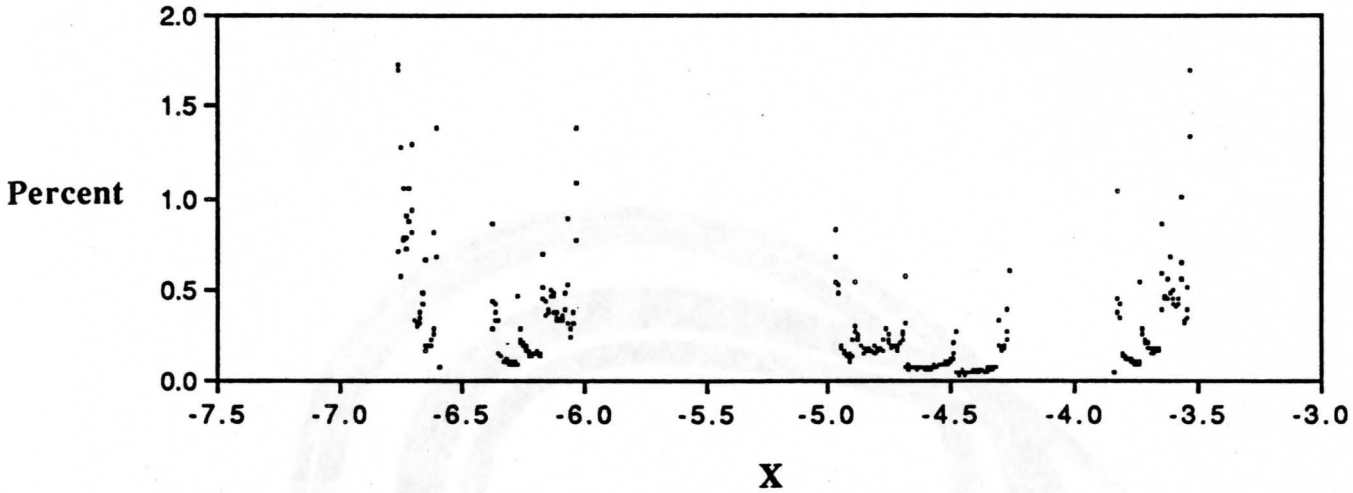

F. 2

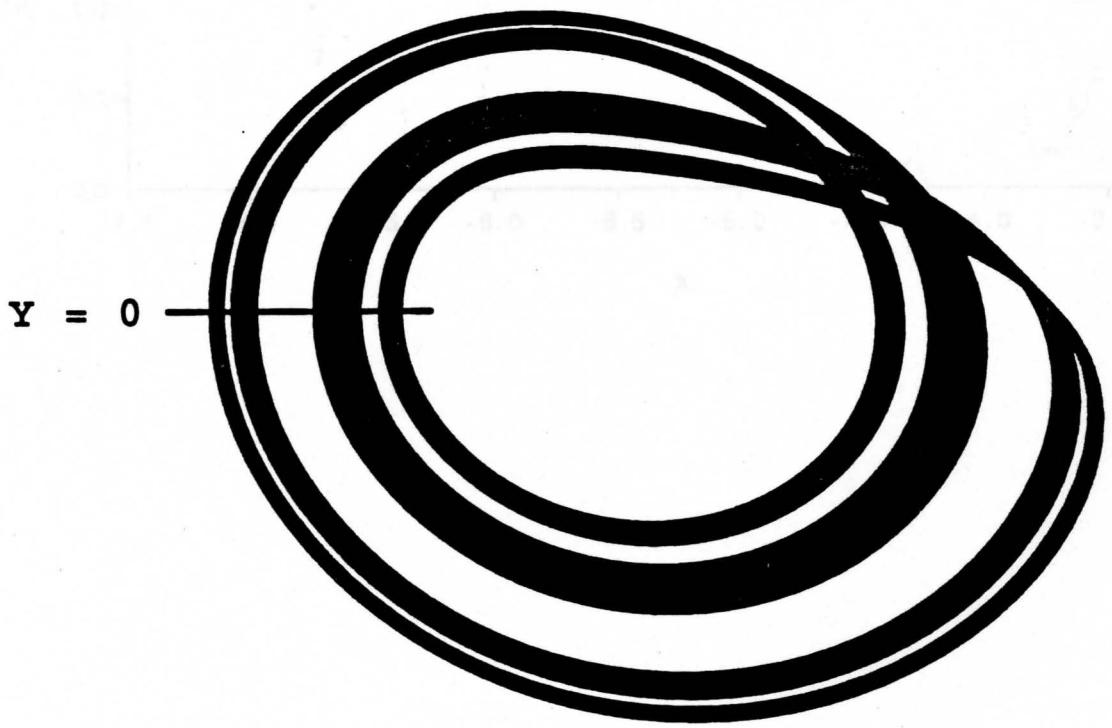

F. 3

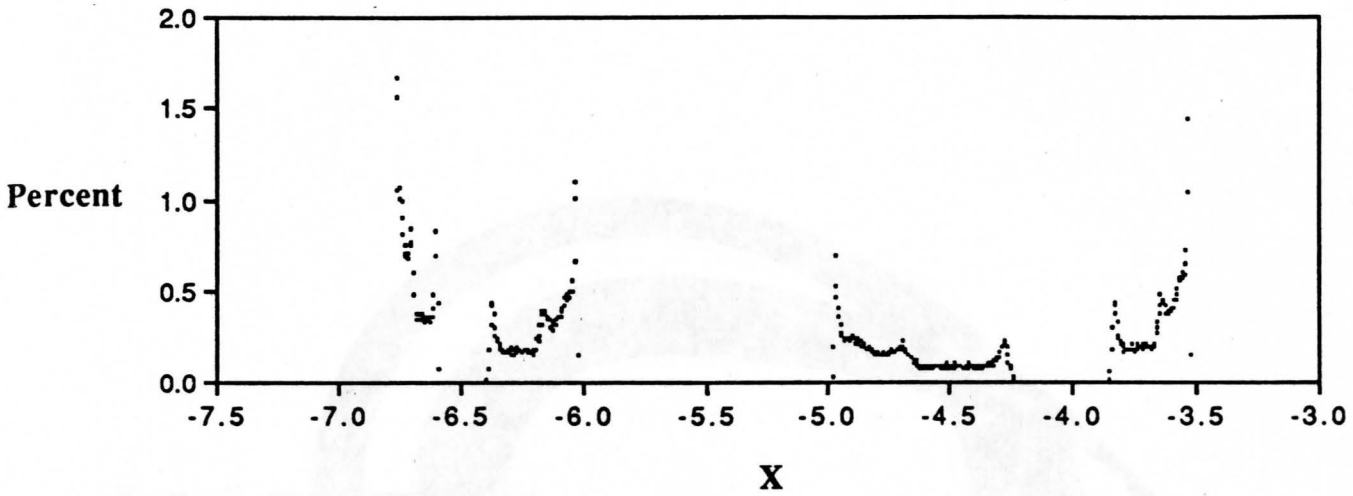
Percent
2.0
1.5
1.0
0.5
0.0
-7.5
-7.0
-6.5
-6.0
-5.5
-5.0
-4.5
-4.0
-3.5
-3.0
X

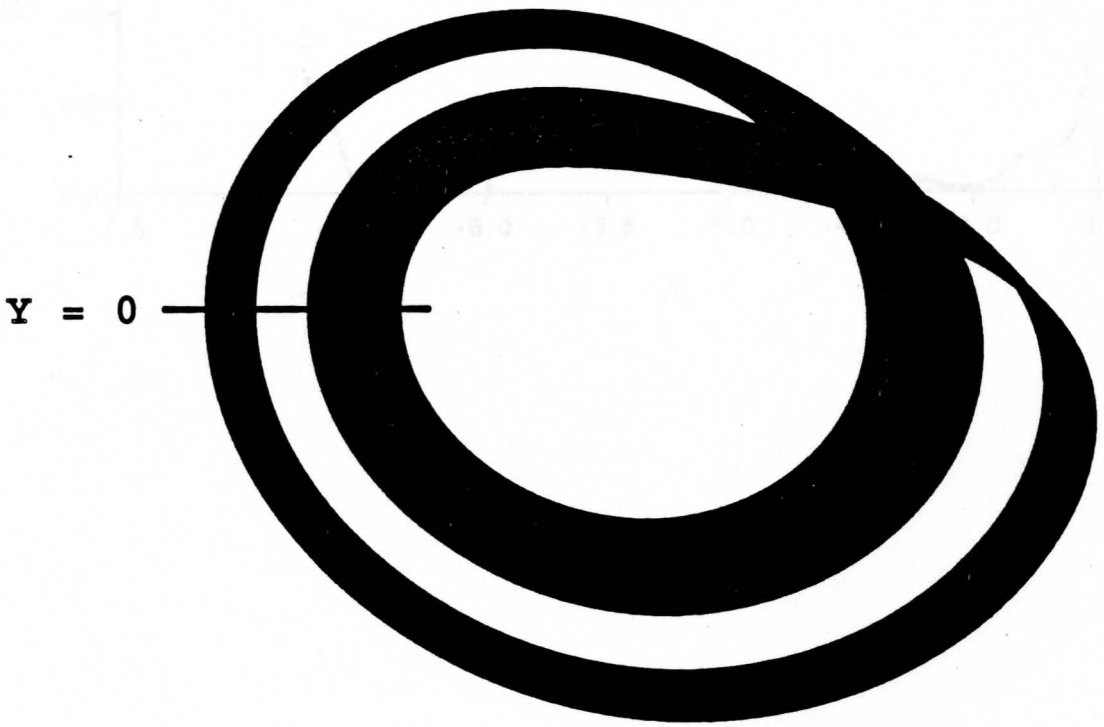

F. 5

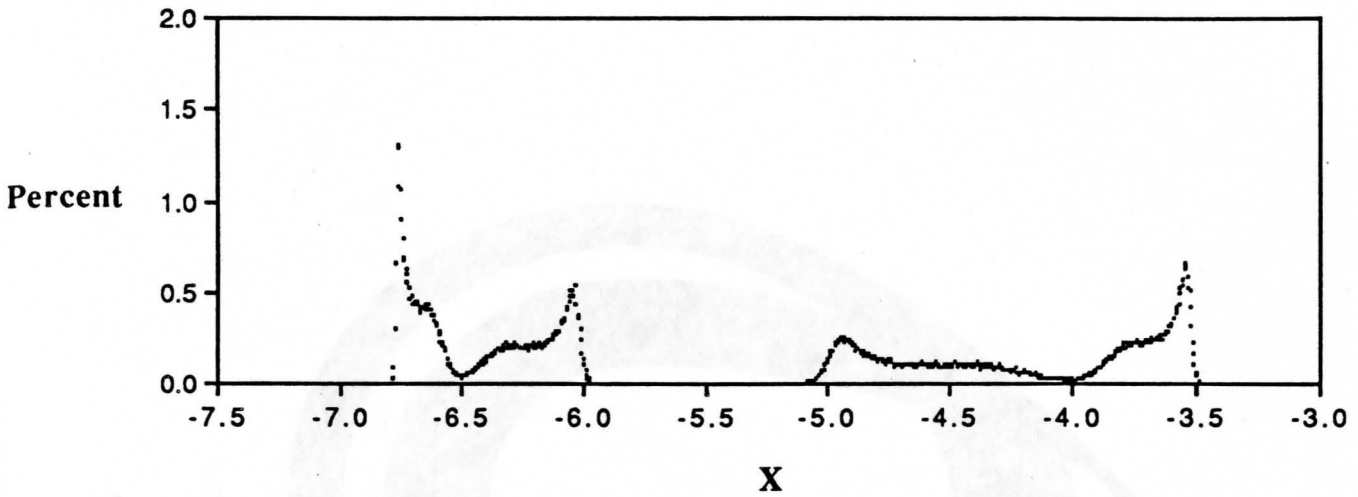

F. 6

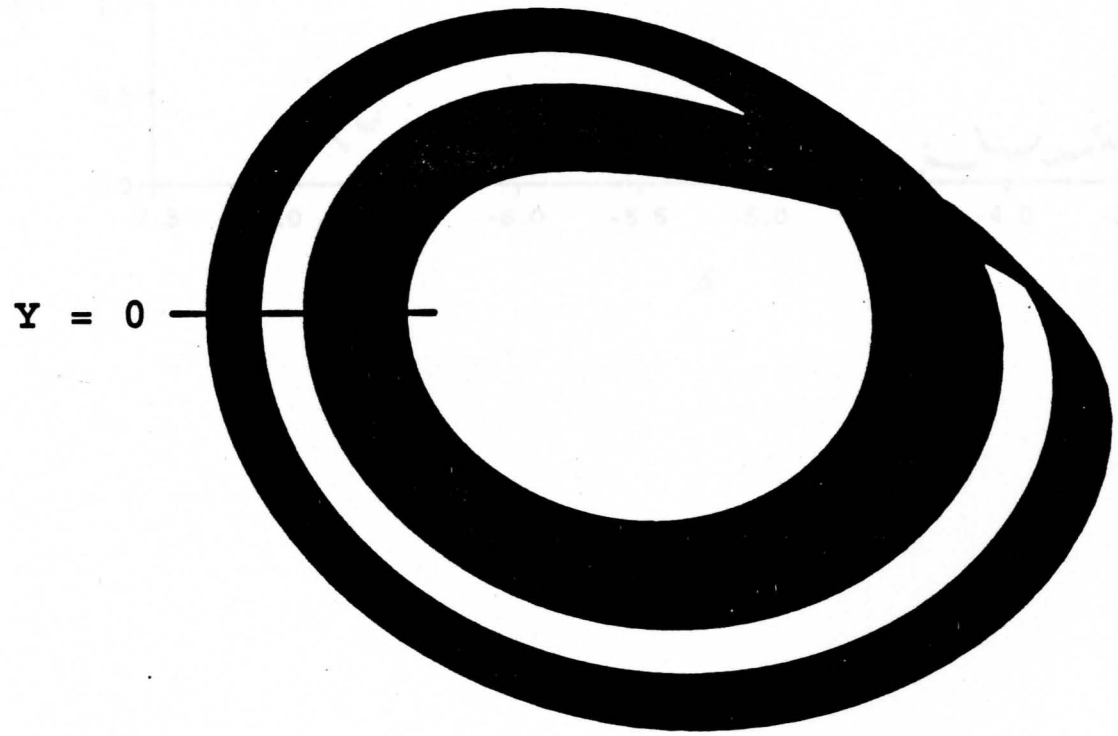
Y = 0

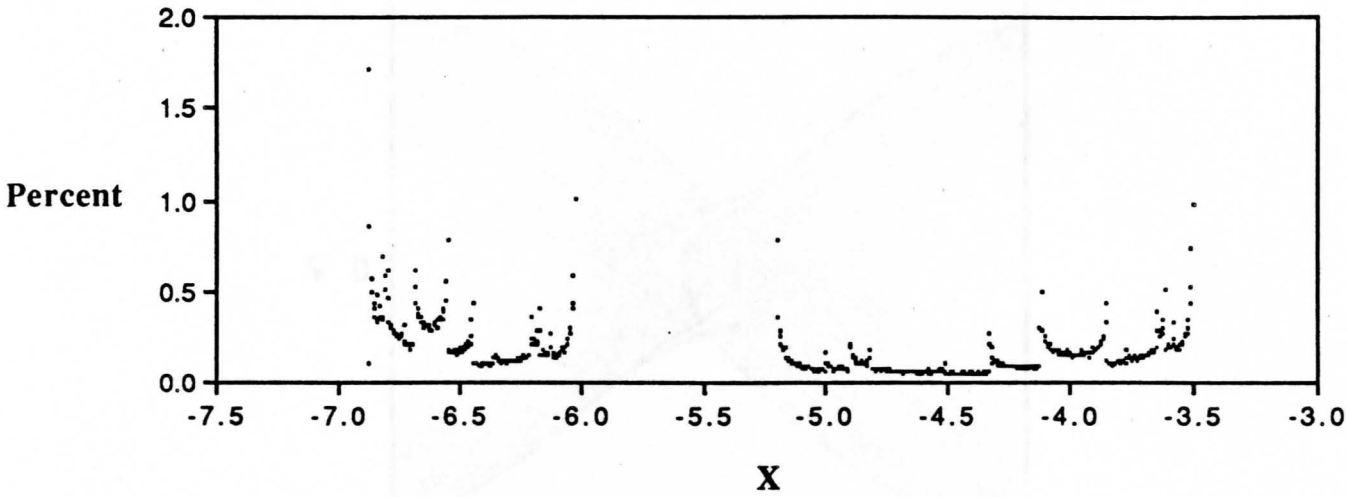
Percent
2.0
1.5
1.0
0.5
0.0
-7.5
-7.0
-6.5
-6.0
-5.5
-5.0
-4.5
-4.0
-3.5
-3.0
X

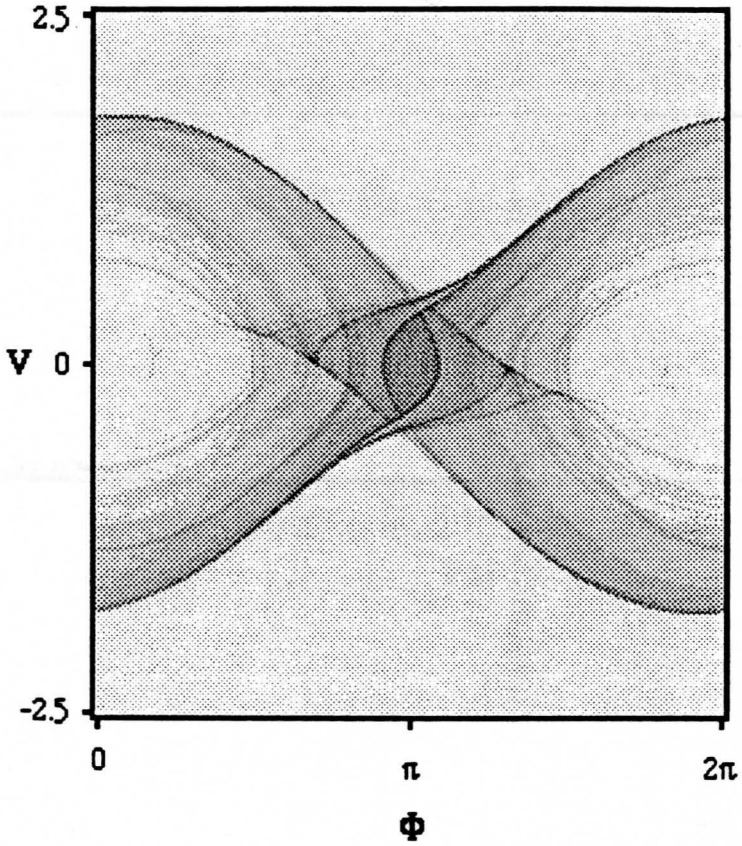
2.5
V 0
-2.5
0
π
2π
Φ

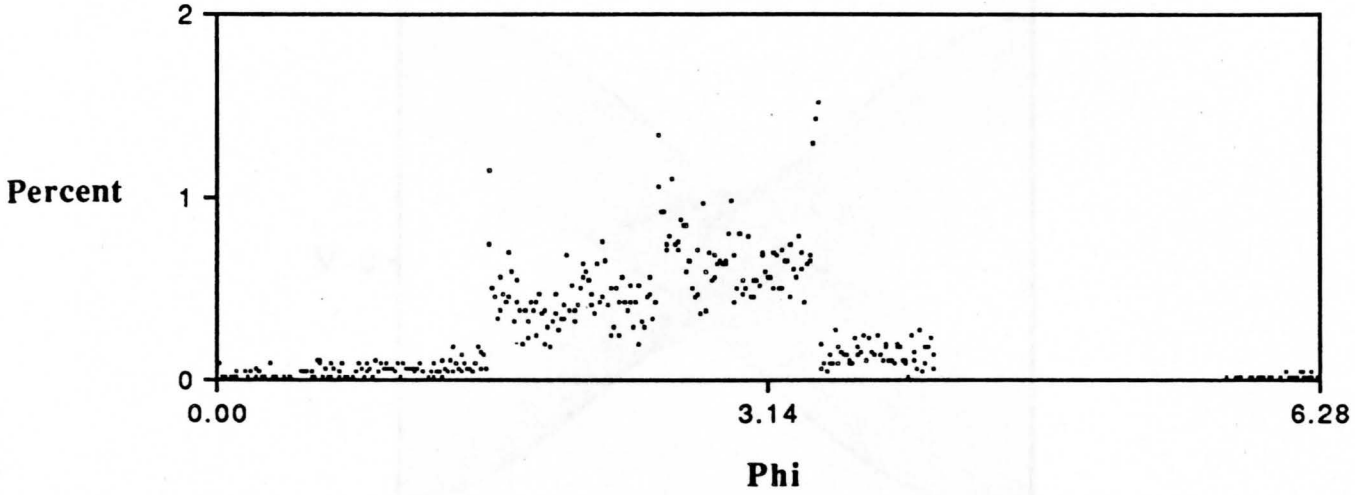
Percent
2
1
0
0.00
3.14
6.28
Phi

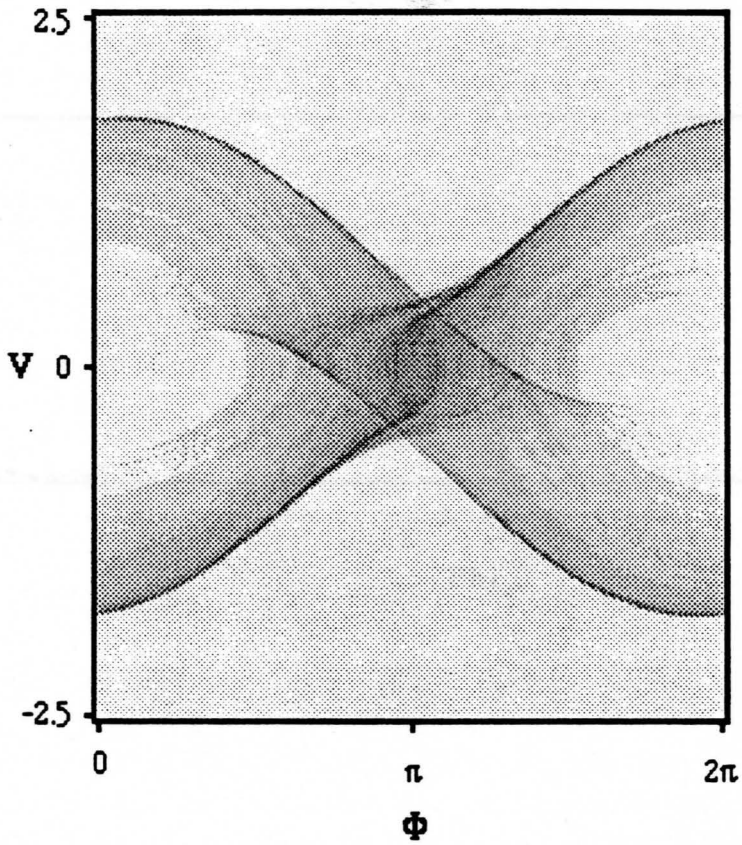
2.5
V 0
-2.5
0
π
2π
Φ

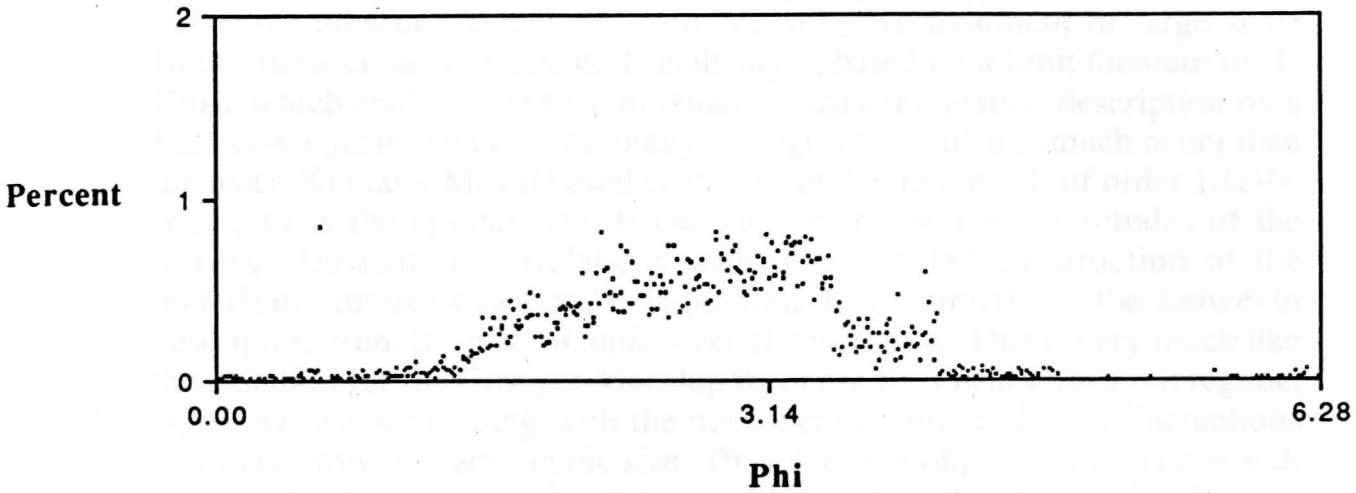
Percent
2
1
0
0.00
3.14
6.28
Phi

Annual Technical Report for Grant: AFOSR-90-0158, "On the Theory of Turbulent Dynamics", for the time period 901001 to 911130 Ronald F. Fox, P.I., (Georgia Tech Project # G-41-613).

In February, 1991 the paper "**Amplification of intrinsic fluctuations by chaotic dynamics in physical systems**", co-authored with Joel Keizer appeared in **Physical Review A43**, pp. 1709-1720. In this paper we present the theory for the quantitative treatment of large scale fluctuations created by chaos. This theory is based on a limit theorem by T. Kurtz which enables one to approximate a master equation description by a Langevin equation with an accuracy of $\text{Log}(\Omega)/\Omega$, which is much better than the usual Kramers-Moyal based central limit theorem result of order $1/\Omega^{1/2}$, where Ω is the system size. If one can determine the magnitudes of the intrinsic fluctuation correlations without a detailed construction of the underlying master equation, it is possible to go directly to the Langevin description from the macroscopic level of description. This is very much like the situation for the Onsager-Machlup theory in the linear relaxation regime, only now we are dealing with the non-linear regime and with fluctuations that may grow to macroscopic size. Thus, the first objective of this research program has been achieved with the establishment of this new approach.

Keizer and I have just finished a long paper on the application of this approach to the Lorenz system for hydrodynamics entitled;"**On the growth of molecular fluctuations for nonstationary systems: hydrodynamic fluctuations for the Lorenz model**". This paper has been submitted to **The Physics of Fluids** and after one round of refereeing we expect the paper to be accepted soon. In it, we present extensive supercomputer simulation results for the Lorenz model including the appropriate fluctuations. This is an example in which the correlations of the fluctuations driving the equations are known independently of a detailed knowledge of the underlying master equation so that the actual construction of the master equation is circumvented. We find that even though there is dramatic amplification of the fluctuations, the stationary probability distribution formed is indistinguishable from the invariant measure for the noiseless simulation. This is in marked contrast with the results, presented in Phys. Rev.A in February, for the Rossler model with fluctuations, and we observe that the reason for this may have to do with the size of the Liapunov exponent which is relatively very large for the Lorenz case. With my student, Tim Elston, whom is subported by this grant, we have looked for a regime in which the Liapunov exponent is smaller and have found several, originally discovered by Sparrow. In these new regimes, clear effects are discernable and we are collecting together our results for publication. In adsdition, by looking instead at the laser-Lorenz model of Haken, in the complex

representation, not only do we also see results like for the Rossler model with a smaller Liapunov exponent, but we also see a period doubling cascade. Another advantage to the model is that it is more closely tied to a real physical system than is the hydro-Lorenz model so that our results can in principle be tested more easily experimentally.

With Elston, I have also been looking at the problem of pattern formation in the Rayleigh-Benard system. This problem is based on the experimental work of the Ahlers group in Santa Barbara, with whom we have had numerous communications. They see a stochastic component to their studies but have found its magnitude to be much bigger than predicted by hydrodynamic fluctuation theory, and this has lead to a bit of a puzzle. While this is not a chaotic system, we thought we should look at it. We found that we could reproduce the fits to experiment with a stochastic theory that included only an initial value distribution (as was suggested to us by M. Rabinovitz) and no stochastic driving force, as opposed to the Ahlers model which uses only a stochastic driving force. This result, "**Stochastic Effects in Rayleigh-Benard Pattern Formation**", has been accepted by **Physical Review A** as a short paper that will appear soon. There is still a puzzle because our initial value fluctuations are also larger than pure thermal fluctuations would be, and we suspect that they have to do with systematic imperfections in the experimental apparatus.

With Raj Roy and one of his students, I have looked at the chaotic amplification of intrinsic fluctuations (spontaneous emission) in a multimode laser. Again, one can go directly to the Langevin description since the intrinsic fluctuation correlations are independently known. Numerical simulation of model equations clearly shows the effect with amplification over many orders of magnitude. Stationary distributions and invariant measures, however, are indistinguishable so that we have studied transient effects in order to see if an experimentally accessible quantity can be identified. In our paper "**Amplification of Intrinsic Noise in a Chaotic Multimode Laser System**", already accepted by **Physical Review A**, we discuss the experimental possibilities. In addition, our transient studies uncovered a new effect of the intrinsic noise that can be seen even in non-chaotic lasers. Thus, the study of noise amplification in a system where noise was originally left out altogether has lead to appreciation of a noise effect totally unexpected. This is mentioned in our paper and will be the subject of subsequent study.

In addition to these completed programs, Elston and I are still working on 2-d turbulence which has lead to numerous computational difficulties. The availability of the Navy supercomputer for this work has been essential.

Georgia Tech has shut down its mainframes this year. The administration's philosophy has been that researchers should shift to workstations instead. This works for those who have access or the wherewithal to obtain access. So far my program has not been adversely affected because the School of Physics purchased an IBM risk workstation to be shared by Flannery, Uzer and myself. Elston does most of his computer program development on this machine and is able to use the supercomputer for big runs. However, I envisage that the growing demand for our risk station by more of the students in our three groups, and by the postdocs, will make this a short term solution. Eventually I will have to procure a dedicated workstation myself, prior to which I will need to procure the funding. Will the Navy-Airforce be able to support such a request in the next year or so?

Final Technical Report for Grant: AFOSR-90-0158, "On the Theory of Turbulent Dynamics", for the time period 900301 to 920930 Ronald F. Fox, P.I., (Georgia Tech Project # G-41-613).

Four papers supported by this grant have appeared in print. They are:

1) "**Amplification of intrinsic fluctuations by chaotic dynamics in physical systems**", R.F. Fox and Joel Keizer, **Physical Review A43**, pp. 1709-1720 (1991).

2) "**Stochastic Effects in Rayleigh-Benard Pattern Formation**", T.C. Elston and R.F. Fox, **Physical Review A44**, pp. 8403-8405 (1991).

3) "**Amplification of Intrinsic Noise in a Chaotic Multimode Laser System**", C. Bracikowski, R.F. Fox and R. Roy, **Physical Review A45**, pp. 403-408 (1992).

4) **"Reply to 'Comments on the Amplification of Intrinsic Fluctuations by Chaotic Dynamics' "**, J.E. Keizer and R.F. Fox, **Physical Review A46**, pp. 3572-3573 (1992).

Two more papers are submitted for publication at this time. They are:

1) "**On the growth of molecular fluctuations for nonstationary systems: hydrodynamic fluctuations for the Lorenz model**", J.E. Keizer, R.F. Fox and J. Wagner, submitted to Physics Letters A (1992).

2) **"Amplification of Thermal Noise by the Lorenz Equations"**, R.F. Fox and T.C. Elston, submitted to Physical Review A (1992).

A book chapter will appear in the Proceedings of the International Workshop on Statisical Physics (IWSP-1992) held at Beijing Normal University, Beijing, P.R. China, October 19-22, 1992. Its title is:

"Amplification of Intrinsic Fluctuations by Chaotic Dynamics", R.F. Fox (1992).

T.C. Elston, the co-author of two of the papers listed above, is a graduate student. The first two years of his research work were supported by this grant which greatly facilitated his ability to focus solely on his research. He is presently completing his thesis with NSF support. I expect him to graduate in May of 1993. C. Bracikowski, the co-author on another paper, was also a graduate student with support from co-author R. Roy.

Elston's research was aided by access to a Navy Cray supercomputer. This facility made possible large scale computations that otherwise could not have been achieved with our local computational resources.

Acceptance of our discovery of amplification of intrinsic fluctuations by chaotic dynamics has been slow. We have been able to identify several of the mental blocks experienced by others and have successfully clarified our position for some of these people. But it has been a slow process. The principal problem has been that some earlier researchers saw amplification of intrinsic fluctuations in their own work but failed to recognize its significance. These include Robert Graham and B. Huberman. The two conceptual insights they have missed are: 1) such amplification invalidates the contraction of the description from the mesoscopic level to the macroscopic level; and 2) the centrality of the Jacobi matrix in the theory since it connects the magnitude (and sign) of the largest Liapunov exponent with the growth of the fluctuations. The first oversight by others follows from their failure to embed the phenomenon in the context of levels of description. Rather, in their work, they have simply added fluctuations to macroscopic equations and investigated what happens. The second oversight results from not suspecting a connection in the first place. I have had success in communicating these thoughts to M. Berry and D. Campbell and am in the process of bringing Robert Graham around as well.

Amplification of intrinsic fluctuations by chaotic dynamics in physical systems

Ronald F. Fox
School of Physics, Georgia Institute of Technology, Atlanta, Georgia 30332

Joel Keizer
Institute of Theoretical Dynamics and Department of Chemistry, University of California, Davis, California 95616

(Received 24 September 1990)

A quantitative method for the treatment of large-scale intrinsic fluctuations amplified by chaotic trajectories in macrovariable physical systems is presented. Paradigmatic results for the Rossler model and preliminary computational results for chaotic Josephson junctions and for chaotic multimode Nd:YAG (yttrium aluminum garnet) lasers are described. These studies are directed towards identification of a real physical system in which experimental confirmation may be realized. The probability distribution on the intrinsic-noise-modified, chaotic attractor is identified as a likely candidate for comparison of experiment and theory.

I. INTRODUCTION

In several recent papers,[1–4] we showed that chaotic dynamics can cause macroscopic growth of intrinsic fluctuations in a macrovariable system. Implications of this effect were suggested for systems as diverse as chemical, hydrodynamic, electronic, and quantum. In this paper, we propose a highly accurate approach to the theoretical description of such large-scale fluctuations. Our proposal is based upon a limit theorem for Markov chains proved by Kurtz[5,6] in 1975, long before its relevance for chaotic dynamics could be appreciated.

That chaotic dynamics and the growth of intrinsic fluctuations are related to each other is a consequence of each being fundamentally tied to a dynamical quantity called the Jacobi matrix.[2] A quantitative characterization of chaos is provided by the largest Liapunov exponent, which when positive, implies chaos.[7] The computation of the largest Liapunov exponent directly utilizes the instantaneous values of the Jacobi matrix.[8] Similarly, the growth of the intrinsic fluctuations is made quantitative by following the time evolution of the covariance matrix.[9,10] Again, the computation of the covariance matrix evolution directly utilizes the instantaneous values of the Jacobi matrix.[2] This dual role of the Jacobi matrix and the consequence that intrinsic fluctuations become very large in a chaotically dynamic system was apparently noticed for the first time only recently.[1,2,4]

In order to make this connection explicit, imagine a macrovariable system described by N macrovariables $M_i(t)$ for $i=1,2,\ldots,N$ satisfying N coupled, nonlinear, ordinary, differential equations

$$\frac{d}{dt}M_i(t)=F_i(\mathbf{M}(t)) \tag{1}$$

in which the F_i's are N, generally nonlinear functions of the M_k's. The Jacobi matrix $J_{ik}(t)$ is defined[7] by

$$J_{ik}(t)=\frac{\partial F_i}{\partial M_k(t)} \tag{2}$$

for each instant of time. It has been shown that the largest Liapunov exponent for this dynamics λ is given by[8]

$$\lambda=\lim_{n\to\infty}\frac{1}{2n}\ln\{\mathrm{Tr}[\underline{J}^{\dagger}(n)\underline{J}(n)]\} \tag{3}$$

in which $\underline{J}^{\dagger}(n)$ is the adjoint of $\underline{J}(n)$. On the other hand, it has also been established that if Eq. (1) is the macroscopic limit of an embedding (see below) master equation (i.e., some "largeness parameter," say Ω, is allowed to go to an infinite limit), and if the scaled linearized deviations from the deterministic solutions to Eq. (1) are denoted by $\mu_i(t)=\Omega^{1/2}\Delta M_i(t)$ [where $\Delta M_i(t)$ is the unscaled deviation], and if the covariance matrix for these deviations (fluctuations) is denoted by $C_{ik}(t)=\langle\mu_i(t)\mu_k(t)\rangle$, where $\langle\ \rangle$ denotes averaging with respect to the master equation's probability distribution, then $C_{ik}(t)$ satisfies

$$\frac{d}{dt}C_{ik}(t)=J_{ij}(t)C_{jk}(t)+C_{ij}(t)J_{kj}(t)+R_{ik}(t)\ , \tag{4}$$

in which $R_{ik}(t)$ is explicitly determined from the master equation. The exponential divergence of fluctuations in the limit of large Ω is reflected in the fact that Eq. (3) is also valid if $\underline{C}^{\dagger}(t)$ and $\underline{C}(t)$ are substituted in place of $\underline{J}^{\dagger}(n)$ and $\underline{J}(n)$ on the right-hand side.[1,4]

The covariance matrix evolution equation involves a linearization of the macrovariable dynamics instantaneously in time. This, of course, produces the Jacobi matrix dependence, but it also means that once the fluctuations have grown even a little bit, the linearized equations lose their validity. In our earlier work[1,2,4] we stressed this point, and noted that while the covariance matrix evolution permitted computation of the largest Liapunov exponent, it did not accurately describe the fluctuations once they grew to macroscopic size. In order to obtain the large-scale fluctuations, a mesoscopic underpinning of the macrovariable equations is required.[2,3] One way to accomplish this is to embed the macrovariable equations in a mesoscopic master equation and deduce the time evolution of the underlying probability distribution.

$$K_i^{(1)}(\mathbf{m},t)=\int d^N m'(m_i'-m_i)W(\mathbf{m}',\mathbf{m}) , \tag{7}$$

$$K_{ij}^{(2)}(\mathbf{m},t)=\int d^N m'(m_i'-m_i)(m_j'-m_j)W(\mathbf{m}',\mathbf{m}) , \tag{8}$$

etc. The Ω properties of W imply[23] that $K^{(1)}\approx O(1)$, $K^{(2)}\approx O(1/\Omega)$, and generally $K^{(n)}\approx O(1/\Omega^{n-1})$. Using these transition moments, the master equation may be rewritten in the equivalent Kramers-Moyal form[24,25]

$$\frac{\partial}{\partial t}P(\mathbf{m},t)=\sum_{n=1}^{\infty}\frac{(-1)^n}{n!}\left[\prod_{j=1}^{n}\frac{\partial}{\partial m_{k_j}}\right] \times[K_{k_1k_2\cdots k_n}^{(n)}(\mathbf{m})P(\mathbf{m},t)] . \tag{9}$$

With these properties, the macroscopic limit, i.e., $\Omega\to\infty$, implies[2]

$$\frac{\partial}{\partial t}P_\infty(\mathbf{m},t)=-\frac{\partial}{\partial m_i}[K_i^{(1)\infty}(\mathbf{m})P_\infty(\mathbf{m},t)] , \tag{10}$$

where the repeated indices in both Eq. (9) and (10) imply a summation and where the subscript (superscript) ∞ denotes the macroscopic limit of the corresponding quantity. This partial differential equation is very special since its derivatives are all first order. This means that if the initial values for the $\mathbf{m}$ components are given precisely, i.e., $P_\infty(\mathbf{m},0)=\delta(\mathbf{m}-\mathbf{m}_0)$, then the solution to Eq. (10) is simply[2]

$$P_\infty(\mathbf{m},t)=\delta(\mathbf{m}-\mathbf{m}(t)) , \tag{11}$$

where $\mathbf{m}(t)$ satisfies the system of coupled ordinary differential equations

$$\frac{d}{dt}m_i(t)=K_i^{(1)\infty}(\mathbf{m}(t)) . \tag{12}$$

Moreover, if we apply the averaging defined in Eq. (16), we obtain the equations

$$\frac{d}{dt}M_i(t)=\langle K_i^{(1)\infty}(\mathbf{m})\rangle=K_i^{(1)\infty}(\langle\mathbf{m}\rangle) =K_i^{(1)\infty}(\mathbf{M}(t)) \tag{13}$$

on account of the Dirac δ-function solution (11). Thus $\mathbf{M}(t)$ is the same as $\mathbf{m}(t)$, since both solve the same equation with the same initial condition $\mathbf{m}(0)=\mathbf{M}(0)=\mathbf{m}_0$. Having constructed the master equation so that $K_i^{(1)\infty}=F_i$ for the F_i's of Eq. (1), we achieve an embedding of the macrovariable equations in the master equation description as the macroscopic limit.

We can also obtain a dynamical description of the intrinsic fluctuations with this master-equation approach. Generally, the intrinsic fluctuations in the macrovariables scale[11] like $1/\Omega^{1/2}$. This means that they simply vanish in the macroscopic limit. In the spirit of the central limit theorem of probability theory,[23] it is possible to rescale the fluctuations so that their limiting behavior may be rigorously deduced. This is done by considering the deviations of the $\mathbf{m}$ components from the deterministic solution to the macroscopic limit equation (12), i.e., $\mathbf{m}(t)$ scaled with $\Omega^{-1/2}$:

$$\mathbf{m}=\mathbf{m}(t)+\Omega^{-1/2}\mu , \tag{14}$$

which defines the scaled intrinsic fluctuations μ. This scaling implies that as $\Omega\to\infty$, the μ components are of order unity. We shift attention from the probability distribution $P(\mathbf{m},t)$ to the probability distribution for the scaled intrinsic fluctuations $\Phi(\mu,t)$. It is then possible to show[2] that in the macroscopic limit (i.e., $\Omega\to\infty$), we obtain

$$\frac{\partial}{\partial t}\Phi=-\frac{\partial}{\partial\mu_i}\left[\frac{\partial}{\partial m_j}K_i^{(1)\infty}(\mathbf{m}(t))\mu_j\Phi\right] +\frac{1}{2}\frac{\partial^2}{\partial\mu_i\partial\mu_j}[R_{ij}^{(2)}(\mathbf{m}(t))\Phi] , \tag{15}$$

in which $R_{ij}^{(2)}$ is defined by

$$R_{ij}^{(2)}=\lim_{\Omega\to\infty}\Omega K_{ij}^{(2)}(\mathbf{m}(t)) . \tag{16}$$

This is a Fokker-Planck equation for a nonstationary, Gaussian, Markov process. The nonstationary results from the explicit dependence on $\mathbf{m}(t)$ in both $K_i^{(1)\infty}$ and $R^{(2)}$. Since this $\mathbf{m}(t)$ is found from (12), the deterministic macrovariable equations, we say that the intrinsic fluctuations "ride on the back" of the deterministic motion. We will refer to the rigorous proof of this result as "Kurtz's *first* theorem."

Several remarks are in order.[2] The time-dependent coefficients of the first-order μ derivatives in Eq. (15) are precisely the components of the Jacobi matrix for the deterministic macrovariable equations [either (1) or (12)]

$$J_{ij}(t)=\frac{\partial}{\partial m_j}K_i^{(1)\infty} . \tag{17}$$

Defining the covariance matrix for the intrinsic fluctuations by

$$C_{ik}(t)=\langle\mu_i(t)\mu_k(t)\rangle , \tag{18}$$

where $\langle\ \rangle$ denotes averaging with respect to $\Phi(\mu,t)$, leads to the equation [derived from Eq. (15)]

$$\frac{d}{dt}C_{ik}(t)=J_{ij}(t)C_{jk}(t)+C_{ij}(t)J_{kj}(t)+R_{ik}^{(2)}(t) . \tag{19}$$

This is exactly (4) of the Introduction [(17) is precisely (2) because of Eq. (6)] and shows how the Jacobi matrix for the deterministic motion arises in the dynamics of the intrinsic fluctuations. The following and final remark is the central issue of this paper. If the deterministic motion is chaotic, then the Jacobi matrix will create an unbounded growth of the C_{ik} components.[2,4] Since the derivation of (15), and hence of (19), assumes that the μ components remain of order unity, it would be inconsistent to use Eq. (19) when the fluctuations grow larger than this. As will be shown below, there exists an alternative treatment[5,6] for this case in which the intrinsic fluctuations can grow large.

One way to express the content of the limit theorem[23] reviewed above is to write

$$\mathbf{M}(t)=\langle\mathbf{m}\rangle_t+O(1/\Omega^{1/2}) , \tag{20}$$

in which $\langle\ \rangle_t$ is the average with respect to $P(\mathbf{m},t)$. This says that the deterministic equations' solution approximates the expected values of the underlying mesoscopic master equation with an error of order $1/\Omega^{1/2}$, i.e., an error the size of the fluctuations. The proper interpretation of this result is that the more fundamental physical description is given by the master equation, whereas the deterministic macrovariable equation is an approximate description. In the macroscopic limit where intrinsic fluctuations may be ignored (provided that they do not grow large), it is far easier to use the macrovariable equations than to use the master equation. However, if the intrinsic fluctuations grow too large for this treatment to be valid (seen as chaos at the macrovariable level), then another limit theorem is available, "Kurtz's *second* theorem."[5,6] Not only does Kurtz's second theorem allow one to handle the large intrinsic fluctuations, but it does so with even greater accuracy than expressed in (20). If we denote the solution to this alternative treatment, to be elucidated below, by $\mathbf{M}_f(t)$, then Kurtz's second theorem[5,6] implies

$$\mathbf{M}_f(t)=\langle\mathbf{m}\rangle_t+O(\ln\Omega/\Omega)\ . \tag{21}$$

$\mathbf{M}_f(t)$ combines both the macrovariable behavior and the large fluctuations and its probability distribution satisfies the Fokker-Planck equation

$$\frac{\partial}{\partial t}P_f(\mathbf{m},t)=-\frac{\partial}{\partial m_i}[K_i^{(1)\infty}(\mathbf{m})P_f(\mathbf{m},t)] + \frac{1}{2}\frac{\partial^2}{\partial m_i\partial m_j}[K_{ij}^{(2)\infty}(\mathbf{m})P_f(\mathbf{m},t)]\ , \tag{22}$$

so that

$$\mathbf{M}_f(t)=\int d^N m\ \mathbf{m}P_f(\mathbf{m},t)\ . \tag{23}$$

When this limit theorem was originally obtained,[5,6] the chaotic amplification of intrinsic fluctuations was not yet clearly understood.[9,10] Since the typical applications involved near equilibrium states or stable steady states away from critical points, for which intrinsic fluctuations remained small, a vanishingly small difference in behavior resulted from using (22) instead of the more tractable (15). Thus this treatment remained largely ignored. On occasion, however, an objection to (22) has been voiced[12] because the averaging defined by (23) implies

$$\frac{d}{dt}(M_f(t))_i=\langle K_i^{(1)\infty}(\mathbf{m})\rangle\neq K_i^{(1)\infty}(\langle\mathbf{m}\rangle) \tag{24}$$

since Eq. (22) does not have a Dirac δ-function solution [cf. Eqs. (10)–(13)]. For intrinsic fluctuations that remain small, the difference between the two expressions on the right-hand side of (24) is only order $O(1/\Omega^{1/2})$, i.e., ignorable. For intrinsic fluctuations that grow large, this same inequality is a sign of the breakdown of the macrovariable limit altogether, as has been shown earlier.[1,2] Therefore, Eq. (22) is perfectly suited to the situation we are confronting.

Because the direct solution to (22) is numerically demanding, we prefer to use a more tractable, equivalent[9] method, the nonlinear Langevin treatment. This is possible because to every probability distribution equation satisfying (22), there is associated a unique Langevin-like equation. However, great care is required in order to express the Langevin equivalent correctly, since there are two valid, yet distinct versions of stochastic calculus by which the equivalence can be realized, the Ito and the Stratonovich versions.[26] The proof of the limit theorem[5,6] that produces Eq. (22) makes use of Martingale properties[26] and in so doing arrives at Eq. (22) in the Ito context. Numerical realizations of Langevin equations in our hands are done in the manner of Stratonovich[27] using the traditional Newtonian calculus. Therefore, we need to obtain the Stratonovich Langevin equation equivalent to the Ito probability distribution Eq. (22). This is done as follows. Suppose $\mathbf{M}_f(t)$ satisfies the stochastic differential equation

$$\frac{d}{dt}(\mathbf{M}_f(t))_i=\alpha_i(\mathbf{M}_f(t))+\beta_{ij}(t)g_j(t)\ , \tag{25}$$

where the derivatives are to be manipulated according to the usual calculus and where the g_j's are statistically independent Gaussian white noises with zero means and covariances of unit strength, i.e.,

$$\langle g_k(t)\rangle=0\ , \tag{26}$$

$$\langle g_i(t)g_k(t')\rangle=\delta_{ik}\delta(t-t')\ , \tag{27}$$

in which $\langle\ \rangle$ denotes averaging with respect to the g_k distributions. The Fokker-Planck equation satisfied by the Stratonovich stochastic process in Eq. (25) is[26]

$$\frac{\partial}{\partial t}P_f(\mathbf{m},t)=-\frac{\partial}{\partial m_i}[\alpha_i(\mathbf{m})P_f(\mathbf{m},t)] + \frac{1}{2}\frac{\partial}{\partial m_i}\beta_{ik}(t)\frac{\partial}{\partial m_j}\beta_{jk}(t)P_f(\mathbf{m},t)\ , \tag{28}$$

which may be rearranged as

$$\frac{\partial}{\partial t}P_f(\mathbf{m},t)=-\frac{\partial}{\partial m_i}\left[\alpha_i(\mathbf{m})P_f(\mathbf{m},t) + \frac{1}{2}\left[\frac{\partial}{\partial m_j}\beta_{ik}(t)\right]\beta_{jk}(t)P_f(\mathbf{m},t)\right] + \frac{1}{2}\frac{\partial^2}{\partial m_i\partial m_j}\beta_{ik}(t)\beta_{jk}(t)P_f(\mathbf{m},t)\ . \tag{29}$$

In both (28) and (29), repeated indices are summed. To identify the correct α and β to be used in Eq. (25), we need only compare Eqs. (22) and (29). Since $K_{ij}^{(2)\infty}$ is a symmetric, non-negative matrix at each instant of time, the square root of $K_{ij}^{(2)\infty}$ will also be symmetric and one finds that

$$\beta(t)=[K^{(2)\infty}(t)]^{1/2}\ , \tag{30}$$

$$\alpha_i(t)=K_i^{(1)\infty}(t)-\frac{1}{2}\left[\frac{\partial}{\partial m_j}\beta_{ik}(t)\right]\beta_{jk}(t)\ . \tag{31}$$

Generally, β is of order $1/\Omega^{1/2}$ so that α differs from $K_i^{(1)\infty}$ only to order $1/\Omega$ and this "Ito-Stratonovich shift" is ignorable,[9] but when the intrinsic fluctuations are large, not only will this difference be important, but (25) will differ markedly from the purely deterministic

macrovariable equation (12) [equivalently (1)].

There is an additional advantage to using Eq. (25) for the study of chaotically amplified intrinsic fluctuations. The only feature of the underlying mesoscopic master equation that remains in Eqs. (25), (30), and (31) is the matrix $K_{ij}^{(2)\infty}$ (the vector $K_i^{(1)\infty}$ is predetermined by the macrovariable equations). Thus we need not know the underlying master equation in full detail, but only the second moment of the transition probability [see (8)]. With physical insight, it may be possible to correctly guess $K_{ij}^{(2)\infty}$ without obtaining the full master equation. Hydrodynamics may be an example of this circumstance.[9]

The description of large-scale intrinsic fluctuations by Eqs. (25)–(27), (30), and (31) combines the macrovariable and the intrinsic fluctuation dynamics in one quantity $\mathbf{M}_f(t)$, unlike the situation for small fluctuations wherein two sets of equations [Eqs. (12) and (15)] are obtained. The intrinsic fluctuations no longer "ride on the back" of the deterministic macrovariables and, indeed, no autonomous macrovariable equation exists [see (24)]. When the intrinsic fluctuations grow large, the distribution function $P_f(\mathbf{m},t)$ becomes broadly spread out, unlike the extremely sharp distribution given by (11), which is only valid when the fluctuations remain small.[9] For this reason, the concept of a deterministic macrovariable is lost. While one may still use (23) to define an "average" value, there is no longer an autonomous dynamics for the $\mathbf{M}_f$ components because of the broadness of the P_f distribution.[2]

The breakdown of the autonomous macrovariable equations associated with large-scale intrinsic fluctuations forces a reassessment of the meaning of chaos in real physical systems. Conceptually, one must shift focus from the wild deterministic macrovariable trajectories to large-scale intrinsic fluctuations. A variety of new characterizations needs to be developed, and the examples that are presented in Sec. IV are meant to indicate some possible avenues for this development. In each of the examples, we will use the approach represented by Eq. (25), since it is the most tractable and is also a highly accurate representation of the mesoscopic level of description.

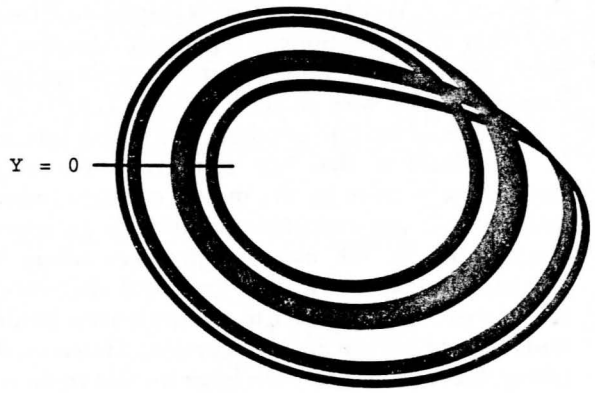

FIG. 1. X-Y plot of the Rossler attractor for $\mu=4.23$ and $\sigma=0$.

One should not confuse this approach with previous work that treats the effects of *extrinsic* noise on macrovariable systems[13,17] using similar equations. In these treatments, some of which have the same form as (25), the α_i's are just the $K_i^{(1)\infty}$'s [i.e., the F_i's of Eq. (1)] and the β_{ik}'s are not connected to the state of the system, i.e., there is no "intrinsic fluctuation-dissipation relation" as in (30), because the fluctuations are *extrinsic* and not *intrinsic*. That is, the strength of the extrinsic noise does not depend on the state of the system. Moreover, if the intrinsic fluctuations have grown by a large scale, the breakdown of the autonomous macrovariable equations implies that extrinsic fluctuations should be introduced directly at the mesoscopic level, not at the deterministic macrovariable level, which is no longer valid.

All the preceding considerations must be qualified by the observation that the growth of intrinsic fluctuations depends upon two quantities, their rate of growth (this is related to the largest Liapunov exponent) and their initial size [this is determined by (30) at $t=0$]. In the Josephson-junction[15] example that follows, both of these quantities are "large," whereas in the laser[16] example,

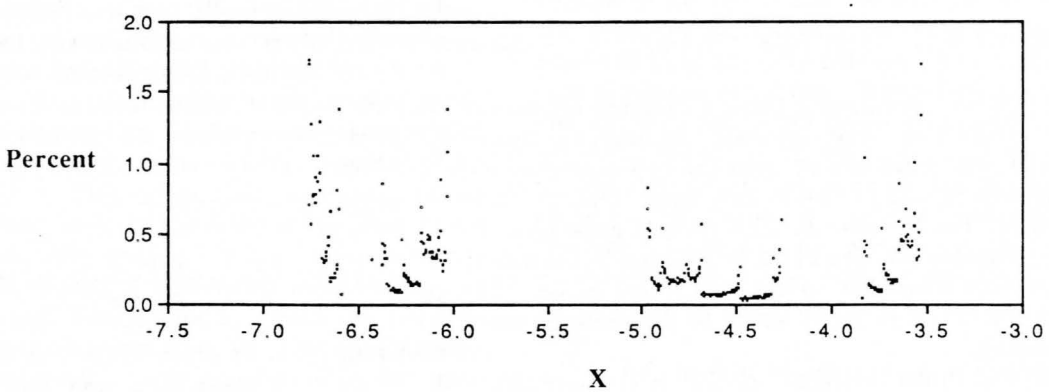

FIG. 2. Invariant measure for the attractor in Fig. 1 projected onto the negative X axis at $Y=0$. The vertical axis gives the percentage of crossing points in an X-axis bin. 1024 bins were used over the range of X values indicated in the figure.

both of these quantities are "small." In the Rossler[14] paradigm, we explore both regimes and motivate our expectations for the real physical systems.

IV. EXAMPLES

The purpose of these examples is twofold. They make the general ideas concrete and they help to make contact with real experiments. Ultimately, we wish to identify a real physical system in which quantitative measurements can be used to explore the amplification of intrinsic fluctuations. Significant progress in this direction is reported.

As our first example, which exhibits behavior like both of the following examples, we look at a purely mathematical model, the Rossler model.[14,28] This model was invented to show the minimal ordinary differential equation system that can have chaos. We have chosen it because of its great simplicity. The route to chaos in this model is period doubling of a limit cycle. The equations, in three independent variables, X, Y, and Z, are

$$\frac{d}{dt}X=-(Y+Z)\ , \tag{32}$$

$$\frac{d}{dt}Y=X+\tfrac{1}{5}Y\ , \tag{33}$$

$$\frac{d}{dt}Z=\tfrac{1}{5}+Z(X-\mu)\ , \tag{34}$$

in which μ is an adjustable parameter. For $\mu=2.6$, the asymptotic state is a simple limit cycle attractor. It has a period of about 5.8 time units. The unit of time is dimensionless, and power spectra show a fundamental at about 0.17 Hz (cycles per unit of dimensionless time). (In the literature,[14] the unit of time is arbitrarily taken to be 0.01 s, so that the fundamental becomes 17 Hz.) For $\mu=3.5$, the limit cycle has bifurcated once, while for $\mu=4.1$, it has done so twice. After this, much smaller changes in μ lead to increasing numbers of bifurcations; until around $\mu=4.2$, infinitely many have occurred and the motion becomes chaotic. For $\mu=4.23$, the largest Liapunov exponent is $\lambda=0.014$.

This system of equations does not describe a real physical system. Therefore, construction of an underlying master equation cannot benefit from physical insight into real molecular substructure. Nevertheless, for the sake of illustration, we can imagine that such an underlying, mesoscopic, molecular picture really does exist. This means that we must construct an underlying master equation for the Rossler model, based on an imagined underlying molecular basis. There are many ways to do this that yield the Rossler model in the macroscopic limit but produce different fluctuations. Whichever specific choice we make, we can circumvent the actual construction of the master equation by invoking Kurtz's second theorem. We do so by merely adding an *intrinsic* noise term to Eq. (34), say, in accord with Kurtz's second theorem as discussed in Sec. III. While arbitrary for the Rossler model, this procedure serves to illustrate how noise amplification can be seen in models of real physical systems, wherein the specification of the added noise is determined entirely by the nature of the physical system. The noise to be added to the Rossler model is Gaussian, white noise with state independent strength, so that no Ito-Stratonovich shift is required.

Note that what we are doing looks similar to what others have done to treat the addition of *extrinsic* noise to the Rossler model. However, the interpretation is significantly different. For extrinsic noise, X, Y, and Z re-

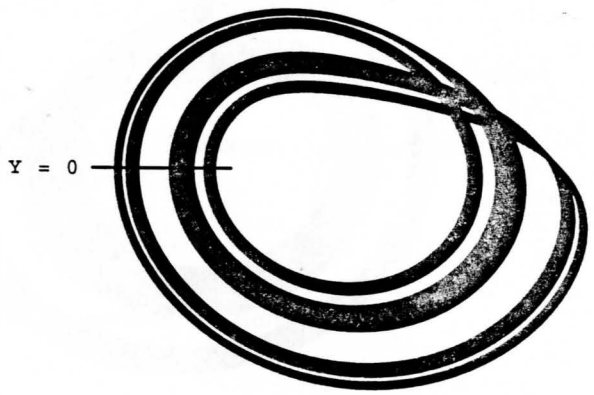

FIG. 3. X-Y plot of the Rossler attractor for $\mu=4.23$ and $\sigma=10^{-8}$.

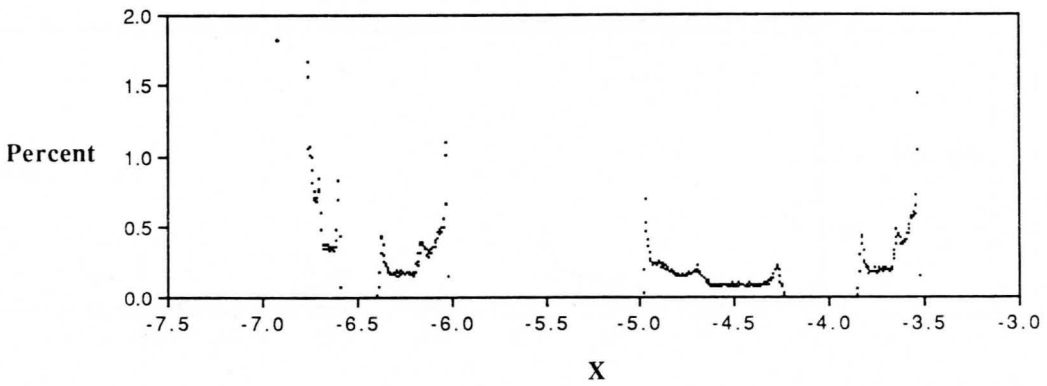

FIG. 4. Probability distribution for the attractor in Fig. 3 projected onto the negative X axis at $Y=0$. All other aspects of the figure are the same as in Fig. 2.

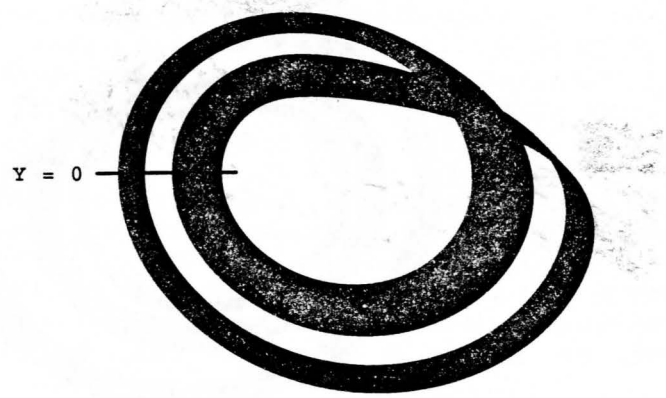

FIG. 5. X-Y plot of the Rossler attractor for $\mu=4.23$ and $\sigma=10^{-6}$.

tain their meaning and their values merely become noisy, but for intrinsic molecular noise, the underlying probability distribution implicitly in mind when we construct the mesoscopic description, either by a master equation or by Kurtz's second theorem, becomes broad because of chaos amplification of noise, and X, Y, and Z cease to be meaningful variables. No autonomous dynamics exists for them. In other words, the macrovariable picture breaks down,[2,4] and the mesoscopic description is required for a correct quantitative treatment.

Let us now return to our *ad hoc* mesoscopic treatment of the Rossler model. The observation of the amplification of intrinsic noise by chaotic trajectories is achieved in the following manner: First, we run Eqs. (32)–(34) numerically and plot the attractor (after the transients have died away) in the X-Y plane (X along the horizontal axis and Y along the vertical axis). This is shown in Fig. 1 for $\mu=4.23$. Also shown is a horizontal line cutting the left-hand portion ($X<0$) of the attractor along $Y=0$. We determine numerically the probability distribution (in the noise-free case, this is called the invariant measure) for X values. This is shown in Fig. 2. Next, we redo all of this with the noise present. As indicated above, this is done by using Eqs. (32) and (33) as is, and by adding Gaussian, white noise with zero mean g to Eq. (34), i.e.,

$$\frac{d}{dt}Z=\tfrac{1}{5}+Z(X-\mu)+g\ , \tag{35}$$

in which g has correlation formula

$$\langle g(t)g(t')\rangle=2\sigma\delta(t-t')\ , \tag{36}$$

in which σ is an adjustable noise strength. In a real physical model, this noise strength would be determined by the underlying physics through the master equation. For our illustrative purposes, it is adjustable so that we can explore how effects depend on its size. Figures 3 and 4 show the results paralleling Figs. 1 and 2 for $\mu=4.23$ and $\sigma=10^{-8}$. It is extremely difficult to discern any differences between Figs. 1 and 3, but there is very clear smoothing of the probability distribution of Fig. 2 in Fig. 4 as a result of intrinsic noise amplification. If, instead, our noise has been instrumental, then we would see it as a smoothing of Fig. 2 with a Gaussian smoothing function with standard deviation equal to $\sigma^{1/2}$, a magnitude of 10^{-4}, that would not produce a visually observable effect on Fig. 2. However, amplification of intrinsic noise produces the clearly observable effect seen in Fig. 4 and shows that the amplification is to macroscopic size (i.e., order unity). Figures 5 and 6 show what happens when $\sigma=10^{-6}$. Now both figures are visually effected and the attractor shows only two bands instead of four. The attractor in Fig. 5 could be mistaken for the more chaotic, noise-free attractor in Fig. 7 obtained for $\mu=4.3$, but the corresponding invariant measure of Fig. 8 is easily distinguished from Fig. 6.

These cases clearly suggest that the way to observe the chaotic amplification of intrinsic noise is to contrast the resulting probability distribution with the noise-free invariant measure. Even when the corresponding attractor plots show no discernible differences, the differences in the probability distributions can be very marked. For big enough noise, even the attractor plots may become distinguishable. The following two examples illustrate this diagnostic approach in models of real physical systems.

The Josephson junction is a real, electronic, physical system in which conditions can be arranged so that it appears to exhibit chaos. A simple mathematical description of the phenomenon in terms of either a macrovariable current, or a macrovariable voltage (or associated

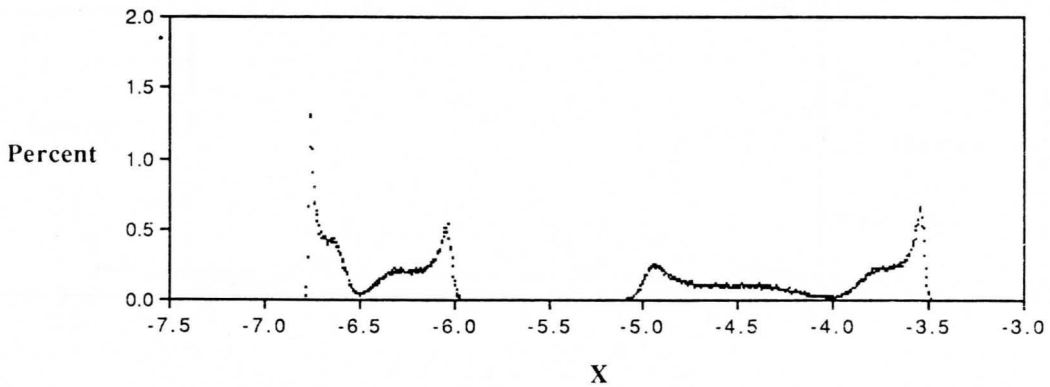

FIG. 6. Probability distribution for the attractor in Fig. 5 projected onto the negative X axis at $Y=0$. All other aspects of the figure are the same as in Figs. 2 and 4.

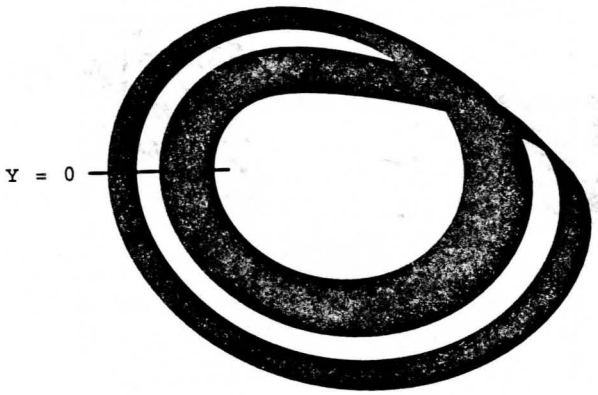

FIG. 7. X-Y plot of the Rossler attractor for $\mu=4.3$ and $\sigma=0$.

phase), also can exhibit chaos. Incidentally, this is one of those examples, alluded to in the Introduction, for which published accounts[15] refer to the chaos in the macrovariable time dependence as a "noise rise." This usage is not what we mean by "chaotically amplified intrinsic noise," and one must make an effort to avoid confusion.

The macrovariable model for superconductor-insulator-superconductor (SIS) Josephson junctions operated in the classical regime (i.e., $eI_0R < k_BT$ to be interpreted below) is[15]

$$C\frac{dV}{dt}+\frac{V}{R}+I_0\sin\phi=I_{\rm dc}+I_{\rm rf}\sin\omega t \ , \tag{37}$$

in which ϕ is the macroscopic quantum phase of the supercurrent, C is the capacitance of the junction, R is its resistance, I_0 is the critical current, $I_{\rm dc}$ is the applied dc current, $I_{\rm rf}$ is the amplitude of the applied rf current with frequency ω, and V is the junction voltage related to ϕ by

$$V=\frac{\hbar}{2e}\frac{d\phi}{dt} \ , \tag{38}$$

in which $\hbar$ is Planck's constant (divided by 2π) and e is the charge of an electron. One may proceed with the two coupled equations (37) and (38), or convert to one second-order equation

$$\frac{\hbar}{2e}\frac{C}{I_0}\frac{d^2\phi}{dt^2}+\frac{\hbar}{2e}\frac{1}{I_0R}\frac{d\phi}{dt}+\sin\phi=\frac{I_{\rm dc}}{I_0}+\frac{I_{\rm rf}}{I_0}\sin\omega t \ . \tag{39}$$

This form of the equation suggests defining the junction frequency ω_0 by

$$\omega_0=\left[\frac{\hbar C}{2eI_0}\right]^{-1/2} \tag{40}$$

and the dimensionless time τ by

$$\tau=\omega_0 t \ . \tag{41}$$

If we also introduce the McCumber parameter[29] $\beta_c=2eI_0R^2C/\hbar$ and the ratios $\rho=I_{\rm dc}/I_0$ and $\rho_1=I_{\rm rf}/I_0$, Eq. (39) becomes

$$\frac{d^2\phi}{d\tau^2}+\frac{1}{\sqrt{\beta_c}}\frac{d\phi}{d\tau}+\sin\phi=\rho+\rho_1\sin\left[\frac{\omega}{\omega_0}\tau\right] \ , \tag{42}$$

which is the canonical form for the Josephson junction and is seen to be the equation for a periodically perturbed, damped, planar pendulum,[30] well known for its capacity to exhibit chaos.

This description of the junction is macroscopic and the macrovariable current represents many Cooper electron pairs. Individual Cooper-pair motions show up as intrinsic fluctuations in the macrovariable current. This is not unlike the picture of current fluctuations in a classical resistor,[9] i.e., Johnson noise, except that the electrons are not paired and, in addition, Johnson noise occurs in a resistor in series with a voltage, whereas Josephson-junction noise occurs with a resistor and a capacitor in parallel with the junction voltage.

In principle, we should now try to construct a master equation that has Eq. (42) as its macroscopic limit and contains the correct physics for the determination of $K^{(2)\infty}$. This is not an easy task. However, in other electronic circuits with a configuration of capacitor and resistance identical to that for Eq. (37) (i.e., in parallel with the voltage), the determination of the strength of the fluctuations through a master equation, has already been obtained successfully.[9] This allows us to use Kurtz's second theorem to obtain a stochastic realization of the

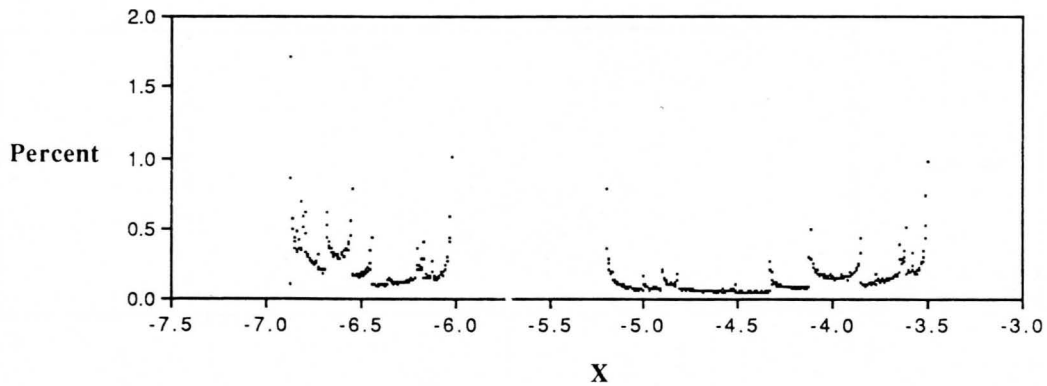

FIG. 8. Invariant measure for the attractor in Fig. 7 projected onto the negative X axis at $Y=0$. All other aspects of the figure are the same as in Figs. 2, 4, and 6.

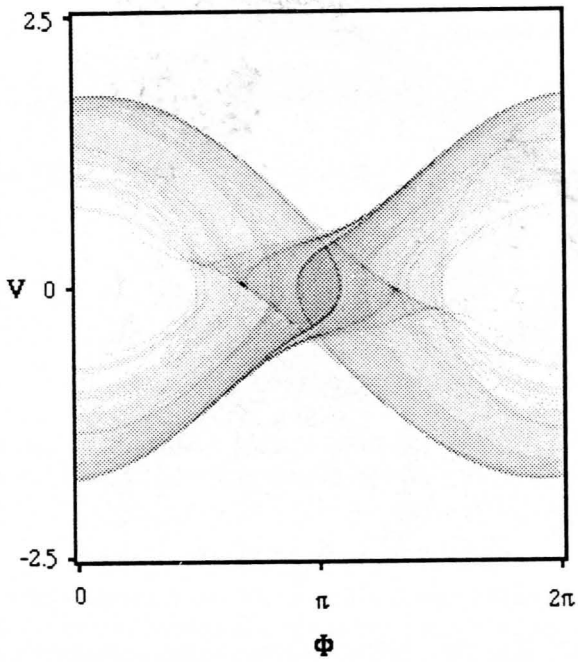

FIG. 9. Invariant measure for the Josephson-junction equations with no noise.

mesoscopic description. The result is to add a stochastic term to the right-hand side of (37) of the form $g\,f(t)$, where f is Gaussian, white noise with zero mean and

$$\langle f(t)f(t')\rangle=\delta(t-t')\ , \tag{43}$$

$$g=(2k_BT/R)^{1/2}\ , \tag{44}$$

in which k_B is Boltzmann's constant, T is the junction temperature, and R is the junction resistance. (Note that for Johnson noise, $g\sim R^{1/2}$ when quantities are expressed as functions of frequency instead of time.) This amounts to the addition of $(g/I_0)\omega_0^{1/2}f(\tau)$ to the right-hand side of (42), where

$$\langle f(\tau)f(\tau')\rangle=\delta(\tau-\tau')\ . \tag{45}$$

Since the numerical integration of this nonintegrable equation is easier to implement as two coupled first-order equations, we recast it as

$$\frac{d\phi}{d\tau}=v\ , \tag{46}$$

$$\frac{dv}{dt}+\frac{1}{\sqrt{\beta_c}}v+\sin\phi=\rho+\rho_1\sin\left[\frac{\omega}{\omega_0}\tau\right]+\left[2\frac{I_T}{I_0}\right]^{1/2}\beta_c^{-1/4}f(\tau)\ , \tag{47}$$

where (46) defines the variable v, and in Eq. (47) we have introduced the "thermal current" I_T defined by

$$I_T=\frac{2ek_BT}{\hbar} \tag{48}$$

and have used the identity

$$\frac{g\omega_0^{1/2}}{I_0}=\left[2\frac{I_T}{I_0}\right]^{1/2}\beta_c^{-1/4}\ . \tag{49}$$

We see from (49) that the fluctuation-dissipation relation maintains its usual significance in this case because the mean square of the fluctuation has a strength proportional to both $2k_BT$ and $\beta_c^{-1/2}$. Moreover, it is inversely proportional to the system size, in this case I_0, which itself is proportional to the cross-sectional area of the junction. The cross-sectional area of the junction is the macroscopic parameter, i.e., Ω, characteristic of this system. A particularly nice feature of this example is that the fluctuation strength is independent of the state of the system (insofar as R is). This is why there is no "β correction to α" [see Eqs. (30) and (31)] in (47). Said another way, the Ito-Stratonovich distinction is irrelevant in this case.

We have done numerical studies of Eqs. (42), (46), and (47). The results are planned to be reported in detail elsewhere.[31] Using physically derived parameters ($\beta_c=4$, $\rho=0$, $\rho_1=0.91$, and $\omega/\omega_0=0.5655$), the scaled parameters in (47) are all roughly of order unity, except for the noise strength given in (49). It works out to be of order 10^{-2}. There is no freedom here because this magnitude is determined by the fluctuation-dissipation relation expressed by (44) and depends on predetermined macroscopic parameters (i.e., T and R). This magnitude is relatively very large. For comparison, a typical hydrodynamics problem cast in dimensionless form, such that the macrovariable magnitudes are order unity, has a

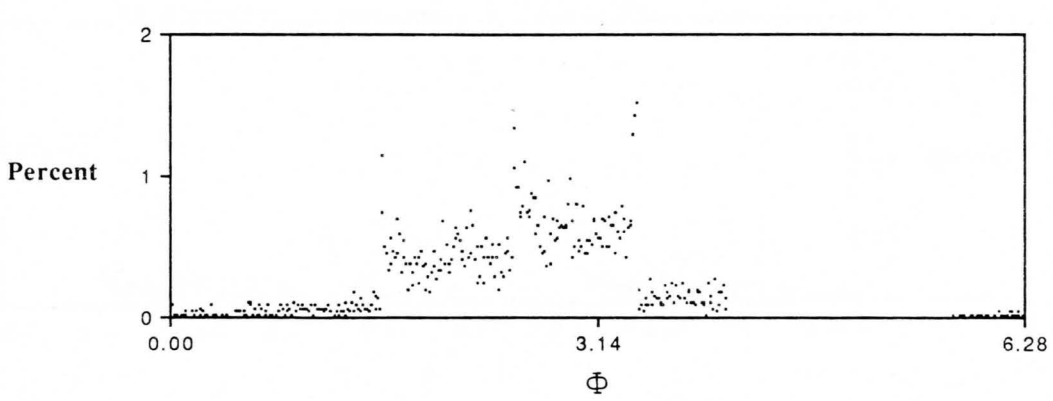

FIG. 10. Projection of Fig. 9 along with $v=0$ axis yielding a the ϕ distribution.

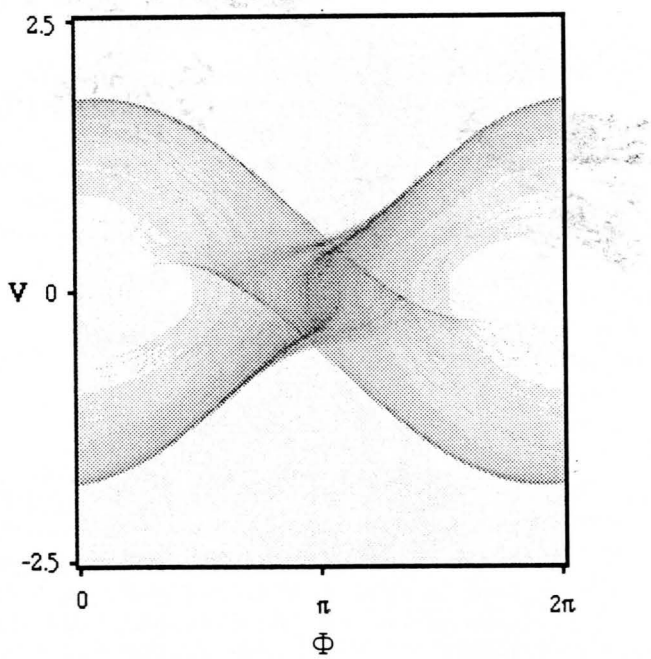

FIG. 11. Probability distribution for the Josephson junction with intrinsic noise.

mean-squared noise strength of order 10^{-10}. Moreover, the largest Liapunov exponent for (42) with the same parameters is $\lambda=0.112$, which implies a sizable amplification of the intrinsic noise in only 10–100 dimensionless time units. This does show up in the attractor plots with the noise compared with those with no noise (see Figs. 9 and 11). This is like the Rossler case of $\mu=4.23$ with $\sigma=10^{-6}$. In addition, dramatic differences in the probability distributions are seen, as is shown in Figs. 10 and 12.

Recent studies of a class-*B* Nd:YAG laser containing a nonlinear intracavity crystal exhibited chaotic output intensity.[16] The dynamics was shown to be very well modeled by equations such as

$$\tau_c \frac{dI_j}{dt} = \left[G_j - \alpha_j - g\epsilon I_j - 2g\epsilon \sum_{k \neq j}^{3} I_k \right] I_j \ , \tag{50}$$

$$\tau_f \frac{dG_j}{dt} = G_j^0 - G_j \left[1 + \beta_j I_j + \sum_{k \neq j}^{3} \beta_{jk} I_k \right] \ , \tag{51}$$

for $j,k=1,2,3$. These equations represent only one of many possible cases studied. In this case, three modes polarized in the same direction have intensities I_j and gains G_j for $j=1,2,3$. In other cases, six, or even eight modes are used and the equations are correspondingly enlarged. The cavity round-trip time τ_c is set equal to 0.2 ns, the fluorescence time τ_f is set equal to 240 μ s, the cavity losses α_j are set equal to 0.01, the nonlinear crystal coupling coefficient ϵ is set equal to 5×10^{-5}, the self-saturations β_k are each set equal to 1, the cross saturations β_{ik} are each set equal to 0.6 and the pump parameters G_j^0 are each set equal to 0.04. The parameter g is a variable configuration parameter depending on the relative orientation of the laser and nonlinear crystals. For different choices (g is always in the interval [0,1]), stable, periodic, chaotic, and intermittent output intensities are produced. The correspondence between the numerical simulation of Eqs. (50) and (51) and real laser measurements for which all of the above parameters were determined is good in the periodic regime when the time course of the total intensity is compared. Spontaneous emission is the physical basis for intrinsic noise in this laser system (pump noise may also prove important, but appears to be very small in this case), and in other laser contexts,[32] it has been very accurately simulated by adding Gaussian, white noise to equations that are the analogs to Eqs. (50) and (51). We may do the same here, in the spirit of Kurtz's second theorem.

Chaos is confirmed for the equations by computing the Liapunov exponent, which turns out to be $\lambda=4.6\times10^{4}$ s^{-1}.[33] The magnitude of the white noise that should be used to model spontaneous emission is of order 10^{-8}. The probability distribution for the total intensity shows a significant effect in our preliminary studies, and this characterization is currently under investigation. A detailed account of the comparison of the theory with experiment is in preparation.[33]

Generally, a numerical simulation of model equations will determine whether or not amplification of intrinsic noise will be significant. If the initial intrinsic noise level is n_0 and the largest Liapunov exponent is λ, then the time required for the noise level to reach n is of the order of[4]

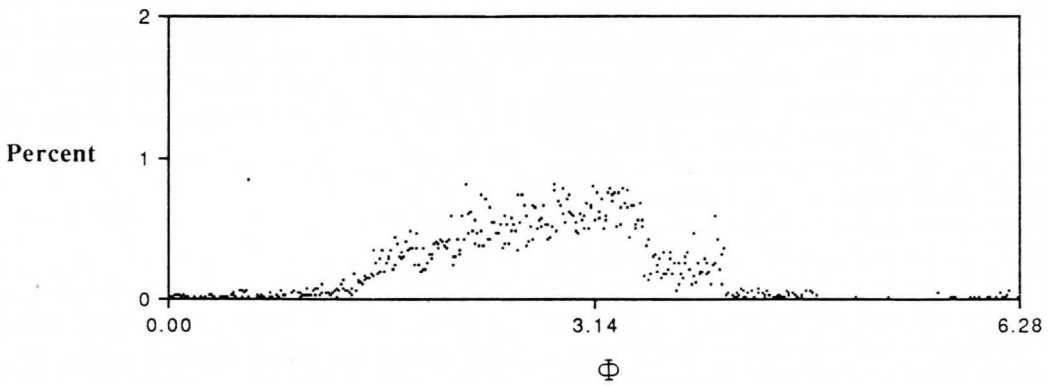

FIG. 12. Projection of Fig. 11 along the $v=0$ axis yielding a the ϕ distribution.

$$t = \frac{1}{\lambda} \ln \left[\frac{n}{n_0} \right] . \tag{52}$$

It may take much longer because this value assumes pure exponential growth, whereas after a certain noise level, nonlinearities will begin to suppress the noise growth.

ACKNOWLEDGMENTS

This work was supported by National Science Foundation research Grants No. PHY-9043227 (R.F.F.) and No. CHE 89-18422 (J.K.) and U.S. Air Force Grant No. AFOSR-90-0158 (R.F.F.). We thank Chris Bracikowski for sharing preliminary results from his ongoing study of laser chaos and John Wagner for his diligent work on the numerical calculations.

[1]R. F. Fox and J. Keizer, Phys. Rev. Lett. **64**, 249 (1990).
[2]R. F. Fox, Phys. Rev. A **41**, 2969 (1990).
[3]R. F. Fox, Phys. Rev. A **42**, 1946 (1990).
[4]J. Keizer, R. F. Fox, and J. W. Tilden (unpublished).
[5]T. G. Kurtz, Math. Prog. Stud. **5**, 67 (1976).
[6]T. G. Kurtz, Stoch. Proc. Appl. **6**, 223 (1978).
[7]A. J. Lichtenberg and M. A. Lieberman, *Regular and Stochastic Motion* (Springer-Verlag, New York, 1983), Sec. 5.2b.
[8]P. Berge, Y. Pomeau, and C. Vidal, *Order within Chaos* (Wiley, New York, 1984), Appendix B, pp. 279–286.
[9]J. Keizer, *Statistical Thermodynamics of Nonequilibrium Processes* (Springer-Verlag, New York, 1987).
[10]J. Keizer and J. W. Tilden, J. Chem. Phys. **93**, 2811 (1989).
[11]N. G. van Kampen, *Stochastic Processes in Physics and Chemistry* (North-Holland, Amsterdam, 1981), pp. 211–213 and 272.
[12]D. K. C. McDonald, Philos. Mag. **45**, 63 (1954); **45**, 345 (1954); Phys. Rev. **108**, 541 (1957).
[13]J. P. Crutchfield, J. D. Farmer, and B. A. Huberman, Phys. Rep. **92**, 45 (1982).
[14]J. P. Crutchfield, J. D. Farmer, N. Packard, R. Shaw, G. Jones, and R. Donnelly, Phys. Lett. A **76**, 1 (1980).
[15]N. F. Pederson and A. Davidson, Appl. Phys. Lett. **39**, 830 (1981).
[16]G. E. James, Ph.D. dissertation, Georgia Institute of Technology, 1990; G. E. James, E. M. Harrell, and R. Roy, Phys. Rev. A **41**, 2778 (1990).
[17]J. P. Crutchfield and N. H. Packard, Phys. D **7**, 201 (1983).
[18]B. J. Berne and R. Pecora, *Dynamic Light Scattering* (Wiley, New York, 1976).
[19]P. Cvitanovic, in *Noise and Chaos in Nonlinear Dynamical Systems*, edited by F. Moss, L. Lugiato, and W. Schleich, (Cambridge University Press, Cambridge, MA, 1990), pp. 270–288.
[20]R. F. Fox, Phys. Rep. **48**, 179 (1978).
[21]T. R. Kirkpatrick, E. G. D. Cohen, and J. R. Dorfman, Phys. Rev. A **26**, 950 (1982); **26**, 972 (1982).
[22]D. A. McQuarrie, J. Appl. Probl. **4**, 413 (1967).
[23]T. G. Kurtz, J. Appl. Probl. **7**, 49 (1970); **8**, 344 (1971).
[24]H. A. Kramers, Phys. **7**, 284 (1940).
[25]J. E. Moyal, J. R. Stat. Soc. Ser. B **11**, 150 (1949).
[26]L. Arnold, *Stochastic Differential Equations* (Wiley, New York, 1974).
[27]R. F. Fox, J. Stat. Phys. **54**, 1353 (1989); **58**, 395 (1990).
[28]O. Rossler, Phys. Lett. A **57**, 397 (1976).
[29]D. E. McCumber, J. Appl. Phys. **39**, 3113 (1968).
[30]J. Guckenheimer and P. Holmes, *Nonlinear Oscillations, Dynamical Systems, and Bifurcations of Vector Fields* (Springer-Verlag, New York, 1983), Sec. 4.6.
[31]J. Keizer, R. F. Fox, and J. Wagner (unpublished).
[32]M. Sargent III, M. O. Scully and W. E. Lamb, Jr., *Laser Physics* (Addison-Wesley, Reading, MA, 1974), Chap. XX.
[33]C. Bracikowski, R. F. Fox, and R. Roy (unpublished).

Stochastic effects in Rayleigh-Bénard pattern formation

T. C. Elston and Ronald F. Fox
School of Physics, Georgia Institute of Technology, Atlanta, Georgia
(Received 15 July 1991)

Results of recent experiments on the Rayleigh-Bénard system indicate that stochastic driving forces are important in the evolution of flow patterns. However, the strength of the noise needed to reproduce the experimental results is four orders of magnitude larger than that of thermal noise. In this report, we present evidence that suggests that the source of noise comes from an uncertainty in the initial conditions rather than from a stochastic driving force.

PACS number(s): 47.20.Ky, 05.40.+j

The Rayleigh-Bénard problem of heating a fluid from below is a classic example from hydrodynamics in which a nonlinear dissipative system undergoes a transition from a spatially uniform state to one of lower symmetry. The important parameter in this problem is the Rayleigh number R, which is proportional to the temperature gradient ΔT across the fluid. Below its critical value R_c, a pure conduction state exists in the fluid with no velocity field present. When R is greater than R_c, the conduction state is unstable and any small perturbation will cause the onset of convection. In most experimental systems, convection will actually occur when R is below R_c because of imperfections in the experimental apparatus. The main source of these imperfections comes from thermal gradients at the boundary due to the differences in thermal diffusivities of the container wall and the fluid. This sidewall forcing not only causes subcritical bifurcations, but also causes the emerging flow patterns to possess the same symmetry as the container. In an attempt to study the effect of stochastic processes on pattern evolution, Meyer and co-workers [1] have constructed an experimental cell whose walls are made from a gel with a thermal diffusivity which is almost identical to that of water, thus eliminating sidewall forcing. When this was done the flow patterns that emerged had randomly oriented convection cells that were not reproduced on subsequent runs of the experiment. These results imply that stochastic processes play an important role in pattern formation.

A more convincing argument for the importance of stochastic processes in this system is found through measurements of the convective heat current j^{conv}. The bifurcation from the conductive to the convective state and the amplitude of the resulting velocity field for R slightly greater than R_c are described by the Landau amplitude equation,

$$\tau_0 \frac{dA}{dt} = \epsilon A - A^3 + h \ , \tag{1}$$

where ϵ is given by $R/R_c - 1$ or $\Delta T/\Delta T_c - 1$, and h represents any imperfections in the system. τ_0 is used to scale time to the vertical thermal diffusion time and for the case under consideration, $\tau_0 = 0.0552$. The $A = 0$ conductive state is a stable solution to the Landau equation when $\epsilon < 0$. When ϵ becomes positive, this solution is unstable and the resulting convective heat current can be found from $j^{\text{conv}} = A^2$. In the experiments performed by Meyer, Ahlers, and Cannell [2], ϵ was ramped linearly in time, i.e., $\epsilon = \epsilon_0 + \beta t$. Using the Landau amplitude equation, Meyer, Ahlers, and Cannell were able to very accurately reproduce experimental data obtained for the convective heat current with h the only adjustable quantity. They found a reasonable fit to the data was obtained with h taken to be constant, however, a stochastic h (stochastic driving force) produced noticeably better results. While this provided convincing evidence for the presence of a stochastic process, the strength of the stochastic force needed to fit the data was four orders of magnitude larger than the strength of the thermal noise predicted by fluctuating hydrodynamics [3,4]. The source of this noise has remained a mystery.

At the suggestion of Rabinovich [5], we decided to investigate the possibility that the noise source in this experiment was an uncertainty in initial conditions rather than a stochastic driving force. Two ramp rates for ϵ were studied, $\beta = 0.27$ and 0.08. For each value of β, the Landau amplitude equation with a time-dependent ϵ was numerically integrated for three different cases. In the first run, h was taken to be a deterministic constant force. For $\beta = 0.27$, $h = 1.10 \times 10^{-4}$ and for $\beta = 0.08$, $h = 1.2 \times 10^{-4}$, which are the same values as those used by Meyer, Ahlers, and Cannell [2]. The second run was preformed with h being a Gaussian white noise driving force. In each case $\langle h(t)h(t') \rangle = 2d\tau_0 \delta(t - t')$, where $d = 5.3 \times 10^{-7}$ for $\beta = 0.27$ and $d = 6 \times 10^{-7}$ for $\beta = 0.08$, which are again identical with the work by Meyer, Ahlers, and Cannell [2]. A final run was made with random initial conditions and no forcing term. The initial value distribution was Gaussian with average value 0 and variance of 8×10^{-6} for $\beta = 0.27$ and 10^{-5} for $\beta = 0.08$. In Fig. 1, we show the results for the case $\beta = 0.27$. The solid line represents the deterministic case and the dashed line represents both the stochastically driven and random initial condition cases since the two curves are nearly identical. Figure 2 is the same as Fig. 1 except with $\beta = 0.08$. Once again there is virtually no difference between the stochastically driven and the random initial condition cases. In Figs. 3 and 4, we show plots of the standard deviation of j^{conv} as a function of time for

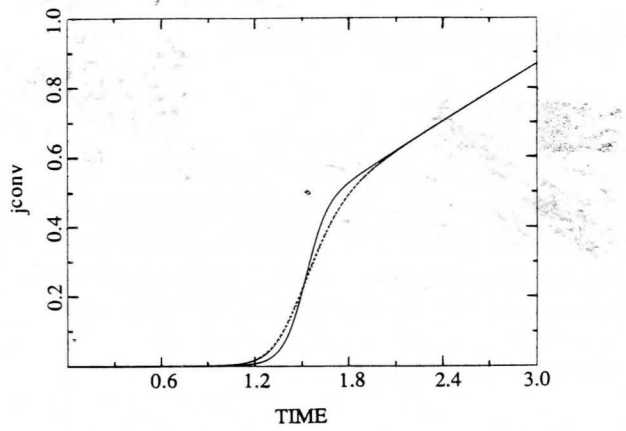

FIG. 1. The convective heat current as a function of time for $\beta=0.27$. The solid line is the deterministic case and the dashed line corresponds to both the stochastic driving force and the random initial condition cases. The time is measured in units of the thermal diffusion time.

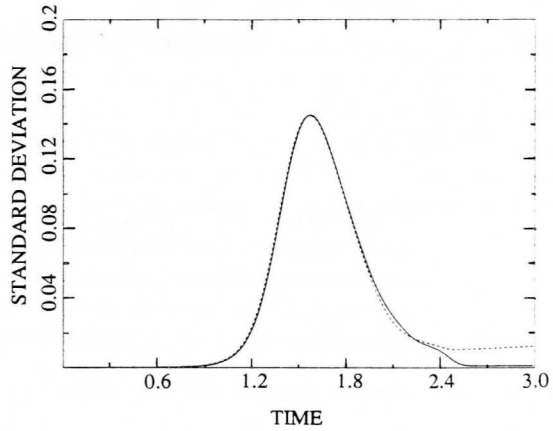

FIG. 3. The standard deviation of the convective heat current as a function of time for $\beta=0.27$. The solid line corresponds to random initial conditions and the dashed line to a stochastic driving force.

$\beta=0.27$ and 0.08 respectively. Here, the solid line represents the random initial condition case, and the stochastically driven case is shown as the dashed line. While slight differences can now be seen, the two curves are very similar. All averages were taken over 10 000 realizations to ensure adequate statistics.

The only notable difference between the work of Meyer, Ahlers, and Cannell [2] and our own is that in their simulations the actual ramp rates varied in time and in ours were constant. This difference, however, only affected the late time magnitudes slightly and none of the qualitative features. We have shown that the source of noise in this experiment need not be attributed to a stochastic driving force, but may well come from an uncertainty in initial conditions. We suspect the initial value fluctuations we get from fitting the data represent some systematic uncertainty in the experimental setup. One possibility is suggested from consideration of the measurement technique used in the experiment. While we do 10 000 stochastic realizations to get a mathematical fit, only a single experiment is performed. This difference is explained [6] by the observation that in this single experiment, a Nusselt-number measurement is performed which effectively integrates the heat transport by many individual patches of convection in different parts of the container. If the detailed states for each patch initially show a variation in the amplitude A comparable with the initial value distribution we have used, then this may be the underlying cause.

It should be noted, however, that the magnitude of the initial value fluctuations is much larger than one would expect from thermal fluctuations. In all of the work

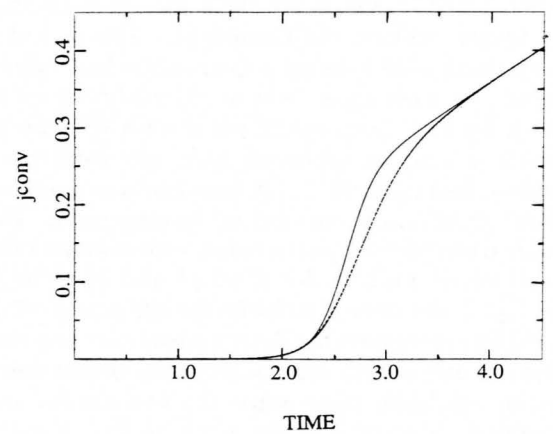

FIG. 2. The convective heat current as a function of time for $\beta=0.08$. The solid line is the deterministic case and the dashed line corresponds to both the stochastic driving force and the random initial condition cases. The time is measured in units of the thermal diffusion time.

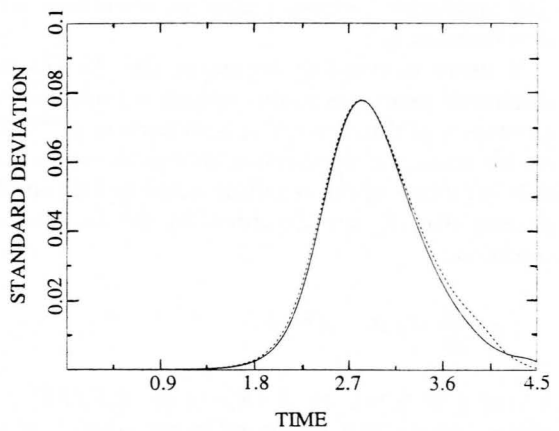

FIG. 4. The standard deviation of the convective heat current as a function of time for $\beta=0.08$. The solid line corresponds to random initial conditions and the dashed line to a stochastic driving force.

quoted above, the origin of time *in the figures*, $t=0$, was chosen as the time when $\epsilon=0$. In fact, Meyer, Ahlers, and Cannell generally took $\epsilon_0=-\beta$ in $\epsilon=\epsilon_0+\beta t$ so that the system aged for a unit time interval before $\epsilon=0$. Thus, *in the equations,* the origin of time is the time when the ramping begins in $\epsilon=\epsilon_0+\beta t$. How does this choice affect the outcome and how does it relate to the size of the initial value thermal fluctuations?

Since $\epsilon_0<0$, the nonlinear term in (1) remains very small and may be ignored during this aging process. The appropriate equation for this stage $(0<t<1)$ is

$$\tau_0\frac{dA}{dt}=(-\beta+\beta t)A+h \ . \tag{2}$$

First consider using only an initial value distribution, i.e., $h=0$. The variance of A grows in accord with (since the mean value remains zero all the time)

$$\langle A^2(t)\rangle=\exp(-2\beta t+\beta t^2)\langle A^2(0)\rangle \ . \tag{3}$$

At time $t=1$ (i.e., when $\epsilon=0$), this yields a factor of $\exp(-\beta)$. As compared with our results for the origin of time used in the figures, taken when $\epsilon=0$, we need only adjust our initial value variance ($\sim 10^{-5}$) by $\exp(\beta)$ in order to get identical results if we start at the earlier time, i.e., at the onset of ramping. This is just a factor of order unity and creates no significant effect.

In order to consider the size of initial-value thermal fluctuations, we must consider another type of aging. The system must be allowed to achieve thermal equilibrium before the ramping begins. During this aging process, the value of ϵ is just the constant ϵ_0 because the ramping has not yet begun. If the only source of initial value fluctuations is thermal fluctuations, then the value for $\langle A^2(0)\rangle$ to be used in (3) would be obtained from the equation

$$\tau_0\frac{dA}{dt}=-\beta A+h_T \ , \tag{4}$$

with h_T representing thermal fluctuations and the origin of time now taken in the very distant past. The variance for h used earlier, d, was of order 10^{-7} to 10^{-6} and was found to be about four orders of magnitude larger than the thermal fluctuation variance. Therefore let us call the thermal variance for h_T in (4) d', so that d' is of order 10^{-11} to 10^{-10}. The equilibrium variance for A resulting from (4) is

$$\langle A^2\rangle=\frac{d'}{\beta\tau_0} \ . \tag{5}$$

The largest this quantity can be for the parameter values used earlier is of order 10^{-8}. This is far short of the $\sim 10^{-5}$ we had to use for $\langle A^2(0)\rangle$. This is why the assertion was made that "the magnitude of the initial value fluctuations is much larger than one would expect from thermal fluctuations."

Nevertheless, we see from this result that if the ramping function is chosen instead to be $\epsilon=-\beta'+\beta t$ in which β' is three or four orders of magnitude smaller than β, i.e., the system is just barely subcritical, and if we let the initial value variance $\langle A^2(0)\rangle$, be determined by

$$\tau_0\frac{dA}{dt}=-\beta' A+h_T \tag{6}$$

instead of by (4), then in place of (5) we obtain

$$\langle A^2\rangle=\frac{d'}{\beta'\tau_0} \ , \tag{7}$$

which is now of order 10^{-5} as required. The description of the experiments [2], however, appears to definitely rule out the possibility of such small values for β', which no doubt would be difficult to achieve. We point out this possibility merely to indicate that slightly subcritical relaxation can enhance the apparent size of initial-value thermal fluctuations.

This work was supported by U.S. Air Force Grant No. AFOSR-90-0158, which includes a graduate research stipend.

[1] C. W. Meyer, G. Ahlers, and D. S. Cannell, Phys. Rev. Lett. **59**, 1577 (1987); G. Ahlers, C. W. Meyer, and D. S. Cannell, J. Stat. Phys. **54**, 1121 (1989).

[2] C. W. Meyer, G. Ahlers, and D. S. Cannell, Phys. Rev. A **44**, 2514 (1991).

[3] G. Ahlers, M. C. Cross, P. C. Hohenberg, and S. Safran, J. Fluid Mech. **110**, 297 (1981); J. Swift, P. C. Hohenberg, and G. Ahlers, Phys. Rev. A **43**, 6572 (1991).

[4] H. van Beijeren and E. G. D. Cohen, Phys. Rev. Lett. **60**, 1208 (1988).

[5] Mikhail I. Rabinovich (private communication).

[6] G. Ahlers (private communication).

Amplification of intrinsic noise in a chaotic multimode laser system

C. Bracikowski, R. F. Fox, and Rajarshi Roy
School of Physics, Georgia Institute of Technology, Atlanta, Georgia 30332
(Received 29 July 1991)

The output intensity of an intracavity-frequency-doubled Nd: yttrium aluminum garnet (YAG) laser can exhibit chaotic variations under certain conditions. It has been predicted that the intrinsic noise due to spontaneous emission present in this laser system can be amplified by the chaotic dynamics. We report here the observation of noise amplification in a mathematical model of this laser system in a parameter regime that produces chaotic intensity variations. The amplification was observed in the evolution of the distribution of an ensemble of noisy trajectories, originating from identical initial conditions. The observed amplification occurred at a rate given by the largest Liapunov exponent and is consistent with the theoretical predictions of Fox and Keizer [Phys. Rev. A **43**, 1709 (1991)]. However, anomalous amplification was also observed and occurred at a rate ~ 10 times the Liapunov exponent. The mechanism for this effect is elucidated.

PACS number(s): 42.50.Lc

I. INTRODUCTION

When a nonlinear potassium titanyl phosphate (KTP) crystal is placed inside a Nd:YAG laser cavity, the output intensity can exhibit chaotic variations [1]. The nonlinear crystal converts some of the 1064-nm fundamental laser light into green light at ~ 532 nm by the processes of second-harmonic generation and sum-frequency generation. Sum-frequency generation creates nonlinear global coupling among the lasing modes (each mode is coupled to all other modes) which causes the laser output to vary periodically or chaotically under certain conditions. We have previously developed a deterministic rate equation model of this laser system which accurately reproduces the experimentally observed stable, periodic, and chaotic dynamics [2-5].

In this paper we present results which show the amplification of intrinsic noise in a parameter regime for which the laser equations produce chaotic intensity variations. A measure of this amplification is obtained by comparing the evolution of an ensemble of 20 noisy trajectories with a deterministic trajectory started from the same initial conditions. Fifteen sets of simulations were performed, each with a different noise strength. The noise strengths varied over 14 orders of magnitude. A plot of the mean time to reach a given separation between noisy trajectories and the deterministic one shows an exponential dependence on noise strength as was predicted by Fox and Keizer [6]. We find good agreement between the rate of the exponential separation and the calculated value of the Liapunov exponent for the dynamics.

In addition to the predicted noise amplification by the chaotic dynamics, we have observed an anomalous amplification of the noise that results in a trajectory separation rate about 10 times the Liapunov exponent.

In Sec. II the laser model that will be used in this paper is reviewed. The theory for the chaotic amplification of noise is discussed in Sec. III. We then describe the numerical observation of noise amplification in these rate equations in a parameter regime producing chaotic intensity variations. Section IV contains an analysis of these results, including a discussion of the mechanism responsible for the observed anomalous noise amplification.

II. LASER MODEL

We have previously developed a deterministic rate equation model of an intracavity-frequency-doubled Nd:YAG laser system which accurately reproduces the experimentally observed stable, periodic, and chaotic dynamics [2–5]. The model includes the polarizations of the cavity modes and the fact that the YAG rod may be birefringent. Figure 1 is a schematic of the intracavity doubled Nd:YAG laser we have modeled. The laser cavity contained a nonlinear KTP crystal which served as the frequency-doubling element. The intensity at the fundamental wavelength is highest within the laser cavity. Since the intensity of frequency-doubled light produced by the KTP crystal is proportional to the square of the intensity at the fundamental wavelength, the KTP crystal was placed inside the laser cavity. The laser is pumped by a ten-element phased-array laser diode with a maximum output power of 200 mW at around 810 nm. The highly divergent and elliptical pump beam is first collimated and then circularized before being focused into the cylindrical YAG rod by a 5-cm focal length lens. The

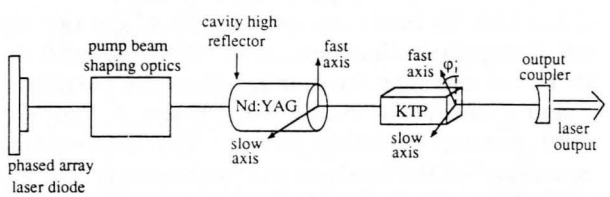

FIG. 1. Schematic of the diode-pumped Nd:YAG (neodymium doped yttrium aluminum garnet) laser with an intracavity KTP (potassium titanyl phosphate) crystal. The KTP crystal produces green light at half the wavelength of the fundamental emission (1064 nm) from the laser.

flat front face of the Nd:YAG crystal served as the cavity high reflector, and was coated to be highly reflecting at both the fundamental (~1064 nm, infrared) and doubled (~532 nm, green) wavelengths and highly transmitting at the pump wavelength. The KTP crystal was antireflection coated at both the fundamental and doubled wavelengths. The laser output coupler was highly transmitting at the doubled frequency and highly reflecting (>99.9%) at the fundamental, such that only the fundamental circulated in the laser cavity; the doubled frequency is simply transmitted by the output coupler. The Nd:YAG and KTP crystals were both 5 mm long and the entire laser cavity was about 3.5 cm long. The threshold pump power for this laser was about 10 mW.

As first pointed out by Oka and Kubota [7], a complete analysis of this laser system must include the polarizations of the cavity modes. These polarizations are given by the eigenvectors of the round-trip Jones matrix M for this laser cavity which are real and orthogonal [2]. These two eignevectors are the only two polarization states that are unchanged after one round trip in the cavity. Since the eigenvectors of the matrix M are real, the laser output will consist of linearly polarized components along one or both of the two orthogonal eigenvector directions.

Nd:YAG normally lases at 1064 nm in the infrared. However, the KTP crystal converts some of this fundamental light into green light at ~532 nm. Green light is produced in the KTP crystal by second-harmonic generation from a single-cavity mode and by sum-frequency generation between pairs of modes. In second-harmonic generation, two photons from the same cavity mode of fundamental frequency ω combine to create one photon of green at frequency 2ω. In sum-frequency generation one photon from a cavity mode at frequency ω_1 and one photon from a different mode at frequency ω_2 combine to create one photon of green at frequency $(\omega_1+\omega_2)$. The amount of green light produced by sum-frequency generation depends on whether the contributing fundamental modes are polarized parallel or orthogonal to each other. The two processes for the generation of green light must be included in the laser rate equations as nonlinear loss terms for the fundamental intensity. The variations in the output intensity that are observed for some parameter values arise from the global coupling created among the lasing modes (each mode is coupled to every other mode) due to sum-frequency generation.

Each cavity mode can exist in one of the two orthogonal eigenpolarization directions, which we label as x and y. Let m and n be the number of modes polarized in the x and y directions, respectively, where $N=m+n$ is the total number of lasing modes. The deterministic rate equations for the fundamental intensities I_k and gains G_k are [2,8]

$$\tau_c \frac{dI_k}{dt} = \left[G_k - \alpha_k - g\epsilon I_k - 2\epsilon \sum_{j(\neq k)} \mu_{jk} I_j \right] I_k \ ,$$
$$\tau_f \frac{dG_k}{dt} = \gamma - \left[1 + I_k + \beta \sum_{j(\neq k)} I_j \right] G_k \ , \tag{1}$$

where τ_c (0.2 ns) and τ_f (240 μs) are the cavity round-trip time and fluorescence lifetime of the Nd^{3+} ion (the active ion in Nd:YAG), respectively; I_k and G_k are, respectively, the intensity and gain associated with the kth longitudinal mode; α_k is the cavity loss parameter for the kth mode; $\gamma(0.05)$ is the small signal gain which is related to the pump rate above threshold; β (0.6) is the cross saturation parameter; and g (0.1) is a geometrical factor whose value depends on the angle between the YAG and KTP fast axes, as well as on the phase delays due to their birefringence. For modes having the same polarization as the kth mode, $\mu_{jk}=g$, while $\mu_{jk}=(1-g)$ for modes having the orthogonal polarization. This difference is due to the different amounts of sum-frequency generated green light produced by pairs of parallel polarized modes or by pairs of orthogonally polarized modes. Here, ϵ (5×10^{-6}) is a nonlinear coefficient whose value depends on the crystal properties of the KTP and describes the conversion efficiency of the fundamental intensity into doubled intensity. In these rate equations we have made the simplifying approximation that the gain γ (0.05) and cross saturation parameter β (0.6) are the same for all modes. The individual mode losses are assumed to differ only slightly, with $\alpha_k \sim 0.01$. The parameter values given above represent typical experimental operating conditions.

As was mentioned earlier, these deterministic rate equations (1) have been found to accurately reproduce experimentally observed periodic and chaotic intensity variations. For the investigation of noise effects it is more convenient to use the entirely equivalent equations for the electric fields

$$\tau_c \frac{d(E_r)_k}{dt} = \left[G_k - \alpha_k - g\epsilon I_k - 2\epsilon \sum_{j(\neq k)} \mu_j I_j \right] \frac{(E_r)_k}{2} \ ,$$
$$\tau_c \frac{d(E_i)_k}{dt} = \left[G_k - \alpha_k - g\epsilon I_k - 2\epsilon \sum_{j(\neq k)} \mu_j I_j \right] \frac{(E_i)_k}{2} \ , \tag{2}$$
$$\tau_f \frac{dG_k}{dt} = \gamma - \left[1 + I_k + \beta \sum_{j(\neq k)} I_j \right] G_k \ .$$

In the remainder of this paper we will discuss how intrinsic noise added into the rate equations is amplified when the model is integrated with parameter values which deterministically produce chaotic variations. This amplification is not present in the case of nonchaotic time traces.

III. AMPLIFICATION OF INTRINSIC NOISE BY CHAOTIC DYNAMICS

Reference [6] contains a detailed account of the theory for amplification of intrinsic noise by chaotic dynamics and of the technique employed to obtain accurate numerical simulations of this effect. To obtain the equations used in the numerical simulations, three steps are followed. In the first step, a mesoscopic master equation is constructed for the time evolution of a probability distribution, the mean values of which correspond to the macroscopic variables, i.e., the quantities I_k and G_k in the

present case. This probability distribution also describes the intrinsic fluctuations, or noise, associated with the macroscopic variables. Kurtz [6] has proved a limit theorem that yields a nonlinear Fokker-Planck equation that is a very accurate approximation to the full master equation. This Fokker-Planck equation constitutes the second step, and its diffusion terms determine the magnitudes of the intrinsic noise correlations. Numerically, both the master equation and the nonlinear Fokker-Planck equation are extremely difficult to implement efficiently. The third step recognizes that there exists a set of Langevin equations, equivalent to the nonlinear Fokker-Planck equation, in which the noise terms are predetermined by the correlations implied by the diffusion terms in the nonlinear Fokker-Planck equation (the fluctuation-dissipation relation in this context). When these correlations are independent of the state variables, i.e., the I_k, E_k, and G_k, the resulting Langevin equations have the form of the original macrovariable equations, Eqs. (2) in this case, with additive Gaussian white-noise terms, Eqs. (3) given below. The correlations of the noise sources are explicitly determined in the manner described above. Since the noise correlations can be determined without actually constructing the master equation, the first two steps may be bypassed, and one simply writes Eqs. (3) directly, as we do below. This is a consequence of the fact that the intrinsic noise is a result of spontaneous emission for which the correlations, Eqs. (4), are already known from earlier work.

Spontaneous emission noise in the laser is included as additive Gaussian white noise in the manner and for the reasons given above:

$$\tau_c \frac{d(E_r)_k}{dt} = \left[G_k - \alpha_k - g\epsilon I_k - 2\epsilon \sum_{j(\neq k)} \mu_j I_j \right] \left[\frac{(E_r)_k}{2} \right] + (f_1)_k ,$$

$$\tau_c \frac{d(E_i)_k}{dt} = \left[G_k - \alpha_k - g\epsilon I_k - 2\epsilon \sum_{j(\neq k)} \mu_j I_j \right] \left[\frac{(E_i)_k}{2} \right] + (f_2)_k , \quad (3)$$

$$\tau_f \frac{dG_k}{dt} = \gamma - \left[1 + I_k + \beta \sum_{j(\neq k)} I_j \right] G_k ,$$

where $(E_r)_k$ and $(E_i)_k$ are the real and imaginary parts of the electric field of the kth mode. Here $(f_1)_k$ and $(f_2)_k$ represent spontaneous emission noise and are Gaussian white (δ correlated) noise terms with the following properties:

$$\langle [f_i(t)]_k \rangle = 0 ,$$
$$\langle [f_i(t)]_k [f_j(s)]_m \rangle = 2D\delta_{ij}\delta_{km}\delta(t-s) , \quad (4)$$

where $i = 1,2$. The strength, $2D$, of the correlations is predetermined by the laser system.

In the integration of these field rate equations, the Gaussian distributed noise terms $(f_1)_k$ and $(f_2)_k$ are calculated using the Box-Muller method [9] from two uniform random deviates $(x_1)_k$ and $(x_2)_k$ on (0,1). When the discrete time step Δt used in the numerical integration is included, the noise terms $(f_1)_k$ and $(f_2)_k$ are given by

$$(f_1)_k = \sqrt{-4D\Delta t \ln[(x_1)_k]} \cos[2\pi(x_2)_k] ,$$
$$(f_2)_k = \sqrt{-4D\Delta t \ln[(x_1)_k]} \sin[2\pi(x_2)_k] \quad (5)$$

such that $(f_1)_k$ and $(f_2)_k$ have zero mean and variance equal to $2D$. The fact that the sine and cosine are used in Eqs. (5) means that $(f_1)_k$ and $(f_2)_k$ are uncorrelated. The fact that, for each k and at each time step two different uniform random deviates $(x_1)_k$ and $(x_2)_k$ are used, means that $(f_1)_k$ and $(f_i)_m$ are uncorrelated. This justifies Eqs. (4).

The integration of the stochastic equations (3) was carried out as follows. The deterministic equations (2) were numerically integrated using the IMSL subroutine DGEAR for intervals of 10 nsec. Noise terms were generated using the algorithm in Eqs. (5) with $\Delta t = 10$ nsec and added to the fields at the end of each interval. The parameter values used in the rate equations are given above in Sec. II. The field rate equations were integrated for various noise strengths from $2D = 10^{-20}$ to 10^{-6} sec^{-1}, each started with the same set of initial conditions. For each noise strength, 20 trajectories were calculated, each trajectory using a different set of random numbers to generate the noise. An integration without noise was also performed. For each noise strength, the total inten-

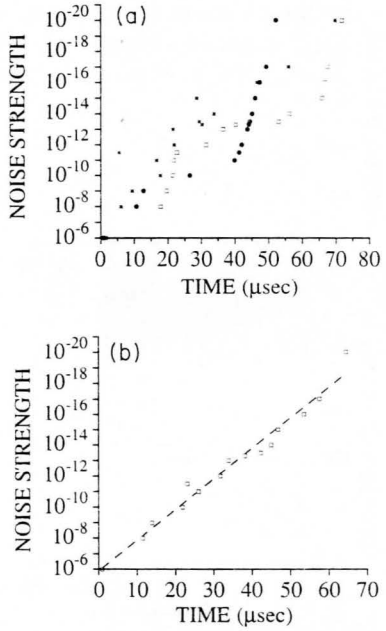

FIG. 2. (a) Time for the separation between noisy and deterministic trajectories produced by an integration of the numerical model to reach 1% of their mean saturated value. The three different symbols represent the different cases of initial conditions (discussed in the text) used in the calculations. (b) Mean time for the separation between noisy and deterministic trajectories produced by an integration of the numerical model to reach 1% of their mean saturated value. The rate of exponential separation is $\sim 4.6 \times 10^5$ sec^{-1}.

sity averaged over 20 realizations was compared with the total intensity for the deterministic trajectory to compute a separation parameter $S(t)$:

$$S(t)=\left|\left[\frac{1}{M}\sum_{k=1}^{M} I_k(t)\right]-I_0(t)\right|, \tag{6}$$

where M is the number of trajectories ($M=20$ in this case here), $I_k(t)$ is the intensity of the kth realization for a particular noise strength at time t, and $I_0(t)$ is the intensity of the deterministic trajectory at time t.

The time for the separation $S(t)$ to reach 1% of the mean saturated value was recorded. This calculation was repeated using the same noise strengths, but starting from a different set of initial conditions. A third set of calculations was done in which the initial conditions for each value of noise strength were different. This last integration was done in order to sample a wider domain of phase space. The mean separation time for each of these three calculations was determined. The time for the mean separation of the trajectories to reach 1% of the mean saturated value (the reference level) is plotted against noise strength in Fig. 2(a) for the three calculations just described. Figure 2(b) shows all three sets of data averaged together. It is very clear that the mean time to reach the reference level increases exponentially as the noise strength decreases, as predicted by Fox and Keizer, and the rate of this exponential increase is $\sim 4.6\times 10^5$ sec^{-1}. If the traditional linearized fluctuation theory were used instead, an average over an ensemble of sufficient size would yield zero for this difference. This is because the linearized theory predicts a symmetric Gaussian distribution of the stochastic trajectories about the deterministic trajectory. Kurtz's nonlinear fluctuation theory [6], however, predicts an asymmetric distribution not centered on the deterministic trajectory. In this case the average of the stochastic trajectories diverges exponentially from the chaotic deterministic trajectory at a rate given by the largest positive Liapunov exponent.

For two of these three cases of initial conditions, the average, largest Liapunov exponent was also computed for the noise strengths $2D=10^{-9}$, 10^{-13}, and 10^{-17} sec^{-1}. The largest Liapunov exponent for these three noise strengths in all the cases considered was about 3.3×10^4 sec^{-1}. The technique used here to compute the largest Liapunov exponent is discussed in Ref. [10]. However, the exponential rate of mean trajectory separation is about ten times larger than the largest Liapunov exponent. This discrepancy is explained below.

For the noise strengths of $2D=10^{-20}$ and 10^{-17} sec^{-1}, the average time for the separation to reach a variable reference level is found to increase exponentially as the reference level increases, as predicted by Fox and Keizer. The rate of this exponential increase is $\sim 2.8\times 10^5$ sec^{-1} and $\sim 2.3\times 10^5$ sec^{-1} for these two cases, respectively [Figs. 3(a) and 3(b)]. These rates are again about ten times the value of the largest Liapunov exponent.

This discrepancy can be understood by analyzing a plot

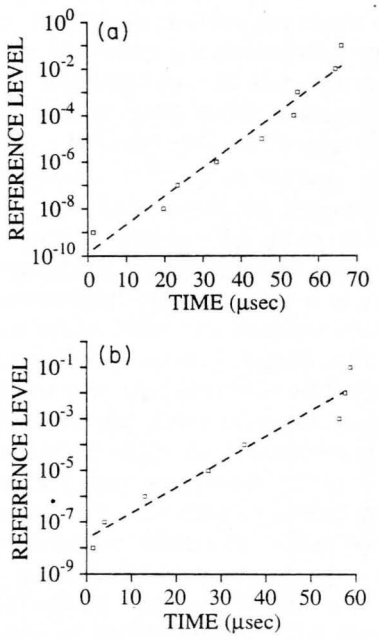

FIG. 3. (a) Mean time for the separation between noisy and deterministic trajectories produced from an integration of the numerical model to reach a variable reference level for a noise strength of $2D=10^{-20}$ sec^{-1}. The rate of exponential separation is $\sim 2.8\times 10^5$ sec^{-1}. (b) Mean time for the separation between noisy and deterministic trajectories produced from an integration of the numerical model to reach a variable reference level for a noise strength of $2D=10^{-17}$ sec^{-1}. The rate of exponential separation is $\sim 2.3\times 10^5$ sec^{-1}.

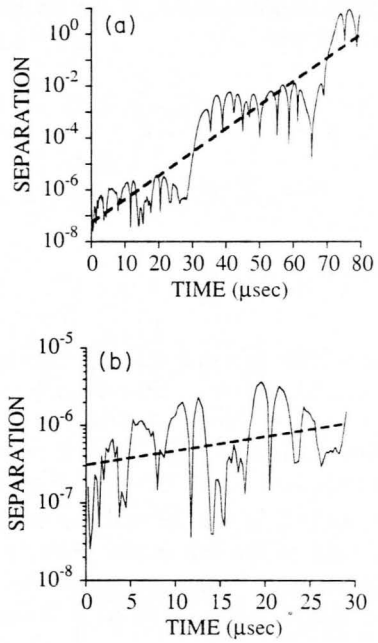

FIG. 4. (a) Separation of a noisy ($2D=10^{-17}$ sec^{-1}) and a deterministic trajectory with time. The rate of exponential separation is $\sim 2.1\times 10^5$ sec^{-1} which is the slope of the linear fit to the data (dashed line). This slope is approximately ten times the value of the largest Liapunov exponent calculated for the data. (b) Close-up view of Fig. 4(a). The rate of exponential separation is $\sim 4.2\times 10^4$ sec^{-1}, which is the slope of the linear fit to the data (dashed line). This slope is approximately equal to the value of the largest Liapunov exponent calculated for the data.

of the separation of a single noisy and the corresponding deterministic trajectory with time as shown in Fig. 4. Figure 4(a) shows that this separation saturates after about 80 μsec. The overall separation is observed to increase approximately exponentially at the rate of $\sim 2.1\times 10^5$ sec^{-1}, which is about the same as the rates of exponential increase discussed above. Note, however, the presence of sudden discrete steps in the difference between the two trajectories. The two steps in Fig. 4(a) occur at about 30 and 65 μsec. Furthermore, Fig. 4(b) shows that, in the first 30 μsec, just prior to the first step the separation increases approximately exponentially at the rate of $\sim 4.2\times 10^4$ sec^{-1}, which is about the same as the value of the largest Liapunov exponent calculated for the dynamics. The calculated value of the largest Liapunov exponent is only negligibly influenced by the presence of the steps since the time over which the steps occur is small relative to the time over which the calculation is performed. However, the time for the difference to reach the reference level is shortened due to the presence of the steps. If the steps did not occur then the separation of the deterministic and noisy trajectories would take place at a rate given by the largest Liapunov exponent just as in the case of the separation of two deterministic trajectories started from slightly different initial conditions (Fig. 5). The reason for the occurrence of the steps in the difference between noisy and deterministic trajectories is explained in Sec. IV.

The Liapunov exponent is the rate at which two initially close trajectories diverge in the complete phase space that is determined by all of the fields and gains. The separation between the total intensities of two deterministic trajectories whose initial intensities differ by 10^{-10} is plotted in Fig. 5. The fit to this data reveals an exponential separation at the rate of $\sim 3.23\times 10^4$ sec^{-1}, which is virtually the same as the Liapunov exponent calculated for the dynamics. Notice that no steps are observed in the plot of the separation. For comparison, when the laser equations are integrated with parameter values that yield a stable time trace, no exponential separation is observed between a noisy ($2D=10^{-10}$ sec^{-1}) and a deterministic trajectory as shown in Fig. 6. The difference plotted in Fig. 6 simply fluctuates about its saturation value of $\sim 5\times 10^{-3}$. When parameters yielding a chaotic trajectory were used, the saturation value of the separation was approximately unity [Fig. 4(a)].

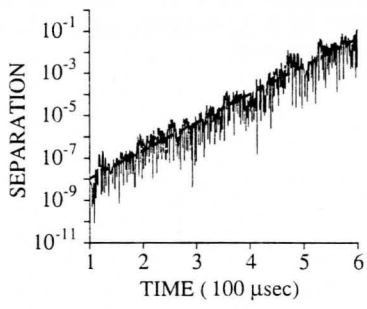

FIG. 5. Separation of two deterministic trajectories produced from an integration of the numerical model whose initial intensities differ by 10^{-10}. The rate of exponential separation is $\sim 3.2\times 10^4$ sec^{-1}. This rate is approximately equal to the value of the largest Liapunov exponent calculated for the data.

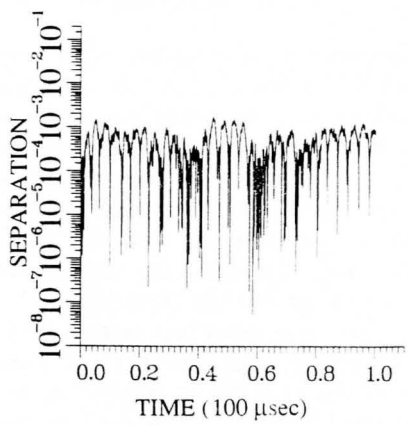

FIG. 6. Separation of a noisy ($2D=10^{-10}$ sec^{-1}) and a deterministic trajectory using parameter values that yield a stable time trace.

Even though gain variations are the driving force behind the intensity variations, the gain terms contribute negligibly to the value of the Liapunov exponent. The gain variations are only about 2% and the intensity variations are about 100% each relative to its respective mean value (Fig. 7). This explains why the exponential divergence rate in Fig. 5 is approximately equal to the Liapunov exponent even though only the total intensities are being considered. We have computed the value of the Liapunov exponent using all intensity and gain terms and using only the intensity terms and have found that they are identical up to eight decimal places.

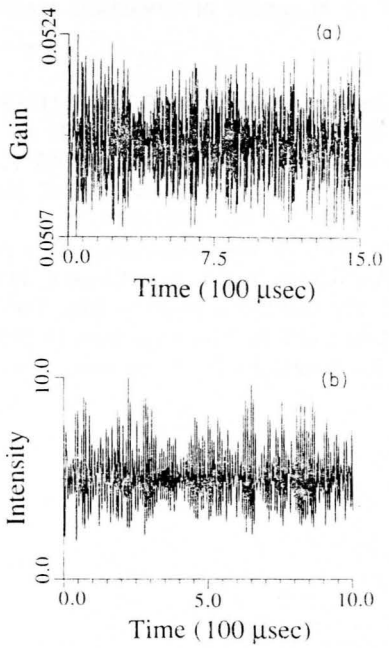

FIG. 7. (a) Gain variations produced from an integration of the numerical model. (b) Intensity variations produced from an integration of the numerical model.

IV. DISCUSSION

The discrepancy of a factor of 10 in the rate of amplification of noise in all of the data described above can be explained by the presence of the steps as shown in Fig. 4(a). It is a property of the laser dynamics here that some of the laser modes may occasionally turn off (perhaps due to the particular initial conditions) when the mode gain G_k remains less than the mode loss α_k for sufficiently long. Typically the modes with the higher losses, being closer to their threshold, will turn off more frequently then than lower loss modes. In a typical deterministic trajectory calculated here, if a mode turns off, the value of the intensity is reduced to an unphysically small value that is less than the spontaneous emission level in the laser. However, in the stochastic trajectory, the added noise prevents the intensity from decreasing to unphysical values such that, when $G_k - \alpha_k$ for that mode becomes positive, the mode will turn back on sooner and the exponential rate of this turn on is given by the value of $G_k - \alpha_k$. We have observed $G_k - \alpha_k$ to be fairly constant over the time in which the mode turns back on. In fact, the value of $G_k - \alpha_k$ is approximately ten times the Liapunov exponent.

We have observed that the large step at ~ 65 μsec [Fig. 4(a)] is caused by only one particular mode that turns off. It then turns back on in the stochastic trajectory (due to the additive noise) before it turns back on in the deterministic trajectory. The difference between the intensity value of this mode in the stochastic and deterministic trajectories was so large that it dominated the total difference between the trajectories, i.e., the total difference was slaved to the difference in this one mode.

It is thus possible to account for the anomalous amplification associated with the "steps." The remaining divergence of the initially close deterministic trajectories and the divergence of a stochastic trajectory (or an average over an ensemble of stochastic trajectories) from its deterministic relative both at a rate given by the Liapunov exponent are manifestations of the chaotic dynamics as predicted by Fox and Keizer [6].

In order to test the Fox and Keizer theory experimentally on a laser system, the laser noise strength must somehow be manipulated and some measurable quantity must be found whose value can change in the presence of noise when the laser is in a chaotic state. An experimental technique to control the amount of intrinsic noise in a laser has been described by Mussche and Siegman [11]. The nonorthogonality of the transverse modes in unstable resonator lasers and gain-guided lasers creates an enhancement of the linewidth and hence excess intrinsic noise. Mussche and Siegman have shown that the amount of excess noise can be changed by varying the geometrical magnification of an unstable resonator. This technique seems promising as an experimental method for examining the effect of spontaneous emission noise in a chaotic system.

In conclusion, the amplification of noise by the chaotic dynamics in the rate equation model of a multimode laser system has been observed. The separation of noisy and deterministic trajectories occurs at a rate given by the Liapunov exponent. In addition to this type of chaos-induced amplification, an anomalous amplification producing trajectory separations at about ten times the value of the Liapunov exponent has also been observed. This effect is a result of the fact that a mode turns on faster with added noise than without, and is not related to the presence of chaos.

ACKNOWLEDGMENTS

We acknowledge support from NSF Grant No. ECS 8722216 (C.B. and R.R.), NSF Grant No. PHY-9043227 (R.F.F.), and AFOSR Grant No. 90-0158 (R.F.F.).

[1] T. Baer, J. Opt. Soc. Am. B **3**, 1175 (1986).
[2] G. E. James, E. M. Harrell, II, C. Bracikowski, K. Wiesenfeld, and R. Roy, Opt. Lett. **15**, 1141 (1990).
[3] K. Wiesenfeld, C. Bracikowski, G. E. James, and R. Roy, Phys. Rev. Lett. **65**, 1749 (1990).
[4] C. Bracikowski and R. Roy, Phys. Rev. A **43**, 6455 (1991).
[5] C. Bracikowski and R. Roy, Chaos **1**, 49 (1991).
[6] R. F. Fox and J. Keizer, Phys. Rev. A **43**, 1709 (1991).
[7] M. Oka and S. Kubota, Opt. Lett. **13**, 805 (1988).
[8] G. E. James, Ph.D. dissertation, Georgia Institute of Technology, 1990 (unpublished).
[9] W. H. Press, B. P. Flannery, S. A. Teukolsky, and W. T. Vetterling, *Numerical Recipes: The Art of Scientific Computing* (Cambridge University, Cambridge, 1989), p. 202.
[10] A. J. Lichtenberg and M. A. Lieberman, *Regular and Stochastic Motion* (Springer-Verlag, Berlin, 1983), p. 264.
[11] (a) A. E. Siegman, Phys. Rev. A **39**, 1253 (1989); (b) **39**, 1264 (1989); (c) P. L. Mussche and A. E. Siegman, Proc. SPIE **1376**, 153 (1990).

Reply to "Comments on the amplification of intrinsic fluctuations by chaotic dynamics"

Joel Keizer
Institute of Theoretical Dynamics, University of California, Davis, Davis, California 95616

Ronald F. Fox
School of Physics, Georgia Institute of Technology, Atlanta, Georgia 30332

(Received 27 March 1992)

We believe that the criticisms of Nicolis and Balakrishnan [preceding Comment, Phys. Rev. A **46**, 3569 (1992)] reflect a misunderstanding of the basis of our claims. Here, we repeat a number of points already made in our papers [Phys. Rev. A **43**, 1709 (1991); **42**, 1946 (1990); Phys. Rev. Lett. **64**, 249 (1990)] in order to dispel ambiguity and misunderstanding.

PACS number(s): 05.40.+j, 05.45.+b

Nicolis and Balakrishnan [1] have criticized our suggestions (i) that chaotic dynamics can amplify spontaneous fluctuations so that the contraction of a master equation description into a macrovariable description is invalid; and (ii) that a nonlinear Fokker-Planck equation of the sort suggested by a theorem of T. G. Kurtz may be used to accurately describe these large-scale fluctuations. These criticisms seem to reflect a misunderstanding, repeated throughout the Comment, of the basis of our claims. We find this surprising since, in Secs. I–III of Ref. [2], these and related issues are addressed rather thoroughly.

A key point that Nicolis and Balakrishnan seem to have missed is that the magnitude of the correlation of the intrinsic fluctuations is not a free quantity but is uniquely determined by the underlying physics in each specific case. Thus, while the limits noted in Eqs. (1)–(3) of their Comment are, indeed, true for ϵ approaching zero, ϵ is not zero for intrinsic fluctuations. It is well known through numerical simulations by us [2] and others [3–5] that the invariant densities in the deterministic case ($\epsilon=0$) and the stochastic case ($\epsilon\neq 0$) are distinct both for discrete maps and for stochastic differential equations. The degree of difference between the two densities depends on the magnitude of ϵ and the dynamics of the chaotic attractor.

Nicolis and Balakrishnan suggest that we incorrectly identify the macrovariables with the mean values rather than with the most probable values, and that "macroscopic behavior is generally not associated with the mean. . . , but rather with the most probable values." In fact, the most probable values of the variables do not satisfy the usual system of autonomous macrovariable equations when the distribution is broad. They do so only asymptotically in the limit of small fluctuations, in which case the Gaussian form of the conditional probability density implies that the mean and the most probable values are the same. When the macrovariable equations possess a chaotic attractor, conditional fluctuations are small for only a brief period of time, after which neither the mean nor the most probable values satisfy the autonomous macrovariable equations. Nonetheless, our simulations, which employ a stochastic modification of the macrovariable equations, make it clear that the macrovariable equations provide the skeleton that supports the flesh of the molecular fluctuations.

Our views about the utility of the nonlinear Fokker-Planck equation are based on two theorems by Kurtz [6,7]. Kurtz's theorems justify various approximations to sample paths of the master equation in the thermodynamic limit. Kurtz's "first" theorem justifies the use of a linear process with a Gaussian conditional probability density for finite times. For that case the most probable and mean values are identical. As we have shown [8], this approximation has a linearly divergent covariance when the mean has a stable limit cycle and an exponentially divergent covariance when the mean behaves chaotically. In the chaotic case the "finite" time interval, which is not otherwise determined by Kurtz's theorem, is of the order of the reciprocal of the largest Liapunov exponent.

For limit cycles and for chaotic attractors, Kurtz's "second" theorem provides a much improved approximation in the following senses: (i) the conditional covariance no longer diverges, despite the fact that the fluctuations may grow to the size of the attractor; and (ii) in the mathematical limit of very small noise, simulations of the probability density derived from the corresponding nonlinear Langevin equation converge to the invariant measure of the deterministic attractor [2]. In this approximation the nonlinearities succeed in saturating the growth of the fluctuations. While Kurtz's second theorem also has been proved only for finite times, it is obviously a much improved approximation to the thermodynamic limit and would appear to work for times much longer than the reciprocal of the largest Liapunov exponent.

Our confidence in the Fokker-Planck equation (or equivalent nonlinear Langevin equation) that is given by Kurtz's theorem is reinforced by recent work of Mareschal and De Wit [5]. Using a direct simulation of the Boltzmann equation, these authors have simulated bifurcation to a limit cycle in a chemical reaction and "find agreement between the microscopic simulation results and a Langevin description . . . below and beyond the bifurcation point [5]." Three types of Langevin description were used in this work to obtain the asympotic, long-time

statistical distribution, including that given by Kurtz's second theorem. All three gave good agreement with the Boltzmann simulations.

In our work, we have used Kurtz's second theorem to obtain an approximate representation of a master equation by a nonlinear Fokker-Planck equation [2,9,10]. This Fokker-Planck equation can be equivalently rendered as a Langevin equation. The Langevin equation happens to be a stochastic version of the macrovariable equation with a well-defined noise correlation determined from this correspondence. Unlike external noise with an arbitrary noise strength, the intrinsic noise is uniquely determined by the underlying physics. In our investigation of the effect of this noise we have considered several classes of examples: two heuristic ones, namely, the Rossler equations [2] and a "master" map for the logistic equation [9], as well as hydrodynamic fluctuations for the Lorenz equations [11], Johnson noise for the Josephson junction [2], spontaneous emission for multimode lasers [10], and chemical noise for mass action kinetics [8]. For each of the examples with a physico-chemical origin, the nonlinear Fokker-Planck equation comes directly from an underlying master equation [12].

We know of no examples in the literature, including those cited by Nicolis and Balakrishnan, which demonstrate that the nonlinear Fokker-Planck equation suggested by Kurtz's second theorem "at best ... may give reasonable results [for] ... a single point attractor although even in this case examples are known for which it can fail badly." While it is true that attempts have been made to formulate other Fokker-Planck equations using completely macroscopic ideas [13], in the thermodynamic limit, even for linear systems, they disagree with the underlying master equation results as one departs from equilibrium (cf. Ref. [12], pp. 173–175).

On the other hand, we agree with Nicolis and Balakrishnan that the growth of molecular fluctuations is "yet another manifestation of the sensitivity to initial conditions of chaotic dynamics." The point, however, is that even in the absence of external noise and uncertainty in the initial conditions, molecular fluctuations destroy the utility of predictions based on the macroscopic kinetic equations within a time of the order of the reciprocal of the largest Liapunov exponent. Furthermore, if the noise is sufficiently large, as seems to be true for the driven Josephson junction [2], the invariant distribution on the chaotic attractor may be modified significantly. Even in cases like the Lorenz system, for which fluctuations have a hydrodynamic origin and are small, one finds an amplification of fluctuations of approximately two orders of magnitude above the values for thermal equilibrium [11]. Such increases in the noise level like that seen near critical points, should be detectable by experiment.

[1] G. Nicolis and V. Balakrishnan, preceding Comment, Phys. Rev. A **46**, 3569 (1992).
[2] R. F. Fox and J. Keizer, Phys. Rev. A **43**, 1709 (1991).
[3] B. White, SIAM J. Appl. Math. **32**, 666 (1977).
[4] P. Jung and P. Hanggi, Phys. Rev. Lett. **65**, 3365 (1990).
[5] M. Mareschal and A. De Wit, J. Chem. Phys. **93**, 2000 (1992).
[6] T. G. Kurtz, J. Appl. Prob. **8**, 344 (1971).
[7] T. G. Kurtz, Stoch. Proc. Appl. **6**, 223 (1978).
[8] J. Keizer and J. Tilden, J. Phys. Chem. **93**, 2811 (1989).
[9] R. F. Fox, Phys. Rev. A **42**, 1946 (1990).
[10] C. Bracikowski, R. F. Fox, and R. Roy, Phys. Rev. A **45**, 403 (1992).
[11] R. F. Fox and J. Keizer, Phys. Rev. Lett. **64**, 249 (1990); J. Keizer, R. F. Fox, and J. Wagner (unpublished).
[12] J. Keizer, *Statistical Thermodynamics of Nonequilibrium Processes* (Springer-Verlag, New York, 1987).
[13] H. Grabert, P. Hanggi, and I. Oppenheim, Physica A **117**, 300 (1983).

Amplification of Intrinsic Fluctuations by Chaotic Dynamics

by

Ronald F. Fox
School of Physics
Georgia Institute of Technology
Atlanta, Georgia, 30332

Abstract

When the deterministic description of a macroscopic physical system exhibits chaotic dynamics, the associated intrinsic fluctuations are amplified, in some situations by many orders of magnitude. This effect has been seen numerically in the Lorenz model, which is a hydrodynamic system, in the Josephson junction, and in a multimode laser system. A related phenomenon occurs for a quantum system that exhibits chaos when treated classically. In this case the variances of the quantum observables initially grow exponentially. These effects may have a variety of experimentally observable consequences.

Introduction

The work reviewed in this paper has appeared in a number of publications[1-9]. While it is clear that much of it has been published, it has not always been easy to get it published and several recent extensions have been pending publication for some time. This is a consequence of the startling implications of the results at least for some people, and I have taken solace at times in the anonymous quote[10]:

> "Every novel idea in science passes through three stages:
> First people say it isn't true.
> Then they say it's true but not important.
> And finally they say it's true and important, but not new."

Fortunately there has also been a fourth stage as well, people understand and accept the idea. In what follows, I will attempt to communicate the essence of the idea in such a way that most of you will reach this fourth stage.

The presentation is divided into two parts: classical, macroscopic physics and quantum mechanical physics. In the first part, the central importance of the Jacobi matrix will be exposed. This quantity simultaneously determines whether the largest Liapunov exponent is positive, the hallmark of classical chaos, and the nature of the time evolution of the fluctuations. When the dynamics is chaotic, the fluctuations are amplified. For the second part it is necessary to initially consider what it will mean to talk about chaos at all since the classical notions of trajectory and Liapunov exponent do not automatically go over into quantum mechanics. Instead, we find that for a system treated classically and found to be chaotic, the corresponding quantum mechanical treatment leads to initially exponential growth of the variances of the quantum observables. This becomes the hallmark of what we will refer to as "quantum chaos". The connection between these two views of the physical world is made with the Wigner distribution[3].

Amplification of Fluctuations by Chaos.

Consider a dynamical system described by N coupled nonlinear ordinary differential equations (ODE's), or by N coupled nonlinear partial differential equations (PDE's). In the latter case, a mode expansion results in infinitely many coupled nonlinear ODE's for the mode amplitudes. Galerkin

truncation of this infinite system to N mode amplitudes again produces a system of N coupled ODE's. This is the context for the following discussion. Such a system is given by the equations

$$\frac{d}{dt} x_i(t) = F_i(\mathbf{x}(t)) \tag{1}$$

in which $\mathbf{x}(t)$ denotes the N variables and the F_i's are generally nonlinear functions of the $\mathbf{x}(t)$ components.

Chaos is extreme sensitivity to the initial conditions of the trajectories produced by solutions of (1). This idea is made quantitative by introducing the Liapunov exponents[11]. If there is a positive Liapunov exponent, the dynamics may be said to be chaotic, and usually the largest positive Liapunov exponent is used to provide a measure of the chaos. If we let $\Delta\mathbf{x}(0)$ denote a small difference in the initial conditions for (1), and if λ is the largest positive Liapunov exponent, then we find

$$\Delta\mathbf{x}(t) \sim e^{\lambda t}\, \Delta\mathbf{x}(0) \tag{2}$$

i.e. there is an exponential separation of initially nearby trajectories. This exponential separation is governed by the time evolution of the Jacobi matrix for system (1), which is defined by

$$J_{ik}(\mathbf{x}(t)) = \frac{\partial F_i(\mathbf{x}(t))}{\partial x_k(t)} \tag{3}$$

To see this, consider the trajectories of two initially nearby points: $\mathbf{x}(t)$ and $\mathbf{x}(t) + \Delta\mathbf{x}(t)$. Clearly, we have (1) and also

$$\frac{d}{dt}(x_i + \Delta x_i) = F_i(\mathbf{x}(t) + \Delta\mathbf{x}(t)) \tag{4}$$

In addition

$$F_i(\mathbf{x}(t) + \Delta\mathbf{x}(t)) = F_i(\mathbf{x}(t)) + J_{ik}(\mathbf{x}(t))\, \Delta x_k + \ldots \tag{5}$$

where the summation over k is implicit. Combining equations (1) and (4-5) yields

$$\frac{d}{dt}\Delta x_i = J_{ik}(\mathbf{x}(t))\,\Delta x_k \tag{6}$$

where the time dependence of the Jacobi matrix is determined by the solution to (1). The formal solution to (6) requires a time ordered exponential:

$$\Delta\mathbf{x}(t) = \mathrm{Texp}\left(\int_0^t ds\, \mathbf{J}(\mathbf{x}(s))\right)\Delta\mathbf{x}(0) \tag{7}$$

It is now clear that the time evolving eigenvalues and eigenvectors of $\mathbf{J}(t)$ will determine the positivity of λ in (2). Thus, the Jacobi matrix is the key to the existence of chaos for system (1).

The Jacobi matrix also governs the time evolution of the fluctuations associated with (1). This statement requires a bit of development since the system (1) does not include fluctuations as it stands. We review the results below, but the reader must go to the references[6] for details. It is possible to invoke a mesoscopic perspective given by a master equation[12,13]. Let $P(\mathbf{x},t)$ be the probability distribution (p.d.) for an N component vector $\mathbf{x}$. We use the notation $\mathbf{x}$ because of the connection with (1), but $\mathbf{x}$ is not $\mathbf{x}(t)$. The $\mathbf{x}$ components are simply coordinates in an N-dimensional probability space. $P(\mathbf{x},t)$ satisfies the master equation

$$\frac{\partial}{\partial t}P(\mathbf{x},t) = \int d^N x'\,(W(\mathbf{x},\mathbf{x}')\,P(\mathbf{x}',t) - W(\mathbf{x}',\mathbf{x})\,P(\mathbf{x},t)) \tag{8}$$

in which $W(\mathbf{x},\mathbf{x}')$ is the transition rate distribution, i.e. the transition probability density per unit time for a change from $\mathbf{x}'$ to $\mathbf{x}$. For certain types of jump processes[14], there exists a macroscopic parameter, Ω, such that the transition moments, $K^{(n)}_{i_1 i_2 \ldots i_n}$, scale with Ω according to:

$$K^{(n)}_{i_1 i_2 \ldots i_n} = \int d^N x'\,(x'_{i_1}-x_{i_1})\,(x'_{i_2}-x_{i_2})\ldots(x'_{i_n}-x_{i_n})\,W(\mathbf{x},\mathbf{x}') \tag{9}$$

$$\sim \Omega^{-(n-1)}$$

The Kramers-Moyal expansion[12] provides an infinite order PDE equivalent to (8) given by:

$$\frac{\partial}{\partial t} P(\mathbf{x},t) = \sum_{n=1}^{\infty} \frac{(-1)^n}{n!} \prod_{j=1}^{n} \frac{\partial}{\partial x_{k_j}} (K^{(n)}_{k_1 k_2 \ldots k_n}(\mathbf{x})\, P(\mathbf{x},t)) \tag{10}$$

in which the summation over the k_j's is implicit. If we now contemplate the limit $\Omega \to \infty$, (10) reduces to Liouville's equation

$$\frac{\partial}{\partial t} P(\mathbf{x},t) = - \frac{\partial}{\partial x_k} (K^{(1)}_k(\mathbf{x})\, P(\mathbf{x},t)) \tag{11}$$

which has the solution

$$P(\mathbf{x},t) = \delta(\mathbf{x} - \mathbf{x}(t)) \tag{12}$$

where $\mathbf{x}(t)$ solves the system of ODE's:

$$\frac{d}{dt} x_i(t) = K^{(1)}_i(\mathbf{x}(t)) \tag{13}$$

These equations are identical with (1) provided that the first moments of the transition rate distribution satisfy

$$K^{(1)}_i = F_i \tag{14}$$

In this way, the master equation description reproduces the deterministic macroscopic description as the limit $\Omega \to \infty$.

There are also two, more delicate limits that produce the dynamics for the fluctuations. The first is in the spirit of the central limit theorem of probability theory[14]. Define the scaled fluctuation in $\mathbf{x}$, $\mathbf{y}$, by

$$\mathbf{x} = \mathbf{x}(t) + \Omega^{-1/2}\, \mathbf{y} \tag{15}$$

wherein $\mathbf{x}(t)$ solves (13). Let $\Phi(\mathbf{y},t)$ denote the p.d. for the fluctuations, $\mathbf{y}$. Φ satisfies the linear Fokker-Planck equation:

$$\frac{\partial}{\partial t} \Phi(\mathbf{y},t) = - \frac{\partial}{\partial y_i} (\frac{\partial}{\partial x_j}\ K^{(1)}_i(\mathbf{x}(t))\, y_j\, \Phi(\mathbf{y},t)) \tag{16}$$

$$+ 1/2 \frac{\partial 2}{\partial y_i \partial y_j} (R_{ij}^{(2)}(\mathbf{x}(t))\ \Phi(\mathbf{y},t))$$

in which $R_{ij}^{(2)}$ is defined by

$$R_{ij}^{(2)}(\mathbf{x}(t)) = \lim_{\Omega \to \infty} \Omega\, K_{ij}^{(2)}(\mathbf{x}(t)) \tag{17}$$

which exists on account of the scaling property (9). In these expressions, $K_i^{(1)}$ and $K_{ij}^{(2)}$ are functions of $\mathbf{x}(t)$. We already see the Jacobi matrix for the deterministic motion given by (13-14) in the first term of the right-hand side of (16). Define the fluctuation correlation matrix, C_{ij}, by

$$C_{ij} = \langle y_i\, y_j \rangle_t \tag{18}$$

in which the averaging symbols, $\langle \ldots \rangle_t$, denote an average with respect to $\Phi(\mathbf{y},t)$. C_{ij} satisfies the equation

$$\frac{d}{dt} C_{ik}(t) = J_{ij}(t)\, C_{jk}(t) + C_{ij}(t)\, J_{kj}(t) + R_{ik}^{(2)}(t) \tag{19}$$

in which J_{ij} is the Jacobi matrix in (3) (cf. (14)). We have shown[1,6] that if the deterministic motion is chaotic, then the presence of $\mathbf{J}$ in (19) implies an exponential divergence of $\mathbf{C}$ (at twice the rate of the largest Liapunov exponent).

Clearly, an exponential growth of the fluctuations will eventually invalidate equation (19) and the linear Fokker-Planck equation (16) from which it is derived. For this eventuality, there is a second limit theorem[15] yielding a nonlinear Fokker-Planck equation

$$\frac{\partial}{\partial t} P_f(\mathbf{x},t) = - \frac{\partial}{\partial x_i} (K_i^{(1)}(\mathbf{x})\, P_f(\mathbf{x},t)) \tag{20}$$

$$+ 1/2 \frac{\partial^2}{\partial x_i \partial x_j} (K_{ij}^{(2)}(\mathbf{x})\, P_f(\mathbf{x},t))$$

in which $K_i^{(1)}$ and $K_{ij}^{(2)}$ are functions of $\mathbf{x}$, not $\mathbf{x}(t)$, and in which we have denoted the p.d. for $\mathbf{x}$ by P_f to distinguish it from the $P(\mathbf{x},t)$ that solves (10) (or (11)).

The physical interpretation of these two limits is as follows. For either a non-chaotic motion, or for the initial fluctuation growth phase for the chaotic motion, we have the equations (13) and (16), i.e. the deterministic equations and the equation for the fluctuation p.d.. The latter has coefficients, the Jacobi matrix and $R^{(2)}$, that depend on the deterministic solution to (13). However, for the time evolved chaotic case, we just have the p.d. equation (20). The distribution P_f is sufficiently non-gaussian and is broad enough that

$$\frac{d}{dt}\langle x_i\rangle_t = \langle K_i^{(1)}(\mathbf{x})\rangle_t \neq K_i^{(1)}(\langle \mathbf{x}\rangle_t) \qquad (21)$$

where $\langle \ldots\rangle_t$ denotes averaging with respect to $P_f(\mathbf{x},t)$. We no longer get the deterministic equations we got from (11-13). Another way to say this is to say that the Dirac delta function solution (12) to Liouville's equation (11) is unstable with respect to fluctuations if the trajectory is chaotic. Thus, we are reduced to a fundamental description at the level of $P_f(\mathbf{x},t)$, given by (20).

Determination of $P_f(\mathbf{x},t)$ requires numerical methods in general, on account of the non-integrability of (20). We achieve the same information by implementing a numerical integration of a Langevin equation equivalent with (20). There are some associated technical matters concerning the Ito-Stratonovich stochastic calculus that must also be dealt with[6]. Furthermore, since only the first two moments of W, $K_i^{(1)}$ and $K_{ij}^{(2)}$, appear in (20), and since $K_i^{(1)}$ is already fixed by (14), only $K_{ij}^{(2)}$ needs to be determined. In the equivalent Langevin treatment[6], this quantity corresponds with the matrix of correlations for the components of the stochastic force. It is in essence the content of the fluctuation-dissipation relation of the Onsager theory for near equilibrium fluctuations. For hydrodynamics, we need only replace the

equilibrium quantities in this relation with their local equilibrium values in order to get this quantity, i.e. $K_{ij}^{(2)}$, for the far from equilibrium situations. This is what we have done in our studies of the Lorenz model.

Quantum Chaos

That concensus on a definition of quantum chaos has not yet been reached is often attributed to the putative fact that the natural definition of chaos in classical systems cannot be carried over into quantum mechanics. In the classical setting, one looks at phase space trajectories and characterizes chaos in terms of the positivity of the largest Liapunov exponent. Since we are taught that quantum mechanics does not allow us to maintain the idea of a phase space trajectory, we no longer can use the Liapunov criterion for a definition of quantum chaos. Many researchers have concluded that the only remaining tactic is to study the quantum mechanical properties of known, classically chaotic Hamiltonian systems; this approach has been dubbed "quantum chaology".[16]

In earlier work[17], we have argued that the Liapunov criterion can be applied in quantum mechanics by looking at expectation value trajectories in a "quantum phase space". Heisenberg's uncertainty principle tells us that these trajectories have associated, non-vanishing variances for all of the variables. This fact does not *a priori* prevent us from using the expectation value trajectories as analogues to the classical trajectories. However, this tactic only remains sensible so long as the root-mean-square deviations from the expectations (i.e. the variances) remain small compared to the expectations.

Sometimes it is asserted that you cannot have chaos in quantum mechanics because the Schrodinger equation is a linear partial differential equation and you need non-linearity for chaos. That this is wrong was shown above. Every classical Hamiltonian system can be recast by the linear Liouville equation for a probability distribution in phase space. This distribution can be taken initially to be a Dirac delta function (localized on the initial coordinates and momenta), and as a consequence of the first order derivative nature of Liouville's equation, the solution will evolve as a Dirac delta function for all time. Thus, for a chaotic system, the Liouville distribution follows the chaotic trajectories precisely.

Earlier, we studied the behavior of a fully quantal system, the periodically kicked pendulum[2,5]. We found that when its classical analogue

was chaotic, the quantum description in terms of an expectation value phase space became very remarkable. The variances grew exponentially fast to large size compared to the expectations, and the quantum expectation trajectories soon bore no resemblance to the classical trajectories. For example, classically, the sequence of pendulum angles from kick to kick was a chaotic sequence that jumped all over the interval $[0,2\pi]$, but quantally the expected angle quickly converged on π (the "down" position). This was a result of the variance of the angle growing so large that the quantum probability distribution for the angle became broadly spread out over all of $[0,2\pi]$. We expect that this will generally be the case for fully quantal treatments of classically chaotic systems[3]. One way to see this is to investigate the behavior of the Wigner distribution,especially in the limit where Planck's constant vanishes. We have shown[3] that this limit can be cast such that it parallels very closely the master equation analysis given above in equations (8-20). Remarkably, we obtain an equation for the quantum fluctuations of the form

$$\frac{d}{dt} C_{ik}(t) = J_{ij}(t)\, C_{jk}(t) + C_{ij}(t)\, J_{kj}(t) \qquad (22)$$

in which $C_{ik}(t)$ is the quantum covariance matrix and $J_{ij}(t)$ is the Jacobi matrix for the associated classical dynamics that is obtained in the limit of vanishing Planck's constant. Thus, when the corresponding classical dynamics is chaotic, the Jacobi matrix engenders an initially exponential growth of the quantum covariances. In parallel with the instability of the Dirac delta function solution to Liouville's equation caused by chaos, and referred to above, a Gaussian, Feynman path integral rendering of quantum mechanical time evolution is also unstable when its classical core is chaotic.

One tantalizing experimental application of this effect occurs in reaction kinetics for molecular beams. Consider a beam of molecules initially prepared in a sharply defined rotation state. Intramolecular rotation-vibration coupling can create chaotic evolution of the rotation state distribution that shows itself as exponential growth in the rotation state variance. This greatly enhances channel availability for reactions with molecules in crossed beams. Reaction rates would appear anomalously greater than would be expected on the basis of the reaction rate for the initial sharp rotation state.

We are also pursuing experimental applications in lasers[8] and in Josephson junctions[6].

Acknowledgements

This work was supported by NSF grants PHY-90-43227 and PHY-92-03878 and by AFOSR grant 90-0158.

References

1) R.F. Fox and J. E. Keizer, Phys. Rev. Lett. **64**, 249 (1990).

2) R.F. Fox and B.L. Lan, Phys. Rev. **41A**, 2952 (1990).

3) R.F. Fox, Phys. Rev. **41A**, 2969 (1990).

4) R.F. Fox, Phys. Rev. **42A**, 1946 (1990).

5) B.L. Lan and R.F. Fox, Phys. Rev. **43A**, 646 (1991).

6) R.F. Fox and J. Keizer, Phys. Rev. **43A**, 1709 (1991).

7) R.F. Fox, Phys. Rev. **44A**, 6193 (1991).

8) C. Bracikowski, R.F. Fox and R. Roy, Phys. Rev. **45A**, 8403 (1992).

9) J.E. Keizer and R.F. Fox, Phys. Rev. **46A**, 3572 (1992).

10) F.M. Harold, *A Study of Bioenergetics*, (W.H. Freeman and Co., New York, 1986), p.57.

11) D. Ruell, *Chaotic Evolution and Strange Attractors*, (Cambridge University Press, New York, 1989).

12) N.G. van Kampen, *Stochastic Processes in Physics and Chemistry*, (North-Holland, Amsterdam, 1989).

13) A. Nordsieck, W.E. Lamb and G.E. Uhlenbeck, Physica (Utr.) **7**, 344 (1940).

14) T.G. Kurtz, J. Appl. Prob. **7**, 49 (1970); **8**, 344 (1971).

15) T.G. Kurtz, Math. Prog. Stud. **5**, 67 (1976); Stoch. Proc. Appl. **6**, 223 (1978).

16) M. Berry, unpublished.

17) R.F. Fox and J.C. Eidson, Phys. Rev. **A34**, 482 (1986); **A36**, 4321 (1987).